AD-A073 034 EFFECTS TECHNOLOGY INC SANTA BARBARA CA F/G 11/6
ASSESSMENT OF THE STATE OF KNOWLEDGE PERTAINING TO SOLID PARTIC--ETC(U)
JUN 79 W F ADLER DAAG29-77-C-0039
UNCLASSIFIED ETI-CR79-680 ARO-14980.1-MS NL

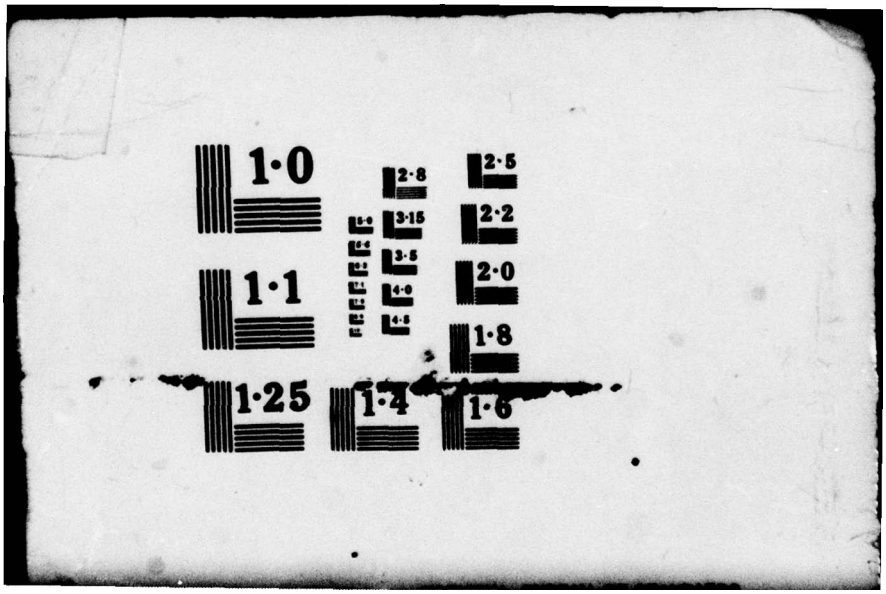
1·0
1·1
1·25
1·4
1·6
1·8
2·0
2·2
2·5
2·8
3·15
3·5
4·0
4·5

THE FINDINGS IN THIS REPORT ARE NOT TO BE CONSTRUED AS AN OFFICIAL DEPARTMENT OF THE ARMY POSITION, UNLESS SO DESIGNATED BY OTHER AUTHORIZED DOCUMENTS.

Unclassified
SECURITY CLASSIFICATION OF THIS PAGE (When Data Entered)

REPORT DOCUMENTATION PAGE

READ INSTRUCTIONS BEFORE COMPLETING FORM

(14) 1. REPORT NUMBER: ET-I-CR79-680 | 2. GOVT ACCESSION NO. | 3. RECIPIENT'S CATALOG NUMBER

(6) 4. TITLE (and Subtitle): ASSESSMENT OF THE STATE OF KNOWLEDGE PERTAINING TO SOLID PARTICLE EROSION,

(9) 5. TYPE OF REPORT & PERIOD COVERED: Final Report,

6. PERFORMING ORG. REPORT NUMBER

(10) 7. AUTHOR(s): William F. Adler

(15) 8. CONTRACT OR GRANT NUMBER(s): DAAG29-77-C-0039

9. PERFORMING ORGANIZATION NAME AND ADDRESS:
Effects Technology, Inc.
5383 Hollister Avenue
Santa Barbara, CA 93111

10. PROGRAM ELEMENT, PROJECT, TASK AREA & WORK UNIT NUMBERS

(11) 11. CONTROLLING OFFICE NAME AND ADDRESS:
U. S. Army Research Office
P. O. Box 12211
Research Triangle Park, NC 27709

12. REPORT DATE: 30 June 1979

13. NUMBER OF PAGES: 150

14. MONITORING AGENCY NAME & ADDRESS (if different from Controlling Office)

(12) 152 p.

15. SECURITY CLASS. (of this report): unclassified

15a. DECLASSIFICATION/DOWNGRADING SCHEDULE

16. DISTRIBUTION STATEMENT (of this Report)

Approved for public release; distribution unlimited.

(18) ARO (19) 14982.1-MS

17. DISTRIBUTION STATEMENT (of the abstract entered in Block 20, if different from Report)

18. SUPPLEMENTARY NOTES

The findings in this report are not to be construed as an official Department of the Army position, unless so designated by other authorized documents.

19. KEY WORDS (Continue on reverse side if necessary and identify by block number)

Solid particle erosion
Analytical modeling
Erosion testing
Impact
Material properties
Ductile materials
Brittle materials

20. ABSTRACT (Continue on reverse side if necessary and identify by block number)

This investigation examines the analyses of solid particle erosion which have been formulated for both ductile and brittle materials. The solid particle erosion process can be described qualitatively for several materials from microscopic examinations of the eroded surfaces, however most of the available erosion analyses are based on material removal models which do not represent the physical processes of material removal as they are presently known. A number of published results have been generally accepted by the erosion community → over

DD FORM 1 JAN 73 1473 EDITION OF 1 NOV 65 IS OBSOLETE

UNCLASSIFIED
SECURITY CLASSIFICATION OF THIS PAGE (When Data Entered)

405 842 LB

20. ABSTRACT (concluded)

without proper scrutiny of the basis for the conclusions reached. Some of these inconsistencies are pointed out and the various analytical approaches used in describing solid particle erosion phenomena are summarized.

The need for an adequately characterized solid particle erosion testing capability is indicated due to the range of test parameters which have been found recently to significantly influence the measured erosion rates. Meaningful advancement in the field is strongly dependent on the development of a reliable experimental data base and experimentation which isolates and clarifies a particular feature of the material removal process.

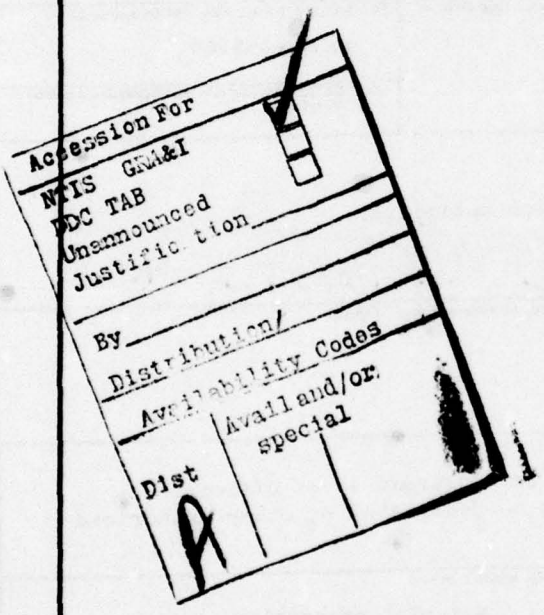

TABLE OF CONTENTS

TABLE OF CONTENTS (concluded)

LIST OF TABLES

LIST OF ILLUSTRATIONS

LIST OF ILLUSTRATIONS (continued)

1.0 INTRODUCTION

Within the last decade a number of investigators have contributed to a clearer understanding of the solid particle erosion mechanisms in both ductile and brittle materials. The erosion process can be qualitatively described for several materials, however most theories of solid particle erosion are based on material removal models which do not represent the actual physical processes of material removal as they are presently known. It became evident to the author that a variety of published results have been generally accepted by the erosion community without proper scrutiny of the basis for the conclusions reached. The objectives of this study are to re-examine both productive and non-productive investigations which have been undertaken in the field of solid particle erosion in order to assess their actual contribution with respect to the current state of the art and to summarize the analyses of the particle impact process and target response which have been pursued as a guide for future activities of this type. This report concentrates on the analysis and modeling of solid particle erosion phenomena, since this aspect of the subject does not appear to have been adequately addressed in the several reviews which have been published (Wahl and Hartstein, 1946; Wellinger and Uetz, 1955; Heymann, 1968; Engel, 1976; Preece and Macmillan, 1977; Evans, 1979; Ruff and Wiederhorn, 1979).

The solid particle erosion literature spans many areas of application and has received the attention of investigators with diverse backgrounds. Motivated for the most part by the need for evaluating the response of materials and coatings to solid particle impingement rather than in understanding the material removal process itself, a diversity of test configurations have been utilized to generate the screening assessments required. Erosion testing has generally been undertaken to satisfy a very specific need for a particular application. Typically a test method is devised representative of the operational environment. A material selection procedure is pursued and then the testing is terminated. It is difficult to construct a coherent series of test

results on this basis. On the other hand there have been a few programs which have been carried out to investigate the erosion process; these have been referred to fairly extensively in the erosion literature. Unfortunately, the available solid particle erosion test results have generally been reported with insufficient information pertaining to the test conditions to provide a valid comparison between the data obtained in one laboratory with that from another laboratory. This situation is complicated further by the fact that changes in the construction of the same test apparatus can significantly influence the delivery of particles to the target material as shown by Uuemois and Kleis (1975), Wolak, et al. (1977), and Maji and Sheldon (1979).

An effort was made to organize and compile the various types of test apparatus used, the test procedures, and the trends in the test results, however it was found that too many voids existed in most publications pertaining to both the description of the apparatus used and information on conducting the tests to make this a meaningful undertaking. Therefore only a limited number of the data trends in the available erosion data are summarized in Section 2 which are relevant to the detailed evaluations of the analytical treatments of solid particle erosion in Section 3.

The scope of this work includes all classes of materials with some emphasis on metals and ceramics exposed to multiple particle impacts ranging from less than a meter per second (ms^{-1}) to an upper limit around 500 ms^{-1} which encompasses most of the work on solid particle impingement of turbine engines, helicopter rotor blades, aircraft window materials, pneumatic transport of solid materials, coal conversion processes, and a variety of additional commonly encountered conditions for which solid particle erosion is an important factor in operational performance. The historical development of the subject is of some interest, but it is not the purpose of this report to provide a complete review of the available literature or to follow an historical perspective.

2.0 GENERAL OBSERVATIONS

Early test devices have been described by Wahl and Hartstein (1946). They divided the test devices used by various investigators into five categories: sand blast equipment, wear chambers, wear pumps, wear nozzles, and other jet devices which pertained primarily to water jets. The use and representative examples of each of these methods for producing wear are described by Wahl and Hartstein.

The most widely used test configuration for solid particle erosion is the sand blast apparatus. Although some version of this device has been used for laboratory-scale erosion evaluations for over seventy years, it has only been quite recently that the test parameters associated with particular types of equipment have been investigaged. The earliest reference provided by Wahl and Hartstein (1946) for laboratory sand blast equipment is to the work of Gary in 1904 (Gary, 1904). The laboratory equipment used for providing a multiple particle field generally worked on the basis of ingestion of particulate matter into a flowing gas stream which subsequently impinges on a test piece. The impact velocity and angle of attack of the particles in the gas stream are governed in part by their size, shape, and density.

Solid particles can also be injected into a flowing gas stream as in a wind tunnel. The specimen is then completely engulfed by the particle-laden gas which offers the advantage of eliminating the transition region around the eroded spot on the test piece when the particles are propelled from a nozzle or tube in the sand blast arrangement. A well-characterized system of this type has been described by Grant and Tabakoff (1975) and Tabakoff and Wakeman (1979).

Rotating arm devices in which the specimen is mounted at the top of a rotor blade and then passes through a stream of falling particles are also used for solid particle erosion evaluations (Kleis, 1969;

Tilly and Sage, 1970; Adler, Morris, and Wahl, 1972). The rotating arm configuration has the advantage of having the specimen impact a graded particle distribution (such as specified by U.S. Military Specification, Mil-E-5007C, which includes particle sizes over the range from 0 to 1000 μm) at a uniform velocity. Such conditions are characteristic of high speed structural components in a dust field where the particles are traveling at considerably lower velocities as for a helicopter rotor. The rotating arm configurations also have potential for being operated at higher impact velocities compared with sand blast and wind tunnel test facilities.

The variations which exist in solid particle erosion test apparatus, even for sand blast devices, make it difficult to discuss typical, or standard, test conditions. Generally the test results are strongly related to the test apparatus used. In addition the testing procedures for solid particle erosion vary widely from laboratory to laboratory, so it is difficult to make an absolute comparison between the results obtained for one set of test conditions to another. Also, as more attention is paid to the test procedures and characterization of the impact conditions, additional factors which influence the impacting particle/target interactions are being discovered (Tilly, 1969; Tilly and Sage, 1970; Uuemois and Kleis, 1975; Grant and Tabakoff, 1975; Wolak, et al., 1977; Young and Ruff, 1977; Tabakoff, Kotwal, and Hamed, 1979; Maji and Sheldon, 1979; Lapides and Levy, 1979). Therefore at the present time the test facility and the test procedure must be considered in conjunction with the test results.

A considerable amount of testing has been devoted to the determination of the so-called "erosion resistance" of a material. Since, as will be demonstrated in Sections 3 and 4, no satisfactory analysis of solid particle erosion exists, it is not possible to provide an expression representing the erosion resistance of a particular material which can be used in a general context involving different particulates,

impact velocities, angles of attack, and so on. Unfortunately, without an adequate analysis of solid particle erosion, the erosion resistance of a material according to a specific definition can only be compared under the same test conditions with another material. Thus, one finds that most of the erosion testing reported in the literature is a ranking of materials for a specific environmental condition. Furthermore, since the majority of solid particle erosion tests have been for the purpose of ranking and comparing the erosion behavior of materials, there has been little concern for quantitatively specifying the test parameters or providing an adequate description of the test apparatus. Faced with this situation several investigators have commented on the general lack of useable test results in the field of solid particle erosion.

The general erosion behavior of a generic material eroded under a specific test condition has the characteristic response illustrated in Figure 2.1. The specimen is weighed before and after exposure to the eroding environment. The mass loss as a function of the exposure to the eroding environments is the raw data obtained from a test. The mass loss/exposure time curve has a general form which consists of an incubation period, acceleration period, and the maximum rate period. Although stages beyond the maximum rate, or steady state rate, of material removal have been defined, the material at this time is so badly eroded that its usefulness for most applications is no longer of interest. Most of the evaluations made for solid particle erosion continue the test until the maximum rate of erosion has been established. This is accomplished by running the test for successive equal time increments and obtaining the same value of the mass loss for these increments. Most of the results reported for solid particle erosion evaluations are expressed as the ratio of the mass of material removed to the mass of the impacting particles for a known exposure time increment. The ratio of the volume of material removed to the mass of the impacting particles or the volume removed per particle impact are also used as measures of the erosion rate. Two types of response to multiple solid particle impacts have been noted.

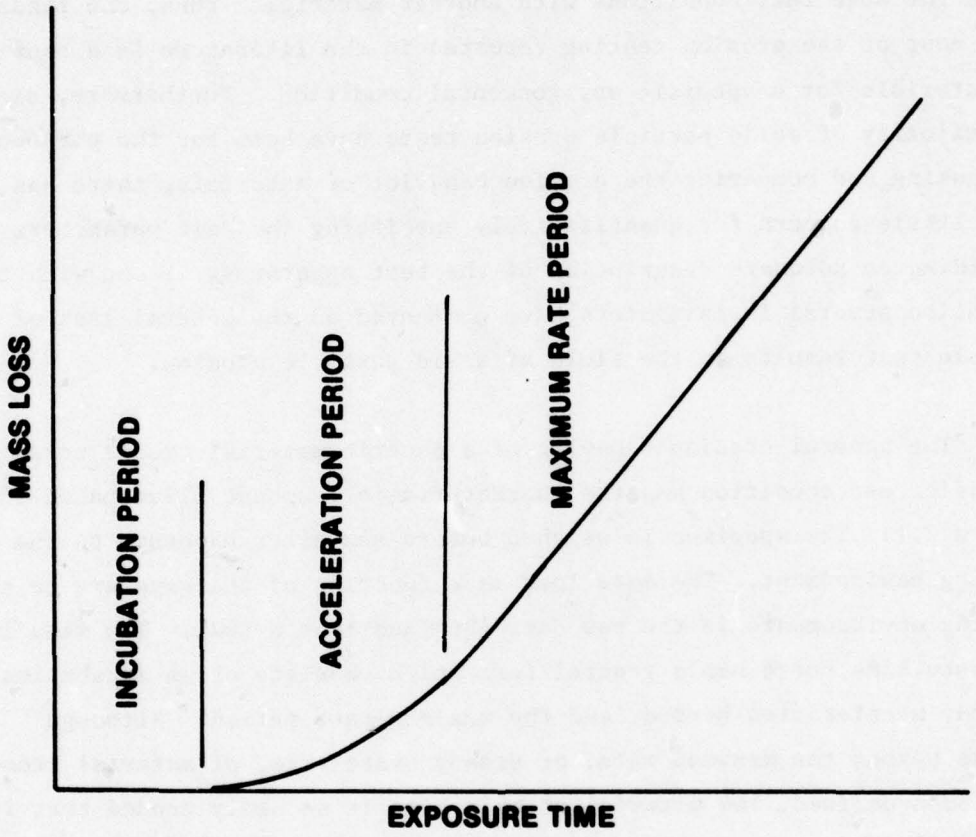

Figure 2.1. Characteristic Mass Removal Curve in Terms of the Time of Exposure to the Erosive Environment.

The first is a ductile response generally associated with metals, while the second is a brittle response associated with glasses and ceramics. The general form of the mass removal rate as a function of the angle of attack for each response is shown in Figure 2.2.

It is a general observation, however, that normally brittle materials exhibit ductile behavior when the particle diameters are less than 100 μm. Sheldon and Finnie (1966a) state that this phenomenon occurs when the zone of material affected by an impacting particle is smaller than the spacing between material flaws or inhomogeneities. Experimentally this transition from brittle to ductile behavior is shown by plotting the erosion rate versus impact angle relationship for different sizes of impacting particles. For larger particles the typical brittle curve is found with its maximum at normal incidence. For very small particles the same material may show a dependence more like the typical ductile curve having a maximum at other than normal incidence. Another indication of ductile behavior is the formation of surface ripples which is characteristic of ductile erosion around the impact angles at which the maximum rate of erosion occurs on brittle materials eroded by very small particles.

The formation of ripples, often very distinct and regular, has been reported by several investigators. Ripples occur only for ductile response and only at impact angles which are oblique. Finnie and Kabil (1965) have proposed a theoretical explanation in terms of the interaction between surface irregularities and the equations of motion of impacting particles. They show that peaks will be attacked less severely than valleys so that irregularities tend to grow. Initially the irregularities will be random, but a certain wavelength is most favored for growth and ripples at that wavelength will eventually be established. The ripple pattern is predicted to move downstream as erosion progresses. Moore (1968) showed that conical brass targets with a 90° cone angle develop almost perfect right-angled steps, whose width and pitch diminish

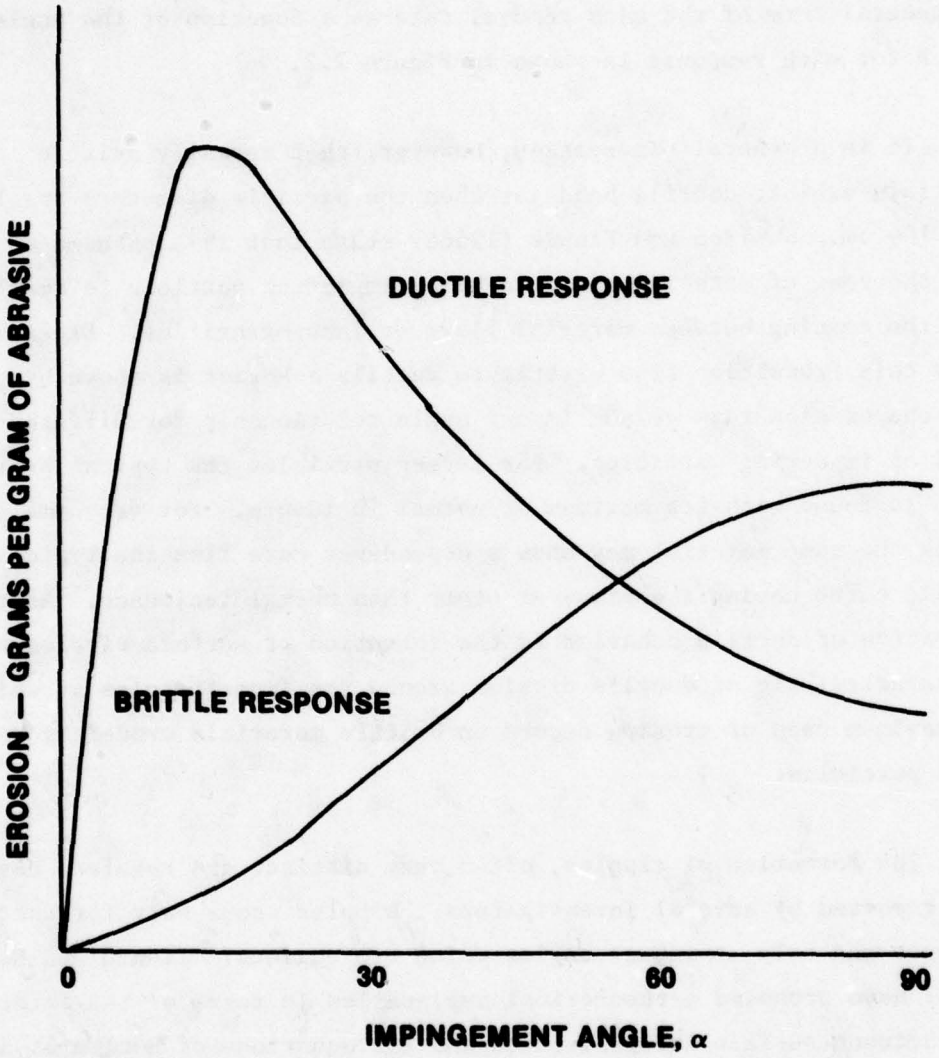

Figure 2.2. Mass Removed by Erosion as Function of Impingement Angle.

with increasing distance from the cone apex when impacted by glass beads. He concluded from photomicrographs that the step formation is a metal flow phenomenon.

There are many factors which influence the material removal process; however the particle size exponent and the velocity exponent will be of primary concern, since these parameters are common to the majority of the solid particle erosion analyses which can be found in the literature. The lack of agreement between the results of the theories based on kinetic energy exchange between the impacting particle and the target has been a perplexing issue in the field of solid particle erosion. The general form of the expression for volume removal (volume removed per particle impact) can be written,

$$\upsilon = g\, V_o^a\, R^b f(\alpha) \qquad (2.1)$$

where g is a functional representing the dependence on all of the parameters not explicitly stated

V_o is the particle impact velocity

R is the radius of the impacting particle

$f(\alpha)$ is a function of the attack angle α

a is the velocity exponent

b is the particle size exponent

The velocity exponent has been generally found to range from two to three for materials displaying ductile behavior for a wide range of particle impact conditions, however higher exponents (up to 4) have been obtained by Grant and Tabakoff (1975) and Tabakoff, et al. (1979). Tabakoff's results are based on detailed observations of the aerodynamics of the particle flow and the rebound characteristics of the particles impacting the eroding surface of the target. The velocity exponents for

brittle materials range from 1 to 6.5 (cp. Gulden, 1979a; Sargent, et al., 1979). The velocity exponent depends on the size, material, shape, and angle of attack of the impacting particle, however it does not appear to be significantly affected by the microstructure of the target material.

The particle size exponent has not been adequately evaluated. It is generally stated that the volume removal in metals is independent of particle size for particle sizes in excess of 100 μm (Tilly, 1969). The variations in particle size effects has already been noted for smaller particle sizes in brittle materials (Sheldon and Finnie, 1966a). Gulden's test data (Gulden, 1979a,b) shows $b \simeq 4$ for magnesium fluoride impacted by quartz particles, however hot-pressed silicon nitride impacted by silicon carbide particles displayed a $b=4$ dependence while impacts by quartz produced a $b=3$ dependence as well as a change in $a=4$ to $a=1$ for particle sizes from 8 to 940 μm. A definite threshold for achieving an $R^4 V_o^4$ relation was found for reaction-bonded silicon nitride impacted by quartz particles. The above results are for normal impacts on the target surface. The dependence of the particle size exponent on the particle material is evident, but it is not known how it would vary with the angle of attack.

The complete characterization of a particular impact condition (particle type and target material) involving the particle size, impact velocity, and impingement angle requires numerous erosion tests. Thus a reliable experimental data base for the development as well as comparison of analytical results is rarely found in the solid particle literature which leaves many aspects of the subject unsettled. The analytical approaches which have been undertaken to describe material removal due to solid particle erosion will be described.

3.0 EROSION CORRELATIONS AND ANALYSES: DUCTILE MATERIALS

A number of concepts have been used as the basis for the development of analytical models of the solid particle erosion process. In general these models do not incorporate an accurate experimentally based description of the material removal process into the mathematical formulation. The mode of material removal is simply a conjecture or is not specified at all in several of these semi-empirical models. However within the last few years experimental studies pertaining to erosion mechanisms have been pursued and so a better physically-based concept of what is taking place can be proposed. These studies are either clever experiments or microscopic observations of metallographically treated surfaces exposed to a small number of particle impacts. Therefore it should be possible within the next few years to develop more physically-based concepts of how material is removed from various material surfaces and to begin to develop a new generation of erosion models.

The mathematical development for many of the existing models will be given in a reasonably unified form. The historical progression of the well-known models of Finnie, Bitter, Neilson and Gilchrist is cited religiously in the introduction to numerous solid particle erosion papers. These correlations and others will be considered here also but in a somewhat more critical way. However a strictly historical approach will not be followed. Recent results on the mechanics of the interactions which can take place between an impacting particle and a solid surface will be used to provide perspective for the real significance of the erosion models or theories.

It is important to note that the physical basis or initial concept for a particular erosion model is based on a moderately detailed analysis of a single particle impact and the material removal process due to multiple impacts is estimated by simply multiplying the material removed by a single particle by the total number of particles or the number of

particles multiplied by an empirical correction (adjustment) factor. The primary defect in this approach is that the surface being eroded by multiple particle collisions is quite different from the initial surface for which the single particle mass loss was originally derived. The detailed modeling effort thereby degenerates to a semiempirical correlation. The transition from isolated impacts to a few overlapping impacts has been investigated to some extent but certainly requires considerable attention (Adler, 1974b, 1976b).

The general categories for the basic elements in the solid particle erosion analyses are the dynamical equations of motion, the Hertzian theory of impact, energy concepts, plasticity, and regression analysis. Due to the prominence of the Hertzian theory in these modeling efforts, the Hertzian relations for a spherical body impacting an elastic half-space are provided in Appendix A for reference.

3.1 Hutchings and Co-workers

Hutchings and co-workers (Hutchings and Winter, 1974, 1975; Winter and Hutchings, 1974; Hutchings, et al., 1976; Hutchings, 1977, 1979) have made significant advances in providing insights into the material removal process due to both single spherical and angular particle impacts by means of a series of clever experiments. The impact conditions are idealized and the particles are scaled to much larger dimensions than those characteristic of multiple particle erosion for high speed photographic analysis of the dynamics of the impacting particle. Each case--spherical particles and angular particles--will be considered in turn. In both cases a compressed gas gun with a 16 mm bore is used to propel the particle. The spherical balls are a hardened steel (with a Vickers hardness of 9.0 GPa) 3 and 9.5 mm in diameter. A few different angular particle configurations have been used in these experiments (Winter and Hutchings, 1974; Hutchings, 1975, 1979). The most recent is to propel square plates, 8x8x1.5 mm, at a stationary inclined target.

Three major categories of oblique particle impacts on ductile materials have been experimentally identified by Hutchings and co-workers in their experimental investigations. The first is a "ploughing" action associated with a spherical particle, a rounded surface on an irregular shaped particle, or the properly oriented flat face of an angular particle as shown in Figure 3.1 a and b. The remaining two categories pertain to angular particles producing cutting deformations (Figure 3.1c). Hutchings and co-workers make a clear distinction between the angle of impact, α , and the orientation of the particle at impact described in terms of the rake angle θ . The rake angle is used in metal cutting technology and is defined in Figure 3.1d. The angle θ is negative if it involves a clockwise rotation between the normal to the surface and the front face of the particle and positive for a counterclockwise rotation. The remaining categories in Hutchings' classification are "Type I cutting" when a forward rotation is imparted to the angular particle and "Type II cutting" when a backward rotation occurs after the particle strikes the target. No criterion has been given in terms of impact velocity, impact angle, and rake angle for determining which of the three categories will prevail. A limited number of transitions can be found in Hutchings experimental evaluations and computer simulations of the impact process.

Characteristic crater profiles are shown in Figure 3.2. Only Type II cutting results in material removal for a single impact due to a micromachining action. For an impact angle of 30°, Type II cutting only occurs at rake angles ranging from 0 to -17°; Type I cutting takes place for rake angles ranging from -17° to -90°. These observations are for a square plate. As illustrated in Figure 3.1b the geometry of the impacting particle will also contribute to the form of the deformation which may occur.

Hutchings (1979) estimates that Type I cutting due to the restricted range of rake angles over which it occurs would only be observed in about one-sixth of the impacts on randomly oriented plates at a 30° impact angle. For Type II cutting and ploughing deformations additional impacts are required to remove the material displaced from the crater.

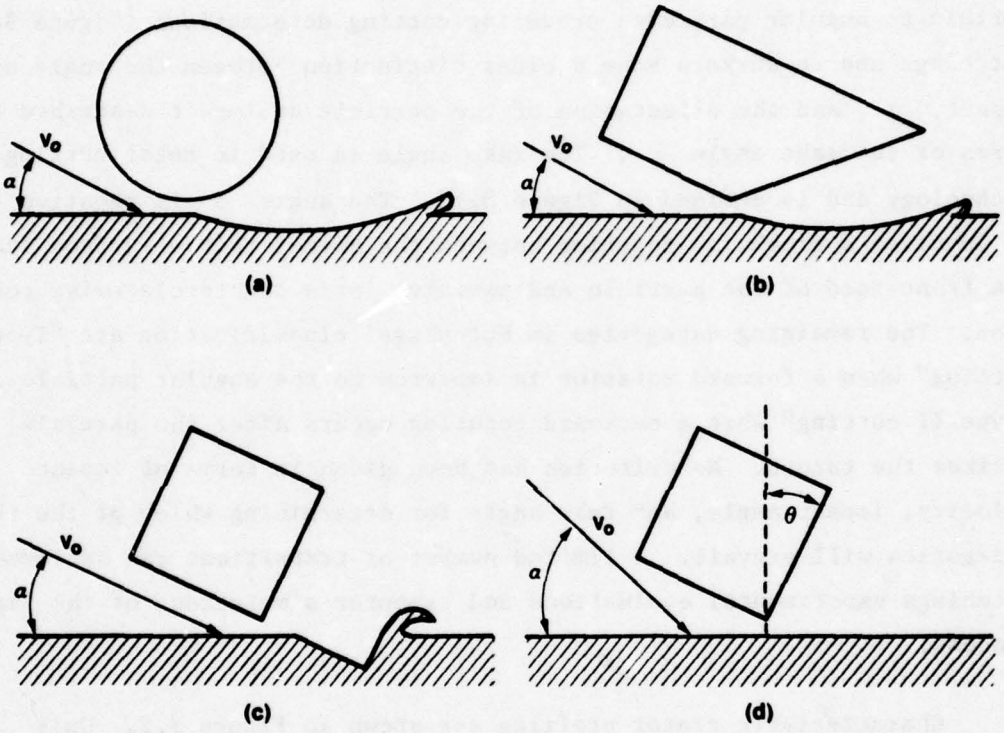

Figure 3.1. Deformation Modes Identified by Hutchings and Co-workers. a) Ploughing Deformation with a Sphere, b) Ploughing Deformation with an Angular Particle, c) Cutting Deformation with an Angular Particle, and d) Definition of the Rake Angle, θ: The Rake Angle shown is Negative by Convention.

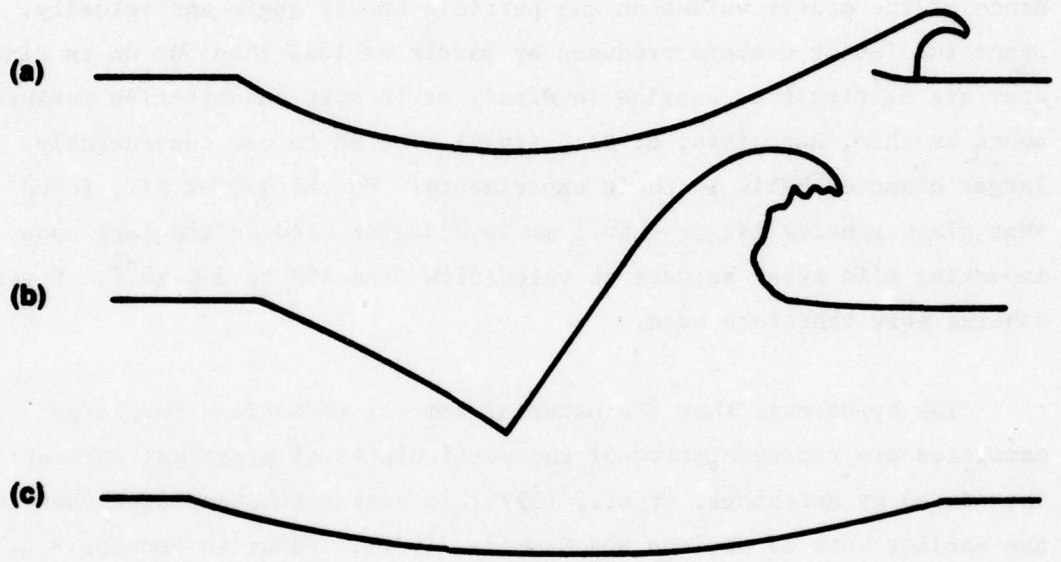

Figure 3.2. Sections Through Impact Craters Showing Typical Shapes. Impact Direction Left to Right.
a) Ploughing deformation by a sphere,
b) Type I cutting, and
c) Type II cutting (Hutchings, 1979).

3.1.1 Spherical Body Impacts on Ductile Targets

The single spherical particle impact experiments were for the purpose of understanding the general character of the indentation in a ductile target and to identify the conditions under which material is removed from the surface. A quantitative study was made of the dependence of the crater volume on the particle impact angle and velocity. Since the impact craters produced by particles less than 500 μm in diameter are difficult to examine in detail or to make quantitative measurements on them, Hutchings, et al., (1976) elected to use considerably larger diameter balls in their experiments. Hutchings, et al., found that glass spheres larger than 1 mm in diameter tend to fragment upon impacting mild steel targets at velocities from 100 to 300 ms^{-1}. Steel spheres were therefore used.

The hypothesis that the material removal mechanisms for large particles are representative of the particulates of practical interest introduced by Hutchings, et al., (1976) is better substantiated than in the earlier work of Sheldon and Kanhere (1972). Refer to Section 3.2. The basis for the comparison made by the authors is Tabor's analysis of a rigid sphere impacting normally on a rigid plastic plane (Tabor, 1951). Tabor predicts that the crater volume will remain constant if the relation

$$\text{density} \times (\text{velocity})^2 = \text{constant} \tag{3.1}$$

is satisfied for spheres of the same diameter. Hutchings, et al., make two unsupported extensions of this result: (1) that it is applicable to oblique impacts; and (2) that for the oblique impact of different diameter spheres, the dimensions of the crater normalized with respect to the sphere diameter will remain constant as long as Eq.(3.1) is satisfied. These conjectures are demonstrated to be valid based on a limited amount of experimental evidence. According to Hutchings, et al. (1976), this comparison provides justification for the experimental evaluations on an enlarged scale and for comparisons with the solid particle erosion literature.

A series of impact craters in mild steel due to a 9.5 mm steel ball impacting over a range of impact angles and velocities was evaluated. The mass of metal removed from the target was measured by weighing the target before and after impact. The volume of the impact crater was determined by machining away all of the material above the level of the undisturbed metal and filling the depression with Plasticine which was then removed and weighed. Thus, direct measurements are made of the mass loss and crater volume as a function of impact angle and velocity. High speed photographic records were used to evaluate the energy lost during the impact process.

A numerical analysis of the collision process was also developed in conjunction with the experimental program. The computational model will be described and then the results of Hutchings' work (Hutchings, et al., 1976) will be discussed.

The temporal progression of a sphere entering and finally leaving the target is determined numerically by solving the equations of motion for incremental time steps with a computer. Hutchings, et al., (1976) write the equations of motion for a rigid sphere impacting a ductile target obliquely as shown in Figure 3.3. They assume the contact surface between the sphere and the deformed material is a circle with diameter $\overline{AB}$. The resisting force acting on the sphere during the penetration phase is taken to be proportional to the contact area determined by $\overline{AB}$ and directed through the center of the sphere. When a frictional force is also allowed to act on the contact area, the equations of motion are

$$\left.\begin{aligned} m\ddot{x} &= -N\sin(\beta+\phi) - \mu N\cos(\beta+\phi) \\ m\ddot{y} &= -N\cos(\beta+\phi) + \mu N\sin(\beta+\phi) \\ I\ddot{\theta} &= R\mu N \end{aligned}\right\} \qquad (3.2)$$

where m is the mass of the impacting sphere, I is the moment of inertia of the sphere, and the remaining quantities are defined in Figure 3.3.

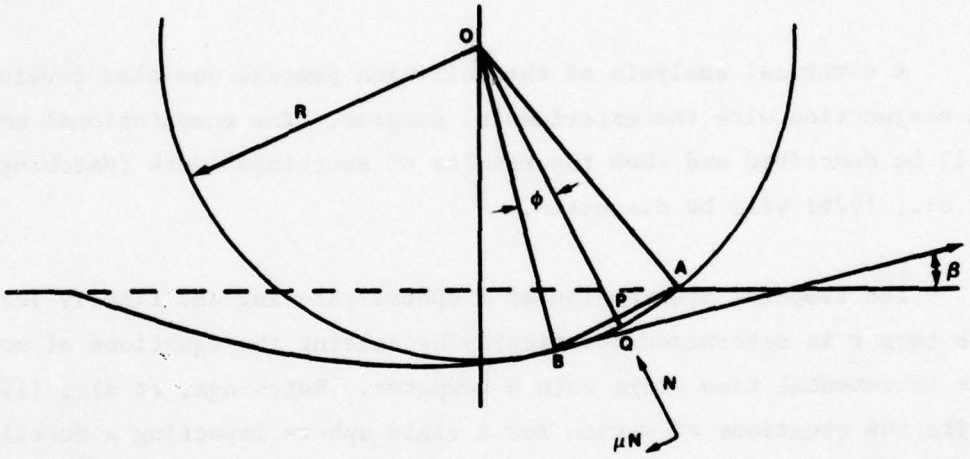

Figure 3.3. Diagram Showing the Region of Contact and the Forces Assumed to Act on the Sphere in the Constant Indentation Pressure Model (Hutchings, et al., 1976).

In Hutchings' equations, Eq.(3.2), the mass, radius, initial velocity, and initial angle of approach of the sphere are prescribed quantities. The value of the normal force, N, and the coefficient of friction, μ, are the only additional parameters which have to be specified in order to integrate the equations of motion. Based on experimental data, μ was assigned a value of 0.05. The force N is determined from the relation

$$N = p \cdot A \tag{3.3}$$

where p is the mean indentation pressure and A is the area of the contact surface (determination of the contact area has been described, but will be discussed at greater length shortly). The pressure p is assumed to be constant throughout the cratering phase and is set equal to 4.0 GPa in the computations reported by Hutchings, et al. (1976). The target material was a work-hardened, low-carbon steel with a Vickers hardness of 2.35 GPa. The magnitude of the quasistatic indentation pressure was adjusted to account for the high strain rates, estimated to be on the order of 10^6 to 10^7 sec^{-1}, encountered during the impact process (Hutchings, 1977).

The determination of the contact area, A, in Eq.(3.3), requires further consideration. The actual contact area is proportional to the area of a spherical segment instead of the approximation of a circle with diameter $\overline{AB}$ introduced into the analysis by the authors. In progressing through the penetration process, one finds the difference between these two views of the contact area can approach more than a factor of two: the area determined by $\overline{AB}$ being the smaller of the two. The calculation also neglects the additional contact area due to the build-up of deformed material around the impact crater: especially in the direction of particle motion.

The significant difference in the magnitude of the contact area can affect the magnitude of the indentation pressure required to match the experimental data. It should of course be realized that the magnitude of the pressure p is not going to be uniform over the contact area: its value will be high in the central portion of the contact zone and it will decrease toward the periphery. The contact area introduced by Hutchings, et al., would probably encompass the primary zone of maximum pressure. On the other hand, the model assumes a rigid-plastic material so that it is necessary for any material in contact with the sphere to be displaced from its path by plastic flow. Hence, on the basis of the material response introduced for the target material, the pressure p should be reached over the complete contact zone in order to maintain continuity with the spherical body. When the kinetic energy of the sphere is no longer able to overcome the resisting force in the direction normal to the target's surface, the sphere begins to move outward from the target by means of the energy in the tangential direction. The assumption of a rigid-plastic target and rigid projectile implies that for an impact normal to the surface of the target, the projectile would penetrate to its maximum depth and remain embedded at this depth in view of the absence of any restoring forces acting on the body. This limiting case illustrates the importance of the tangential velocity component in the model and the necessity for elastic-plastic response if normal impacts on real materials are to be described as considered by Mamoun (Section 3.7). The difference between the calculated and experimental rebound velocities should provide a reasonable estimate of when the elastic response is significant. For this reason, Hutchings, et al., did not carry their computations beyond impact angles of 75°.

The experimental data for the mass loss and crater volume as a function of the impact velocity and angle is shown in Figure 3.4 to 3.7. Excellent agreement is found between the experimental determination of the energy lost in the collision process and the model predictions. The energy lost computation is relatively insensitive to changes

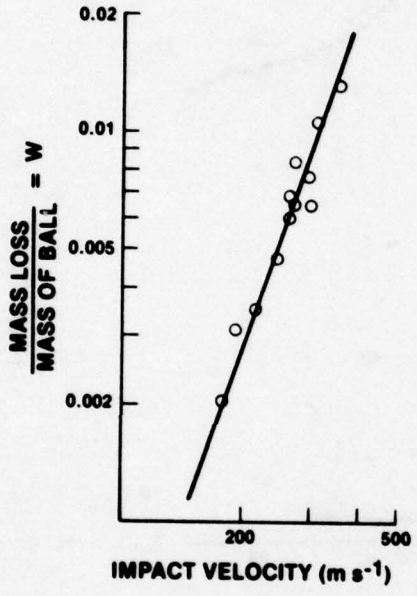

Figure 3.4. Mass Losses for 9.5 mm Steel Balls Striking Mild Steel Specimens at 30° Impact Angle. The Solid Line Represents the Relation

$$W = 5.82 \times 10^{-10} V_o^{2.9}$$

(Hutchings, et al., 1976).

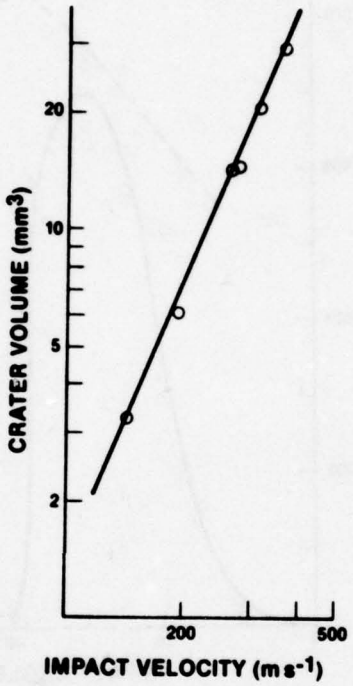

Figure 3.5. Crater Volumes for 9.5 mm Steel Balls Striking Mild Steel Specimens at 30° Impact Angle. The Solid Line is Theoretically Derived from Hutching's Model and has a Slope of 2.4 (Hutchings, et al., 1976).

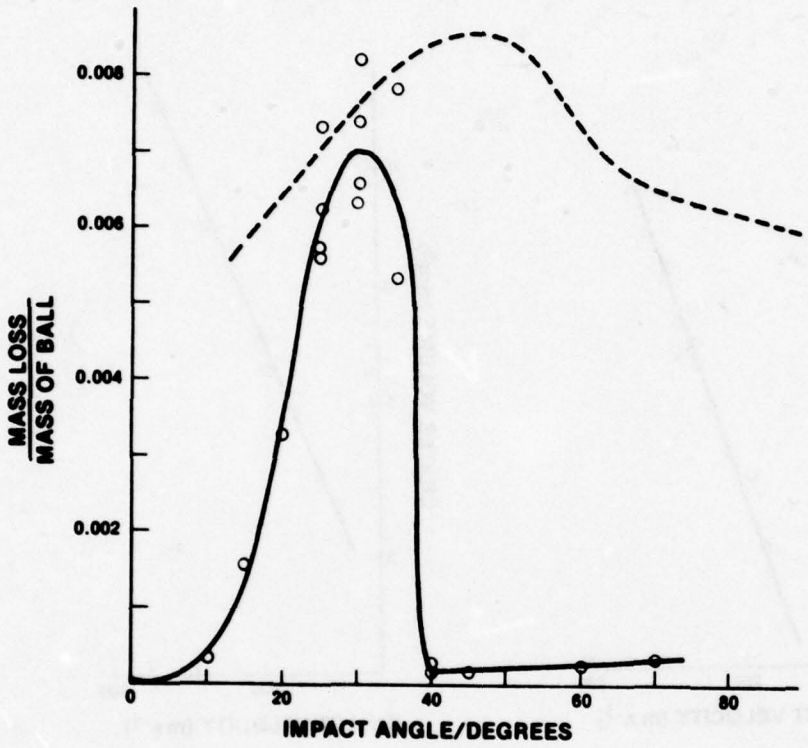

Figure 3.6. The Variation of Mass Loss with Impact Angle for 9.5 mm Steel Balls Striking Mild Steel at 270 ms^{-1}. The Broken Line Represents the Results of Kleis (1969) for Multiple Impacts of Round Iron Shot on Mild Steel Scaled to 270 ms^{-1} Impact Velocity (Hutchings, et al., 1976)

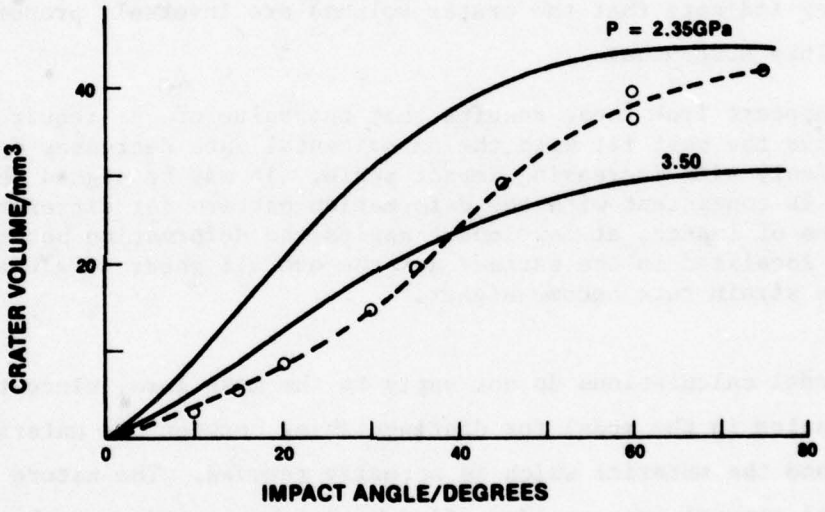

Figure 3.7. The Variation of Crater Volume with Impact Angle for 9.5 mm Steel Balls Striking Mild Steel at 270 ms^{-1}. The Solid Curves are Theoretically Derived from the Model, Assuming the Plastic Indentation Pressure to be 2.35 GPa and 3.50 GPa. Note the difference in form compared with the experimental data: dashed curve (from Hutchings, et al., 1976).

in the value of the plastic indentation pressure p : the experimental data is fit quite well when $p = 4.0$ GPa . On the other hand, the model predictions in Figure 3.7 do not reflect the general trend in the data. The match appears to be reasonable for $\alpha \leq 30°$, however for $\alpha > 30°$ sizable deviations in the predicted and experimental crater volumes occur. The crater volume as a function of impact velocity shown in Figure 3.5 when $\alpha = 30°$ happens to be a condition which shows excellent agreement between experiment and theory when $p = 4.0$ GPa. Hutchings, et al. (1976), attempt to fit the experimental crater volume measurements in Figure 3.7 by varying the value of p , however the general trend in the data does not appear to be reproduced as long as p remains constant. They indicate that the crater volumes are inversely proportional to p . They state that

> "It appears from these results that the value of p required to give the best fit with the experimental data decreases appreciably with increasing impact angle. It may be argued that this is consistent with the deformation pattern for different angles of impact; at low impact angles the deformation becomes more localized in the surface and the overall shear strain and hence strain rate become higher."

The model calculations do not apply to the mass loss, since there is no mechanism in the model for distinguishing between the material displaced and the material which is actually removed. The nature of the material removal process identified by Hutchings and co-workers will now be described for rounded body impacts based on their idealized experimental conditions.

The major impetus for Hutchings to use large particles was to better understand the material removal process. The value of this understanding is to identify the way in which the properties of a material control its erosive response. For essentially rigid spheres impacting mild steel targets obliquely, metal is displaced from the resulting crater by: (1) accommodation of the displaced material through bulk

deformation of the material surrounding the crater, and (2) creation of a shear lip at the end of the crater where the particle leaves the surface. The volume of material comprising the shear lip ranges from 1/12 to 1/4 of the total displaced volume. Hutchings' experiments indicate that a critical velocity exists for each impact angle below which the lip remains attached and above which it is removed. A band of intense shear deformation is observed at the base of the lip. Separation of the lip, when it takes place, occurs along this shear band.

Sheldon and Kanhere (1972) made an essentially similar observation for the material removal mechanism for 20 and 90 degree impacts on aluminum targets using 2.3 mm steel spheres and 3 mm glass beads. These investigators observe for a 20° impact angle and velocity of 232 ms^{-1} (760 fps) that the surface material flows in front and to the sides of the advancing particle until it is strained sufficiently to fracture resulting in material loss. They note that material builds up on the forward side of the crater, but the volume of this material is much less than the total displaced volume. The forward lip appears to fracture sooner for the work-hardened 6061 aluminum compared with specimens in the annealed state and most of the displaced material fractures leaving a cavity with no extruded material at the periphery. The greater susceptibility to fracture of the work-hardened surface appears in the higher mass loss recorded for this condition over th annealed state. The experimental data shows that there is an impact velocity below which the work-hardened surface may reduce the mass loss. It may be that the mass loss differences are related to the strain rates which increase with impact velocity.

Sheldon and Kanhere find the same material removal mechanism applies to 90° impacts at 232 ms^{-1}. They speculate that material now flows evenly around the periphery of crater due to the impact by glass and steel spheres and observe that a relatively small ridge exists at the periphery of the crater. The details of the material removal process

are not as well documented as in the work of Hutchings, et al., 1976. From Sheldon and Kanhere's mass loss measurements it is seen that there is relatively little variation in the absolute magnitude of the mass loss between the 20° and 90° glass bead impacts over the velocity range investigated. A wider variation between the mass loss for these two impact conditions is found for steel shot. It would be of interest to differentiate between mass loss and crater volume in the manner developed by Hutchings to try to better understand the material removal process in aluminum and to examine a broader range of impact angles.

It is significant to note that according to Hutchings, et al., only a portion of the displaced volume is removed during a single collision. The work of Sheldon and Kanhere would indicate a significantly larger portion of the displaced volume is removed from 6061 Aℓ. Most analyses for erosion rates develop expressions for the volume of material displaced, but then employ heuristic arguments to make the material removal rates conform to the experimentally determined values.

3.1.2 Angular Plate Impacts on Ductile Targets

The investigation of the impact of angular particles on ductile targets undertaken by Hutchings and Winter (Winter and Hutchings, 1974; Hutchings, 1977, 1979) parallels the investigation of spherical body collisions. The first point to be considered is the scaling of the impact damage due to small particulates on the order of 100 μm to that produced by steel plates on the order of 10 mm. This point is not adequately substantiated. The initial comparison (Hutchings and Winter, 1974) is for spherical bodies and this comparison is simply adopted for angular bodies (Hutchings, et al., 1976). Winter and Hutchings (1974) note that it is found experimentally that the erosion of metals by angular particles greater than 100 μm is independent of particle size (Tilly, 1969). However this leaves open the question as to whether the mode of material removal for a single particle impact is identical to

that due to multiple particle impacts on a completely obscured surface. These investigators also refer to the experimental justification for scaling presented by Sheldon and Kanhere (1972). However, once again, the work of Sheldon and Kanhere pertains to spherical bodies and, as will be shown in Section 3.2, the basis for their verification is questionable. Thus, adequate justification cannot be found in Hutching's publications for the exactness of the representation of the mode of deformation associated with angular-shaped erosive particulates by geometrically idealized particles with dimensions of several millimeters. On the other hand, the qualitative features of the damage produced under the idealized experimental conditions Hutchings employs are quite instructive in understanding the events which can take place when an angular particle impacts a ductile target.

The effect of particle orientation can be expressed in terms of the rake angle as indicated in Figure 3.1. However, in addition to the impact angle, α , and the rake angle, θ , the location of the center of mass of the particle is also a factor in determining which of the three classifications (ploughing, Type I cutting, and Type II cutting) identified by Hutchings (1979) will occur (Winter and Hutchings, 1974). The effect of the shape of the particle (distribution of mass) on the material removal process is illustrated in Figure 3.1. The influence of the frangibility of the impacting particle was also described by Winter and Hutchings (1974).

In subsequent work (Hutchings, 1977), the particle geometry was restricted to a square plate which removed the influence of particle shape, other than the angularity of the particle, on the material removal process. The plate was propelled from a gas gun such that a corner of the plate impacted the inclined plate at a predetermined rake angle. The relevant two-dimensional analysis is analogous to that already described for spherical body impacts. The plate is assumed to be rigid impacting upon a rigid-plastic target. The equations of motion

for this condition are then formulated and integrated incrementally with respect to time to calculate the position and orientation of the plate while in contact with the target. The time-dependent contact area is computed and a uniform indentation pressure is assumed to act on this area. Frictional forces are neglected. Several possibilities are likely to occur for the square plate impact as depicted in Figure 3.8. Determination of the contact areas for the conditions in Figure 3.8 b, c, and d become a part of the problem. The equations of motion cannot be written explicitly, but depend on the temporal evolution of both the translation and rotation of the plate while in contact with the target. Hutchings (1977) divides the general problem into four cases representing the current location of the contact zone and its new location due to an incremental rotation. The computational scheme reformulates the governing differentiation equations after each time step. The volume displaced during the complete impact sequence can be computed as a function of the initial impact angle, impact velocity, and rake angle. Energy partitioning before and after impact is readily evaluated. Examples of the computational results can be found in Hutchings (1977).

The solid particle erosion studies undertaken by Hutchings and co-workers at the University of Cambridge over the last five years have made a significant contribution to understanding the modes of material removal for angular particles impacting ductile targets obliquely. Prior analyses have been quite conjectural as to the nature of the particle/target interactions. The computer studies in conjunction with micrographic studies of single and multiple particle crater configurations associated with carefully graded particulates should provide much additional valuable information on the true volume removal rates for a variety of impact conditions.

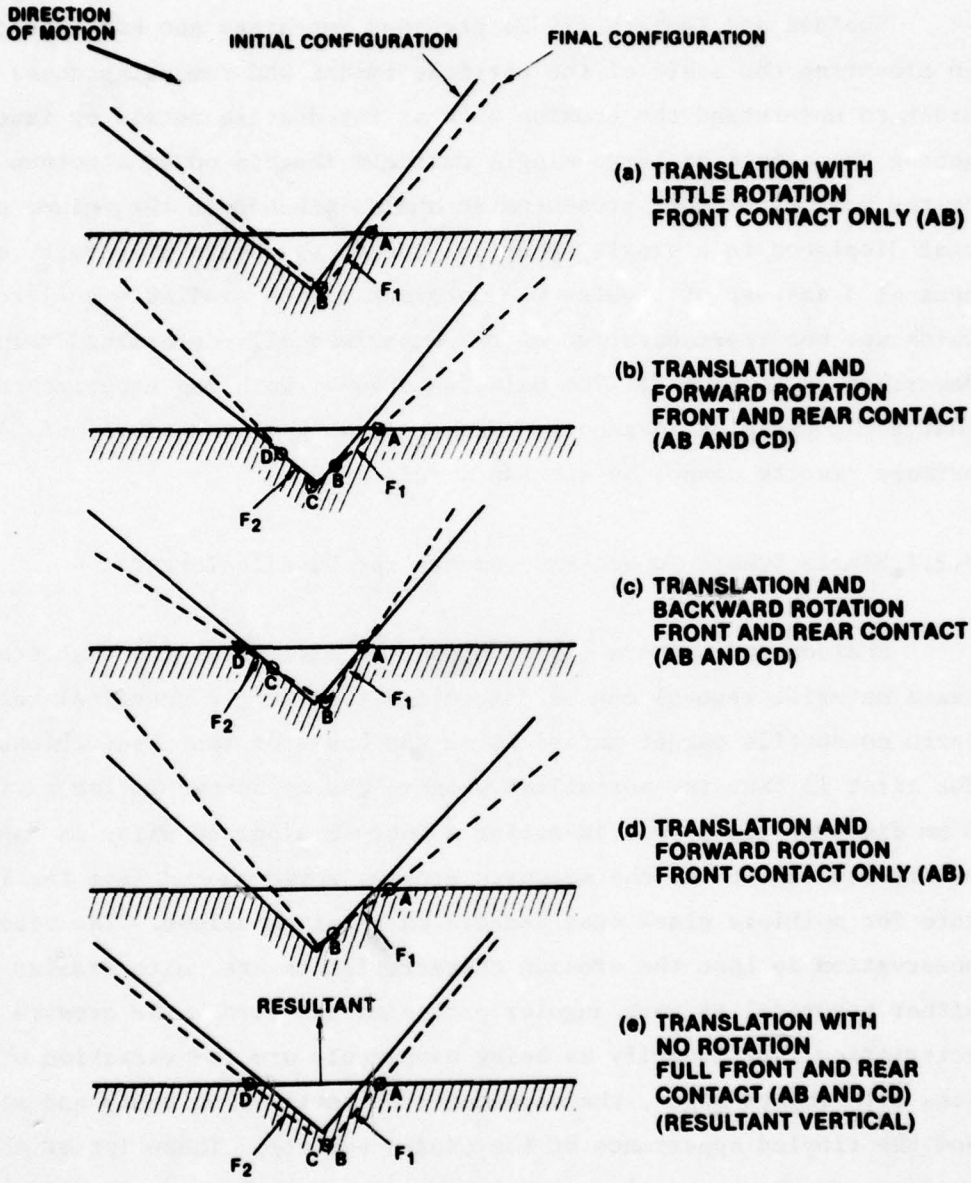

Figure 3.8. Dynamics of Square Plate Impacts on a Ductile Target (Hutchings, 1978).

3.2 Sheldon and Kanhere

Sheldon and Kanhere (1972) preceded Hutchings and his associates in elevating the scale of the particle impact and removal process in order to understand the erosion process for ductile metals by investigating the effect of large single particle impacts on an aluminum alloy. In the same paper they presented an analysis based on the volume of material displaced in a single spherical indent to obtain a velocity exponent of 3 instead of 2 which was inherent in the available analyses but which was not representative of the experimentally-determined values as described in Section 2. The main features of both the experimental and analytical parts of Sheldon and Kanhere's work will be reviewed. The primary results cannot be substantiated.

3.2.1 Single Sphere Impact Experiments for Ductile Targets

Sheldon and Kanhere (1972) support their contention that steady-state material removal can be determined from single spherical bead impacts on ductile target materials on the basis of two observations. The first is that the normalized weight loss measurements for a single 3 mm diameter glass bead impacting a 6061-TO aluminum alloy is "approximately equivalent" to the measured erosion rates quoted from the literature for multiple glass bead impacts on aluminum alloys. The second observation is that the erosion characteristics are quite similar when either spherical or very angular particles are used. The erosion characteristics they identify as being comparable are the variation of mass loss with impact angle, the dependence on particle velocity and size, and the rippled appearance of the eroded surface. These latter observations are the authors' personal views in that they are simply stated without any supporting evidence to convince the reader that they are indeed valid comparisons. The authors conclude on the basis of the above that the same material removal mechanisms are operative when either angular or rounded particles are the eroding medium. This conclusion

considerably broadens the relevance of their single particle impact studies. The basis for this conclusion will be considered in terms of the data Sheldon and Kanhere present in their paper.

In support of the equivalence between the material removed by a single glass bead impact and multiple glass bead impacts, Sheldon and Kanhere provide the data in Table 3.1, which has been augmented by additional values which can be obtained from the references cited. Our interpretation of this data is provided in the lower half of Table 3.1. It is not stated whether pure aluminum or an aluminum alloy was used in Nielson and Gilchrist's erosion tests (Nielson and Gilchrist, 1968). It is thought that Aℓ 2618 was used in the work of Tilly and Sage (1970) based on the composition reported in their paper. The experimental data from these two papers is shown in Figure 3.9. The comparison between the rounded and angular particle data is shown in Figure 3.9b for impact angles from 0 to 90°. This direct comparison from Tilly and Sage (1970) shows a decisive difference between the two conditions which in itself weakens the relationships Sheldon and Kanhere are trying to establish. One also notes a significant change in the shape of the experimental curves reported by Nielson and Gilchrist (Figure 3.9a) and Tilly and Sage (Figure 3.9b) for glass beads. Furthermore, there appears to be an inconsistency in the data reported by Tilly and Sage in that the values of the mass loss for 90° impact data for glass beads does not agree with the values read from plots of the velocity dependence of the mass removal rates found in the same paper. The mass loss read from the plot of the velcotiy dependence of 125-150 μm glass beads impacting normally onto aluminum targets is shown in parentheses in the last line of Table 3.1. The relevant multiple glass bead erosion data does not appear to be very consistent in toto.

Sheldon and Kanhere state that the mass loss due to single particle impacts was determined by accurately weighing the test specimen before and after impact. Three particles mounted in a styrofoam sabot were

TABLE 3.1. Comparison of Single and Multiple Glass Particle Erosion Tests on Aluminum.

PARTICLE DATA		EROSION (mg/g)	
VELOCITY fps(ms^{-1})	IMPACT ANGLE (degrees)	MULTIPLE IMPACTS	SINGLE IMPACTS
260 (79)	20	0.36 *	0.12
800 (244)	20	0.40 **	1.8
800 (244)	90	2.5 **	1.8
260 (79)	20	0.35 *	0.11
800 (244)	20	.36 **	1.7
260 (79)	90	.073 *	0.14
800 (244)	90	2.4 (5.9)*	1.9

* Neilson and Gilchrist (1968).

** Tilly and Sage (1970).

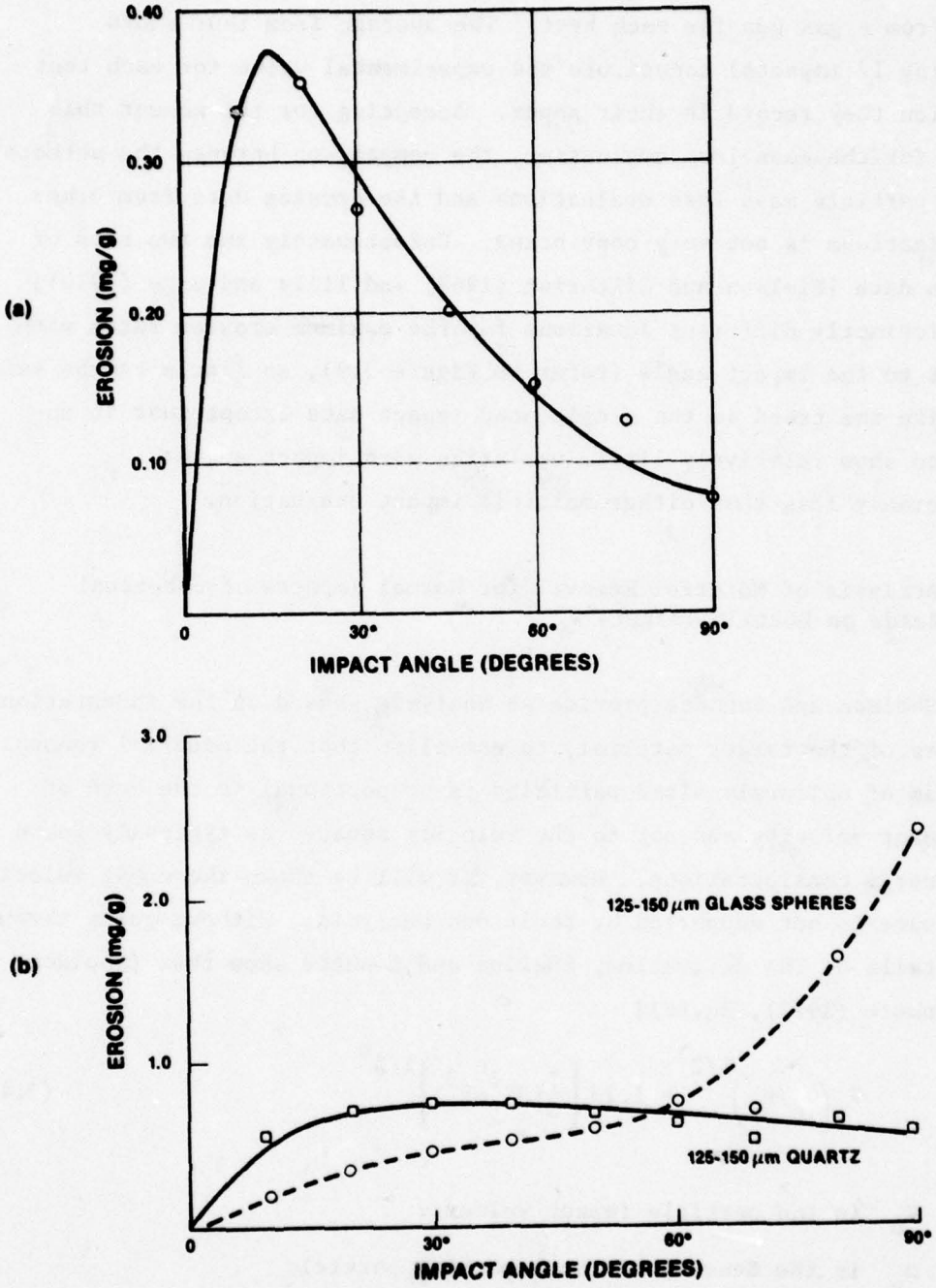

Figure 3.9. Impact Angle Dependence for Erosion of Aluminum Alloys. a) 475 μm Glass Spheres Impacting at 79 ms^{-1} (Neilson and Gilchrist, 1968); b) Impact Velocity: 244 ms^{-1} (Tilly and Sage, 1970).

fired from a gas gun for each test. The average from four shots (totaling 12 impacts) constitute the experimental value for each test condition they record in their paper. Accepting for the moment this method for the mass loss evaluation, the comparison between the authors' single particle mass loss evaluations and the erosion data from other investigations is not very convincing. Unfortunately the two sets of erosion data [Nielson and Gilchrist (1968) and Tilly and Sage (1970)] show distinctly different locations for the maximum erosion rates with respect to the impact angle (refer to Figure 3.9), so little can be said regarding the trend in the single bead impact data except that it appears to show relatively little variation with impact angle: considerably less than either multiple impact evaluation.

3.2.2 Analysis of Material Removal for Normal Impacts of Spherical Beads on Ductile Targets

Sheldon and Kanhere provide an analysis, based on the indentation hardness of the target material, to establish that the material removal per gram of uniformly sized particles is proportional to the cube of the impact velocity and not to the velocity squared as typically found from energy considerations. However, it will be shown the cubic velocity dependence is not supported by their own analysis. Without going through the details of the derivation, Sheldon and Kanhere show that [Sheldon and Kanhere (1972), Eq.(8)]

$$V_o\left(\rho_p/H_v\right)^{1/2} = 1.23\left[\frac{1}{3}(3\chi^2-\chi^3)\right]^{1/2} \qquad (3.4)$$

where V_o is the particle impact velocity

ρ_p is the density of the impacting particle

H_v is the Vickers hardness of the target material

$\chi = \frac{2q}{D}$ $(\chi<1)$

q is the depth of the impact crater

D is the diameter of the impacting sphere.

This relation is obtained from an energy balance between the kinetic energy of a sphere impacting normal to the surface of the target and the work done in creating the final crater dimensions in accordance with Meyer's hardness relation. For $\chi \leq 0.3$, the final crater depth is proportional to the impact velocity. For $0.3 < \chi < 1.0$, the term involving χ^3 becomes more significant as χ increases to introduce some nonlinearity into the χ-V_o functional dependence which is not indicated on the authors' plot of Eq.(3.4). On the basis of Eq.(3.4) and the experimental results for single bead impacts on 6061-T0 aluminum, Sheldon and Kanhere conclude that

$$q \propto V_o \tag{3.5}$$

This result does not appear unreasonable although one wonders why the experimental data for 20° impacts appears to cluster around the analytical values for 90° impacts (Curve I in Figure 3.10), while the trend in the crater depth measurements from 90° impact experiments (Curve II in Figure 3.10) are *displaced from* the computed depth-velocity relation. It is to be noted that the experimental data is quite sparse. In Figure 3.10 a straight line is drawn through data points representing four different impact conditions. It is seen that if taken on an individual basis, each impact condition shows a distinctly different trend than that for the consolidated data.

Sheldon and Kanhere make the perplexing statement that "since the dimensions of the crater formed by impact are all proportional to q , and since the amount of material removed is nearly the full crater size, then, it is to be expected that material removal per particle," W , would be proportional to the cube of the maximum penetration depth, q ,

$$W \propto q^3 \tag{3.6}$$

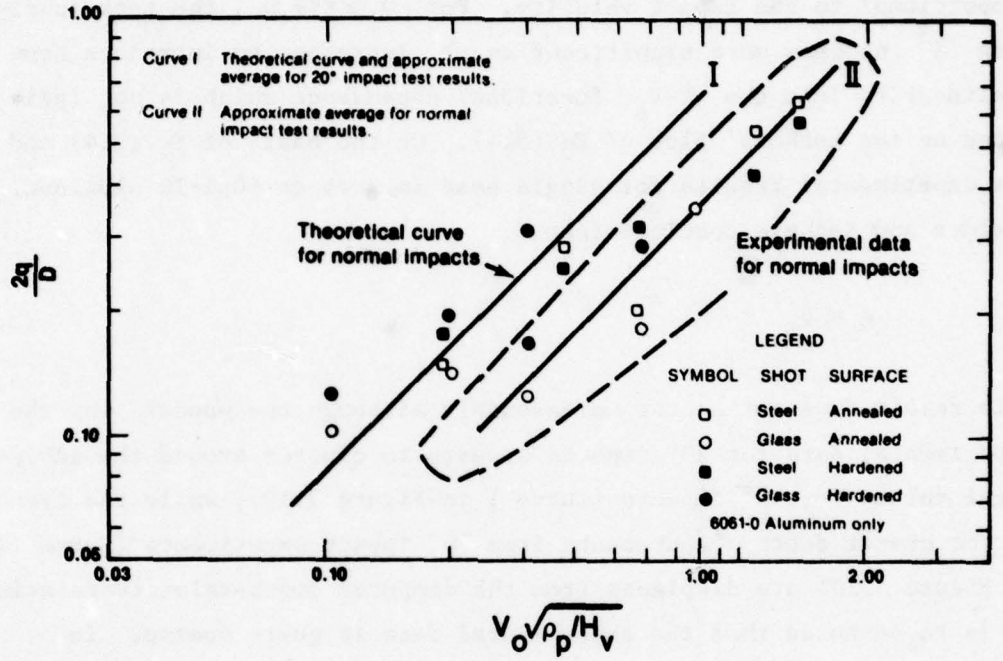

Figure 3.10. Comparison of the Hardness Penetration Theory (Curve I) with Experimental Erosion Results. Note discrepancy between theoretical prediction and experimental data for normal impacts. (from Sheldon and Kanhere, 1972).

So, according to Eq.(3.5), $W \propto V^3$. The volume of the indent is actually more strongly proportional to the square of the penetration depth as shown in Eq.(B4) of Appendix B.

Returning to Eq.(3.4), the term in brackets is identified as being proportional to the volume of an incomplete spherical cap, υ , referring to Eq.(B4) in Appendix B

$$\upsilon = \pi\left(\frac{D}{2} q^2 - \frac{1}{3} q^3\right) \tag{3.7}$$

which can be rewritten

$$\upsilon = \frac{\pi D^3}{8}\left[\frac{1}{3}(3\chi^2 - \chi^3)\right] \tag{3.8}$$

Substituting into Eq.(3.4),

$$\upsilon = \frac{1}{(1.23)^2} \frac{\pi D^3}{8} V_o^2 \left(\frac{\rho_p}{H_v}\right) \tag{3.9}$$

The corresponding expression obtained by Sheldon and Kanhere is

$$\upsilon \propto q^3 = \frac{1}{(1.23)^3} \frac{D^3}{8} V_o^3 \left(\frac{\rho_p}{H_v}\right)^{3/2} \tag{3.10}$$

[with minor corrections]. However, this result is based on a highly erroneous measure of the crater volume. A similar observation was made by Hutchings in his Ph.D. thesis (Hutchings, 1978).

Eq.(3.9) is a consistent result for the model used by Sheldon and Kanhere as the basis for their analysis: the material removal rate remains proportional to the square of the impact velocity. The incorrect assumption made in Eq.(3.6) is the reason for the velocity cubed

dependency which the authors state as a principal conclusion from their analysis. According to Eq.(3.9), the Vickers hardness is once again inversely proportional to the rate of material removal consistent with Finnie's experimental data (Finnie, Wolak, and Kabil, 1967) and not to the (-3/2) power which the authors cannot justify on the basis of the available experiment data.

In summary, Sheldon and Kanhere's work does not develop a valid experimental basis for establishing a correspondence between single spherical particle impacts and the material removal rates for multiple irregular shaped particles. In addition, the paper does not provide a sound analytical derivation for demonstrating that material removal rates proportional to the cube of the particle impact velocity can be achieved. Therefore, both the experimental and analytical results contained in this paper are of questionable value.

3.3 Finnie

Finnie provided a simple analysis of the erosion of ductile metals due to angular particle impacting at oblique angles of attack (Finnie, 1958; 1960). The equations obtained in 1958 have remained essentially unchanged to the present time. The general approach will be described. The derivation of the basic equations was reformulated in 1965 (Finnie and Kabil, 1965) and summarized with the assumptions necessary for their derivation in 1972 (Finnie, 1972). A modification of the original equations was proposed in 1977 which provided a variable velocity exponent which was greater than 2 (Finnie and McFadden, 1978). These equations have been reviewed recently by Finnie (Finnie, Levy, and McFadden, 1979). Finnie's model and associated analysis have been widely referenced in the solid particle erosion literature over the intervening two decades. Relatively few new conceptual models or detailed particle impact experiments have provided better insights into the material removal process during this period, except for the innovative studies of Hutchings and his colleagues.

The erosion of ductile metals was described by Finnie in terms of the volume removed by a single angular particle impacting obliquely. The volume removed is determined by writing the equations of motion for a single particle interacting with the surface and then estimating the volume removed from the particle's trajectory as it cuts through the surface layer of the target material. The analysis assumes that the target material is rigid-plastic and that material is removed due entirely to the displacing or cutting action of the impacting particle. Finnie's analysis is a special case of Hutchings' analysis for angular particles. The conceptual model upon which Finnie's analysis is based is Type I cutting as defined by Hutchings (1979). Hutchings' results would indicate that Finnie's cutting mechanism is a single particle material removal mechanism, but the conditions necessary for its operation in a random distribution of impacting particles may occur for only a small number of particle impacts.

Finnie's concept of an angular-shaped particle impacting a ductile surface at an acute angle is shown in Figure 3.11. The dynamical equations governing the motion of the particle after it strikes the surface are:

$$m\ddot{x}_c + F_x = 0 \tag{3.11}$$

$$m\ddot{y}_c + KF_x = 0 \tag{3.12}$$

$$I\ddot{\Phi} + F_x r = 0 \tag{3.13}$$

The equations are written for motion relative to the center of mass of the particle. The particle has a uniform width, b. The horizontal resisting force of the ductile target material, F_x, is equal to the flow stress, σ_f, for the ductile target times the area of the cutting face of the particle in contact with the material as the particle penetrates the target. The area of the contact zone normal to the horizontal

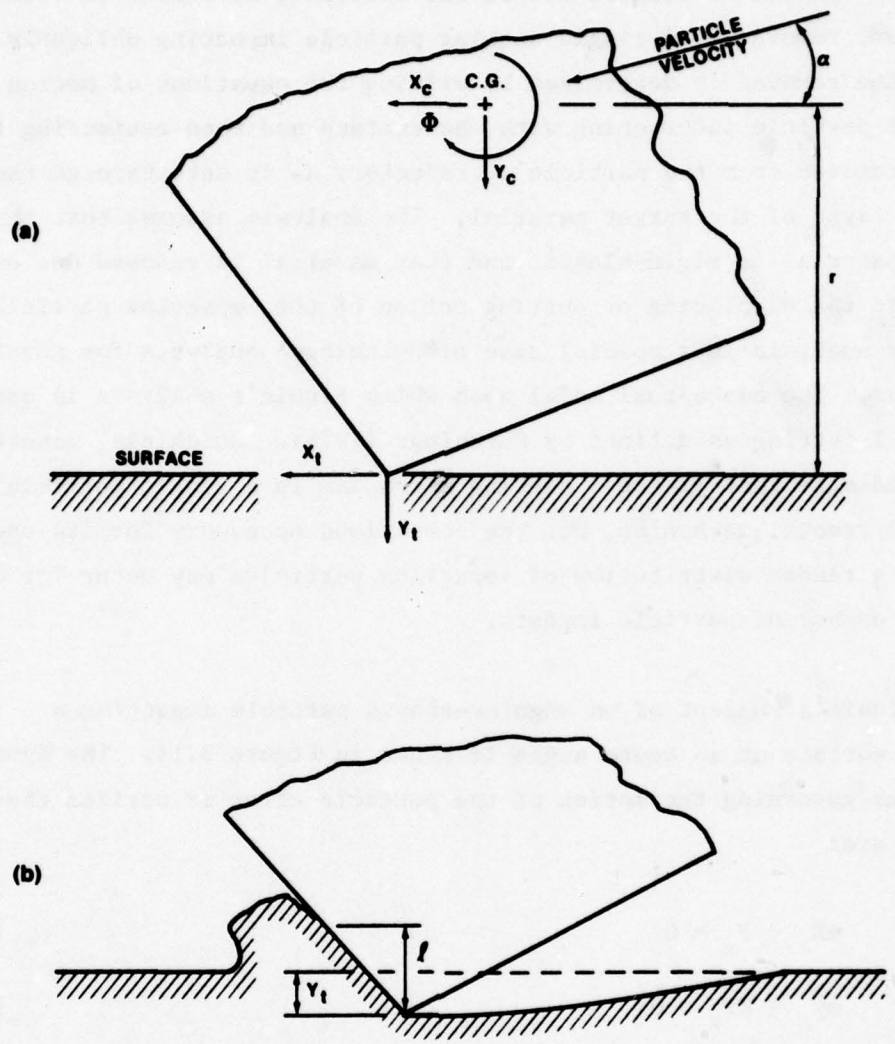

Figure 3.11. Finnie's Model for Material Removal.
a) Idealization of an Angular Particle Striking a Ductile Surface
b) Idealization of an Angular Particle Removing Material.

force component is, in accordance with Figure 3.11,

$$A = \ell b = \left(\frac{\ell}{y_t}\right) b y_t \tag{3.14}$$

so

$$F_x = p\psi b y_t \tag{3.15}$$

Finnie assumes that during the cutting process the ratio $\psi = \frac{\ell}{y_t}$ is a constant and that $y_t = y_c$ (Finnie, 1958). The latter relation requires that the particle be rigid and its rotation during the cutting process is negligible. Finnie further assumed that the ratio of the vertical force component, F_y, to the horizontal force component, F_x, is a constant K. Arguments based on metal cutting are presented to provide numerical estimates for the constants ψ and K (Finnie, 1958, 1960).

It is seen that the model is essentially for a rigid cutting tool removing a chip of material. This correspondence is further emphasized in that the particle rotation during the period of contact is taken to be small. It is now known from the work of Hutchings (Hutchings, 1977, 1979) that this is a somewhat restrictive assumption. In Finnie's model the entire forward face of the particle which penetrates the target defines the contact area. This condition will not prevail if particle rotations are permitted as shown in Figure 3.8. The assumption of a constant ratio, K, between the vertical to horizontal force fixes the direction of the force vector acting on the contact area. Thus, there is no provision in Finnie's analysis for variations in the orientation of the particle prior to impact. These two primary assumptions enable Finnie to solve the governing differential equations analytically.

The volume removed by the cutting action of the particle is simply

$$v = b\int_o^{\hat{x}} y_t dx_t \tag{3.16}$$

as illustrated in Figure 3.11. There are two conditions which can be realized: the particle's kinetic energy is dissipated before the chip is removed so the particle motion terminates while it is still in contact with the surface, or the particle completes the cut and leaves the surface. These conditions will be used in conjunction with Eq.(3.16) upon completion of the integration.

In Finnie (1958) the equations of motion were integrated and explicit expressions obtained for x_t and y_t which were then used to evaluate Eq.(3.16). A slightly more direct approach was used in Finnie and Kabil (1965) and utilized in the continued discussion of the model presented in Finnie (1972). The latter derivation will be given in moderate detail to indicate the basic elements of Finnie's theory.

For a rigid particle in Finnie's analysis

$$\ddot{x}_t = \ddot{x}_c + r\ddot{\Phi} \tag{3.17}$$

Substituting Eq.(3.11) and (3.13) into Eq.(3.17) yields

$$\ddot{x}_t = \frac{-\sigma_f b \psi}{m}\left(1 + \frac{mr^2}{I}\right) y_t = -\Gamma y_t \tag{3.18}$$

where F_x is given explicit form from Eq.(3.15). Substituting Eq.(3.18) into Eq.(3.16),

$$v = -\frac{b}{\Gamma}\int_o^{\hat{x}_t} \ddot{x}_t dx_t \tag{3.19}$$

where $\hat{x}_t$ is the value of x_t for which the cutting action terminates at a time t_c. Note that

$$\int_o^{\hat{x}} \ddot{x}dx = \int_o^{t_c} \ddot{x}\,\dot{x}\,dt = \frac{1}{2}\int_o^{t_c} \frac{d}{dt}(\dot{x})^2 dt = \frac{1}{2}\dot{x}^2 \Big|_o^{t_c}$$

The initial condition

$$\dot{x}_t \Big|_{t=0} = V_o \cos\alpha \tag{3.20}$$

can be introduced, and Eq.(3.19) becomes

$$\upsilon = \frac{b}{2\Gamma}\left(V_o^2 \cos^2\alpha - \dot{x}_t^2 \Big|_{t=t_c}\right) \tag{3.21}$$

It is now necessary to evaluate the critical conditions as indicated in the discussion following Eq.(3.16). The first condition is simply

$$\dot{x}_t \Big|_{t=t_c} = 0 \quad , \tag{3.22}$$

the second condition is the value of $\dot{x}_t$ when $y_t=0$. The expression for y_t is determined from Eq.(3.12) which can be written

$$\ddot{y}_t + \beta y_t = 0 \tag{3.23}$$

where $\beta = \sigma_f K\psi b/m$. The solution to this differential equation is

$$y_t = C_1 \sin \sqrt{\beta}\, t + C_2 \cos \sqrt{\beta}\, t \tag{3.24}$$

subject to the initial conditions

$$y_t \Big|_{t=0} = 0 \quad \text{and} \quad \dot{y}_t \Big|_{t=0} = V_o \sin\alpha \tag{3.25}$$

Hence

$$y_t = \frac{V_o \sin\alpha}{\sqrt{\beta}} \sin \sqrt{\beta}\, t \tag{3.26}$$

and it is seen that $y_t = 0$ when $t = \frac{n\pi}{\sqrt{\beta}}$ where $n = 0, \pm 1, \pm 2 \ldots$ Finnie selects the value, $t_c = \frac{\pi}{\sqrt{\beta}}$. The explicit expression for $\dot{x}_t$ can be obtained from Eq. (3.18), so

$$\dot{x}_t \Big|_{t=t_c} - \dot{x}_t \Big|_{t=0} = \frac{\Gamma}{\beta} V_o \sin\alpha \left(\cos\sqrt{\beta}\, t \Big|_{t=t_c} - \cos\sqrt{\beta}\, t \Big|_{t=0} \right)$$

$$\dot{x}_t \Big|_{t=t_c} = V_o \cos\alpha - \frac{2\Gamma}{\beta} V_o \sin\alpha \tag{3.27}$$

The two conditions represented by Eq.(3.22) and (3.27) can now be substituted into Eq.(3.21) to give the final result,

$$\upsilon = \frac{b}{2\Gamma} V_o^2 \cos^2\alpha \tag{3.28}$$

$$\upsilon = \frac{bV_o^2}{\beta}\left(\sin 2\alpha - \frac{2\Gamma}{\beta}\sin^2\alpha\right) \tag{3.29}$$

Introducing the expressions for Γ and β,

$$\upsilon = \frac{mV_o^2}{2\sigma_f\psi\left(1 + \frac{mr^2}{I}\right)}\cos^2\alpha \tag{3.30}$$

$$\upsilon = \frac{mV_o^2}{\sigma_f K\psi}\left(\sin 2\alpha - \frac{2}{K}\left(1+\frac{mr^2}{I}\right)\sin^2\alpha\right) \tag{3.31a}$$

$$= \frac{mV_o^2}{2\sigma_f\psi\left(1+\frac{mr^2}{I}\right)}\frac{2}{P}\left(\sin 2\alpha - \frac{2}{P}\sin^2\alpha\right) \tag{3.31b}$$

using the notation from Finnie (1972) where $P=K/\left(1+\frac{mr^2}{I}\right)$. In his work Finnie has provided some rationale from an analogy with metal cutting for letting $\psi=2$ and $K=2$. The value $\psi=2$ is implicitly incorporated into the results presented in Finnie (1972). In 1958 Finnie selected $I = \frac{mr^2}{2}$, while $I = \frac{mr^2}{3}$ is used in Finnie (1972); otherwise, the expressions are identical. These mass moments of inertia do not relate to a particular particle geometry but appear to be determined on the basis of Finnie's intuition as to the forms which would be representative of the angular particles in his model.

The expressions in Eq.(3.30) and (3.31), or equivalently Eq.(3.28) and(3.29), provide the functional relations for the angular dependence of the steady-state erosion rates, indicate the volume removed is proportional to the kinetic energy of the impacting particle, and contain only one material parameter, the flow stress σ_f , representing the response of the target. The general features of the curves corresponding to Eq.(3.30) and (3.31) will be examined.

The curves corresponding to Eq.(3.30) and (3.31) are plotted in Figure 3.12 for $0 \leq \alpha \leq 90$. The solid curve is the one used by Finnie to correlate erosion data; the conditions for the point at which the two curves cross and the maximum in the erosion curve can be obtained from the explicit relations for the angular dependence. The maximum value is found by differentiating Eq.(3.31) with respect to α and setting the result to zero, then the value of α corresponding to maximum erosion is determined from

$$\tan 2\alpha_m = P = \frac{K}{1 + \frac{mr^2}{I}} \tag{3.32}$$

The expressions in Eq.(3.30) and (3.31b) are equal for the value of α_o determined from

$$\tan\alpha_o = P/2 \tag{3.33}$$

The relative locations of the angles represented by Eq.(3.32) and (3.33) are shown in Figure 3.12. The variation in the magnitude of these angles with Finnie's specifications for I can be evaluated. For K=2 the maximum erosion occurs when $\alpha_m = 16°\text{-}51'$ and the erosion curves are equal when $\alpha_o = 18°\text{-}26'$ with $I = \frac{mr^2}{2}$. The corresponding values of α when $I = \frac{mr^2}{3}$ are 13°-17' and 14°-2' .

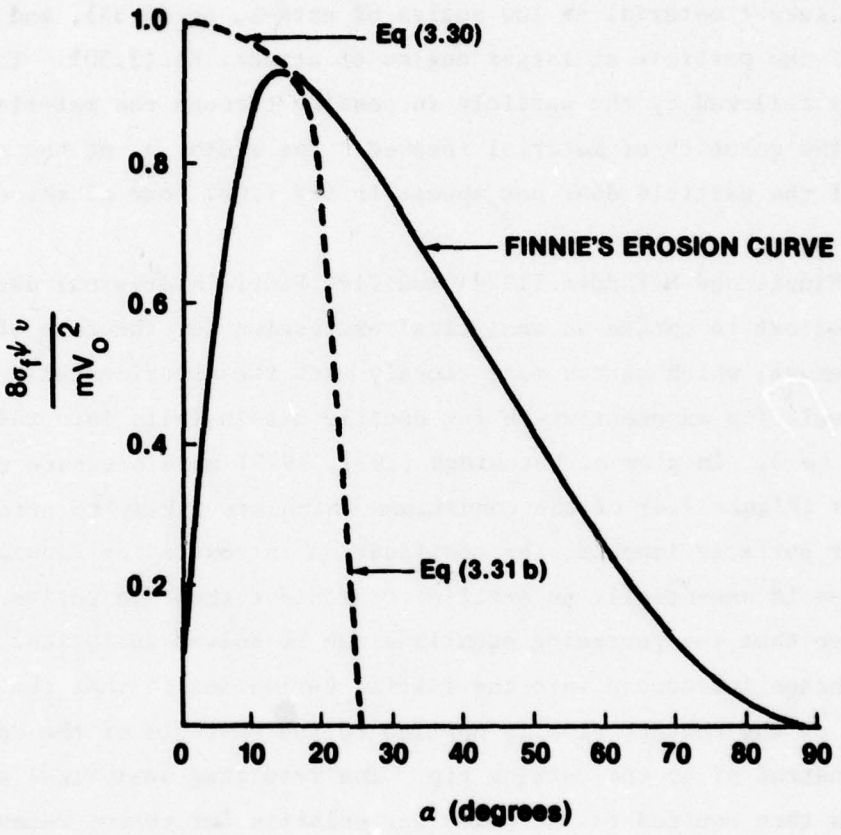

Figure 3.12. Form of the Erosion Curve for Oblique Impacts on Ductile Targets based on Finnie's Analysis when K=2 and $I = 1/3 \frac{mr^2}{3}$.

The general range of applicability of Finnie's model is taken to be for rigid particles greater than 100 μm and for values of α from 0 to 45° (Finnie and McFadden, 1978; Finnie, et al., 1979). The governing equations determine two conditions: the completion of a cut in the target material at low angles of attack, Eq.(3.31), and embedding of the particle at larger angles of attack, Eq.(3.30). The trajectory followed by the particle in passing through the material determines the quantity of material removed. The width b of the contacting face of the particle does not appear in the final form of the equations.

Finnie and McFadden (1978) modified Finnie's original derivation in an effort to obtain an analytical expression for the rate of material removal which agrees more closely with the experimentally-determined velocity exponent which for ductile metals falls into the range from 2 to 3. In view of Hutchings (1977, 1979) more accurate representations (Figure 3.8) of the conditions which are likely to arise for angular particle impacts, the modification introduced by Finnie and McFadden is essentially an artifice to achieve their objective formulated so that the governing equations can be solved analytically. The only change introduced into the initial derivation is that the force acting on the contact area is applied to the centroid of the contact area instead of at the cutting tip. The resulting analytical expression is then equated to the power law relation for volume removal which is essence is equivalent to assuming the result they want to derive.

The direction of the applied force and orientation of the contact face are held constant throughout the time the particle is in contact with the target. This change does not influence Eq.(3.11) or (3.12) but Eq.(3.13) is modified as follows

$$I\ddot{\phi} + F_x(r-y) - 2KF_x y = 0 \qquad (3.34)$$

where y is the distance to the centroid of the contact area. The same procedure is followed for solving the revised equations as has been outlined for the initial formulation. The new equation corresponding to Eq.(3.31b) is

$$\frac{\beta\upsilon}{b} = V_o^2 \left[\left(\sin 2\alpha - 4\sin^2\alpha \right) + \frac{15\pi}{4} \frac{V_o \sin^3\alpha}{r\sqrt{\beta}} \right] \tag{3.35}$$

where as before $\beta = \frac{\sigma_f K \psi b}{m}$ and a value of $P = \frac{1}{2}$ has been assumed (compare Eq.(3.31b)).

This expression for the volume removed, υ , in Eq.(3.35) has the general form

$$\upsilon = (A + BV_o)V_o^2 \tag{3.36}$$

On the basis of the experimental data, Finnie and McFadden assume

$$\upsilon = CV_o^n \ . \tag{3.37}$$

The velocity exponent is determined by equating the analytical result to the power law relation representative of the experimental mass-loss data indicated in Eq.(3.37), so

$$(A + BV_o)V_o^2 = CV_o^n \tag{3.38}$$

The explicit form of Eq.(3.38) expressed as the ratio of the volume removed at two different impact velocities, U_1 and U_2 , is then used to evaluate the exponent n ,

$$\left(\frac{U_2}{U_1}\right)^{n-2} = \frac{\sin 2\alpha - 4\sin^2\alpha + (15/4)\pi(U_2/U_1)\lambda_1 \sin^2\alpha}{\sin 2\alpha - 4\sin^2\alpha + (15/4)\pi\lambda_1 \sin^2\alpha} \tag{3.39}$$

where $\lambda_1 = \frac{U_1 \sin\alpha}{\sqrt{\beta}\, r}$ which is the maximum depth of cut relative to the particle radius.

According to Finnie and McFadden the value predicted for the effective exponent n for a given α and λ_1 is quite insensitive to the ratio of the impact velocities, so the volume removed plotted against impact velocity should be essentially a straight line on a log-log scale.

This is the result when the particle leaves the surface and applies for angles of attack less than approximately 20°. The evaluation of the expression for the volume removed corresponding to the condition when the particle's trajectory terminates in the target is somewhat more involved. Representative values of n were not evaluated by Finnie and McFadden for this latter condition.

Finnie's analysis (Finnie, 1958) for ductile materials was the first of its kind in the solid particle erosion literature and therefore deserves recognition for the contribution made in providing a basis for correlating erosion data. However the restriction of being able to integrate the equations of motion analytically removes many features of the dynamic penetration process occurring for oblique impacts of angular particles and may no longer be a realistic objective. A velocity exponent greater than 2 comes out of Hutchings numerical analyses which describe more representative impact conditions fairly directly as opposed to the imposition of the highly idealized impact conditions assumed by Finnie and McFadden (1978) in order to obtain an analytic solution.

3.4 Bitter

Finnie's theory of erosion of ductile materials is based on a model of the cutting action by the impacting particle and therefore did not account for material removal for particle impacts at normal incidence. The experimental data shows that material removal does occur for angular particle impacts on ductile materials at normal incidence which is a limitation on the application of Finnie's correlation to values of α greater than 45° as previously noted. Bitter (1963a) provided a fairly detailed analysis for the normal collision of an elastic sphere on an elastic-plastic half-space as a model for material removal in a solid particle erosive environment. The main elements of Bitter's approach will be described, but reference to the original publication is advised in order to follow the details of Bitter's discussions of the material response. The general features of Bitter's concept of the material removal mechanisms are presented as interpreted by the author, but the physical process by which material is removed is not reflected in the final semi-empirical correlation.

Bitter divides the general erosion process into two categories: deformation wear and cutting wear. Finnie's analysis of cutting wear was already published, however Bitter developed an analytical approach for deformation wear as well as an alternative derivation of the cutting wear analysis. Bitter's analyses are for a single spherical particle impacting an elastic-plastic target material. The deformation wear analysis is based on an energy balance whereby the kinetic energy of a single impacting particle is divided into recoverable elastic and elastic-plastic deformational energy and non-recoverable plastic deformation. The cutting wear relations are obtained from the equations of motion for a single spherical particle striking an elastic-plastic target obliquely. Bitter (1963a,b) notes that both de Haller (1939) and Wellinger (1949) recognized that the material removal process due

to multiple particle impacts was influenced by the hardness of the target material (the flow stress in Finnie's analysis for ductile targets) and the impingement angle.

3.4.1 Deformation Wear Model

Bitter (1963a) described the material removal mechanism due to deformation wear as a process of strain hardening and embrittlement of the ductile target. He argues that no material removal will occur when the states of stress in the target material do not exceed the elastic limit except for fatigue damage due to the repetitive impact cycles. When the particle impacts are severe enough to produce plastic deformation, the repetitive impacts produce a plastically deformed surface layer which becomes work hardened and brittle and loses its capacity for further plastic deformation. During the embrittlement process the elastic limit increases until it represents the strength of the target material. Stresses in excess of the elastic limit for the strain-hardened material can no longer be tolerated through further plastic deformation and therefore fracture is initiated apparently in a brittle mode. Bitter's analysis was strongly influenced by Davies' analysis of a solid sphere impacting a ductile half-space using the Hertzian theory of impact (Davies, 1949). Using either the Tresca or von Mises yield condition, Davies found that the maximum principal stress difference (onset of yielding) occurred along the axis of symmetry at a point approximately one-half the contact radius for a steel ball impacting a steel plate. Thus locating the maximum stress condition within the target for the onset of yielding, Bitter equates this to the point at which the strength of the material is exceeded and envisions cracks developing parallel to the contact area in the plastically-deformed surface layer. Material fragments are assumed to be removed in the form of flakes. The mathematical development is guided by the conceptual model described above.

The general single particle impact at normal incidence is shown in Figure 3.13 as idealized by Bitter. For low impact velocities the impact is purely elastic and the Hertzian theory of impact is assumed to be applicable (Appendix A). The applied pressure distribution is paraboloidal. When the elastic load limit is exceeded, plastic stresses develop as shown in Figure 3.13b for an elastic-perfectly plastic material.

Bitter's expression for material removal due to deformation wear is based on a partitioning of the initial kinetic energy of the impacting particle into plastic, elastic-plastic, and plastic deformations of the target material. The energy balance is

$$Q = \frac{1}{2} mV_o^2 = Q_e + Q_{pe} + Q_p \tag{3.40}$$

The term Q_e is the fully recoverable elastic deformation energy associated with the loading function up to the load level at which yielding in the target initiates. Up to this load level the impact is described in terms of the Hertzian theory of impact which has a major role in Bitter's analysis. The elastic-plastic response of the target is considered to comprise a further elastically recoverable component, Q_{pe}, and a pure plastic (permanent) deformation of the target absorbing the energy Q_p. The rebound velocity of the spherical projectile from the elastic-plastic target, V, is governed by the elastic deformational energy stored in the target, so

$$\frac{1}{2} mV^2 = Q_e + Q_{pe} \tag{3.41}$$

Using the explicit representations for Q_e, Q_{pe}. and Q_p, Bitter is able to show that

$$Q_{pe} = \sqrt{15/4\ Q_e Q_p} = 1.936\sqrt{Q_e Q_p} \tag{3.42}$$

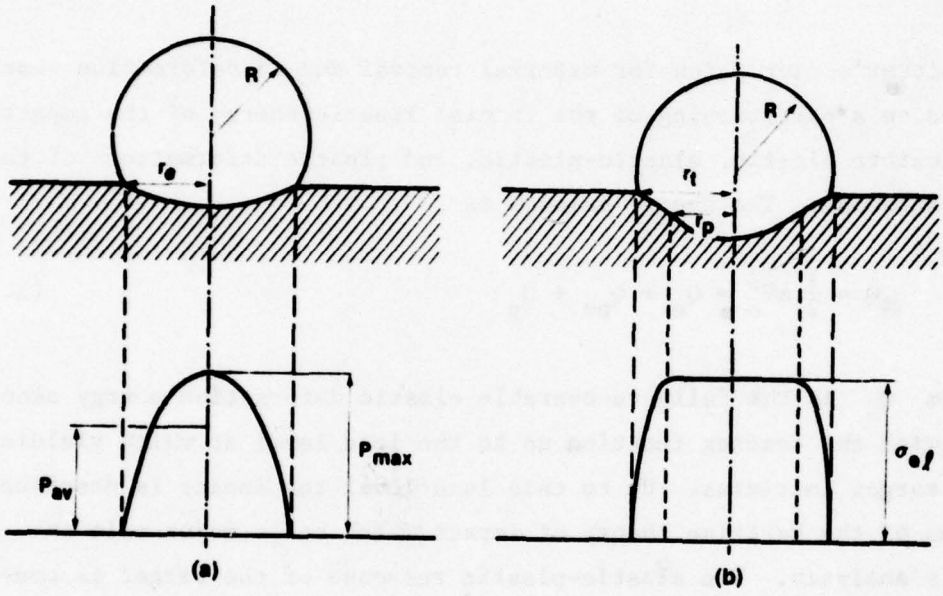

Figure 3.13. Surface Pressure Distribution Over Contact Area (Bitter, 1963a). a) Elastic Impact, b) Elastic-Plastic Impact.

Eliminating Q_{pe} from Eq.(3.40),

$$Q = Q_e + 2\sqrt{Q_e Q_p} + Q_p - 0.064\sqrt{Q_e Q_p} \tag{3.43}$$

which Bitter approximates by

$$Q_p \approx \left(\sqrt{Q} - \sqrt{Q_e}\right)^2 \tag{3.44}$$

Bitter defines the measure of deformation wear, υ_D, as

$$\upsilon_D \equiv \frac{Q_p}{\xi} \tag{3.45}$$

where ξ is an empirical parameter representing the amount of energy required to remove one unit volume of material. υ_D is due solely to the energy absorbed by plastic deformation of the target material.

With the introduction of the empirical parameter ξ, Eq.(3.45) is essentially no more than an assumed representation for the deformation wear response. Substituting Eq.(3.44) into (3.45), using the definition of Q in Eq.(3.40) and

$$Q_e = \frac{1}{2} m V_e^2 \tag{3.46}$$

which defines the portion of the initial kinetic energy contributing to the purely elastic deformation of the target material, Eq.(3.45) becomes

$$\upsilon_D = \frac{\frac{1}{2} M(V_o \sin\alpha - V_e)^2}{\xi} \tag{3.47}$$

It is assumed that only the normal component of the initial particle impact velocity, V_o, will be effective in producing deformation wear and

that the steady-state erosion rate is simply a linear accumulation of the damage produced by a single particle with the introduction of the total mass, M, for all the particles striking the target. No erosion takes place when $V_o \sin\alpha \leq V_e$. The original definition of deformation wear, Eq.(3.45), has now been generalized to oblique impacts and to multiple spherical body impacts.

Although the Hertzian theory is used extensively in Bitter's analysis, only the velocity V_e is related explicitly to the material properties of the impinging spherical bodies and the target in accordance with the following relation

$$V_e = \frac{\pi}{2\sqrt{10}} \sigma_{e\ell}^{5/2} \frac{1}{\rho_1^{1/2}} (k_1+k_2)^2 \tag{3.48}$$

This expression is derived from the straightforward application of the Hertzian theory of impact which is taken to be valid up to the value of the average applied pressure, $\sigma_{e\ell}$, at which yielding within the target material is initiated. (Bitter refers to $\sigma_{e\ell}$ as the elastic load limit and denotes it by the symbol y.) The remaining parameters are the density of the impinging sphere, ρ_1, and the elastic moduli of the sphere and the target, k_1 and k_2, as defined in Eq.(A3) of Appendix A.

Despite the lack of a sound basic derivation of the deformation wear expression in Eq.(3.47), it has been one of the major correlating functions for solid particle erosion test results.

Rebound tests for hardened steel balls impacting plates of various materials are used to indicate the independence of V_e on the particle size (mass). Hardened steel balls of different mass were dropped from a constant height of 85.7 cm and the rebound height was measured. The rebound height is taken to be dependent on the recoverable elastic energy in Eq.(3.40) which is the sum of Q_e and Q_{pe}. The energy balance can

now be written

$$Q = (Q_e + Q_{pe}) + Q_p \tag{3.49}$$

$$\frac{1}{2} mV_o^2 = \frac{1}{2} mV^2 + \frac{1}{2} m(V_o - V_e)^2 \tag{3.50}$$

where the definitions in Eq.(3.40) and (3.41) and Bitter's result in Eq.(3.44) have been used. Bitter obtains from Eq.(3.50)

$$V^2 = 2V_o V_e - V_e^2 \tag{3.51}$$

which can be solved for V_e ,

$$V_e = \left(1 - \sqrt{1-e^2}\right) V_o \tag{3.52}$$

where $e = \frac{V}{V_o}$ is the coefficient of restitution. According to this expression the functional dependencies of V_e are identical to those of e (Goldstein, 1960; Adler, 1961). When e=1 , the collision is perfectly elastic and $V_e = V_o$, so according to Bitter's hypothesis no material loss will occur. All of the initial kinetic energy will be dissipated in plastic deformation when e=0 . In general e varies with both the mass of the impacting particle and its velocity, as well as numerous other properties of the particle and target material: e is a dynamics parameter which represents all of the modes of energy dissipation which occur for a particular impact condition in real materials.

The experimental determinations of V_e are used to evaluate $\sigma_{e\ell}$ from Eq.(3.48). The empirical parameter ξ is determined from the erosion test data. Bitter elected to use the experimental erosion rate (mass removal/mass of impinging particles) at $\alpha = 60°$ to obtain the

value of ξ . Eq.(3.47) then provides the explicit variation in angular dependence for the erosion rate associated with solid particulates impacting at a specified velocity V_o on a specific material.

$$W_D = \frac{\rho_2 v_D}{M} = \frac{\rho_2}{2\xi} (V_o \sin\alpha - V_e)^2 \tag{3.53}$$

where ρ_2 is the density of the target material. W_D is expressed in terms of the mass of material removed per unit mass of impacting particles. Some material properties are included explicitly in V_e , Eq.(3.48), however the material properties influencing the target's response in an erosive environment are primarily represented in the parameter ξ . Bitter provides a brief discussion of this factor.

3.4.2 Cutting Wear Model

Bitter derived the equations governing cutting wear on the basis of an elastic-plastic analysis. Bitter considered the two particle impact conditions which Finnie described; namely, the particle cuts through the surface with a nonzero final velocity, or it becomes embedded in the surface before completion of the cutting action. In the first case

$$W_{C1} = \frac{\rho_2}{2\phi}(V_o^2 \cos^2\alpha - \dot{x}_f^2) \tag{3.54}$$

where $\dot{x}_f$ is the tangential velocity which the particle has as it leaves the surface and ϕ is the cutting wear factor which is the energy required to "scratch" a unit volume of material from the surface. Again, W_{C1} is expressed in terms of the mass of material removed per unit mass of impacting particles. Bitter does not provide any additional information on the cutting wear factor except that it depends on the mechanical properties of the target. For the second impact condition when $\dot{x}_f = 0$ before completion of the cut,

$$W_{C2} = \frac{\rho_2 V_o^2 \cos^2\alpha}{2\phi} \tag{3.55}$$

Bitter finds that a correction factor is required in Eq.(3.55) if the condition $\dot{x}=0, \dot{y}=0$ is achieved when the maximum depth of cut occurs.

Bitter's cutting wear analysis involves the determination of the final horizontal component of velocity, $\dot{x}_f$, in Eq.(3.54) and the indicated correction factor for Eq.(3.55). The approach used is based on the oblique impact of a spherical particle which is equivalent to an angular-shaped abrasive particle. The size of the irregular-shaped body is approximated by a spherical radius R. The particle is assumed to have rounded edges and to be fairly equiaxed. A smaller rounded portion of the particle with a radius of curvature r penetrates the ductile target and the mass of the particle is expressed in terms of this apparent radius, so

$$m = \frac{4}{3} \pi \rho' r^3$$
$$\rho' = (R/r)^3 \rho \tag{3.56}$$

where ρ' is the fictitious density of the equivalent particle and ρ is the density of the actual particle. The velocity $\dot{x}_f$ is then determined from the equations of motion for the oblique impact of the equivalent spherical body.

$$m\ddot{x} = -A\phi = F_x \tag{3.57}$$

$$m\ddot{y} = \pi r_p^2 \sigma_{e\ell} + \pi r_e^2 \frac{2}{3} \sigma_{e\ell} = F_y \tag{3.58}$$

where F_x is the horizontal shearing force resisting motion tangential to the surface of the target by the spherical body and F_y represents the elastic-plastic penetration force after the maximum Hertzian pressure exceeds the elastic stress limit, $\sigma_{e\ell}$, of the target material. The area A is for the vertical cross section of that part of the particle which has penetrated the target (roughly equivalent to the region shown in

Figure B1, Appendix B)*, and ϕ is the cutting wear factor. The vertical resisting forces correspond to the condition in Figure 3.13 already described for the deformation wear analysis. Bitter's equations of motion exclude frictional effects and rotation of the spherical body as it cuts through the surface of the material. The depth of the cut is determined from the normal velocity component.

It is noted in passing that Surette (1971) identified the primary mode of volume removal to be failure of the impacted surface in shear due to sliding friction between the impinging particle and the surface. He indicates that his model is based on first principles and that the parameters required are combinations of readily obtainable engineering data. A somewhat confusing derivation of the governing relations is presented.

Surette writes the equations of motion for a rigid spherical body impacting a ductile target obliquely, however these equations require some interpretation due to the lack of precise meanings assigned to the notation used. Referring to Figure 3.14,

$$m\ddot{x} + f_s(\sigma_s A_d) = 0 \tag{3.59}$$

$$m\ddot{y} + N = 0 \tag{3.60}$$

$$I\ddot{\theta} - f_s(\sigma_s A_d)R = 0 \tag{3.61}$$

---

*Bitter states $A=4/3r_pH$, where H is the plastic penetration depth in the target, however the author was not able to derive this expression for the area A. It is not obvious what approximations were used in Bitter's derivation.

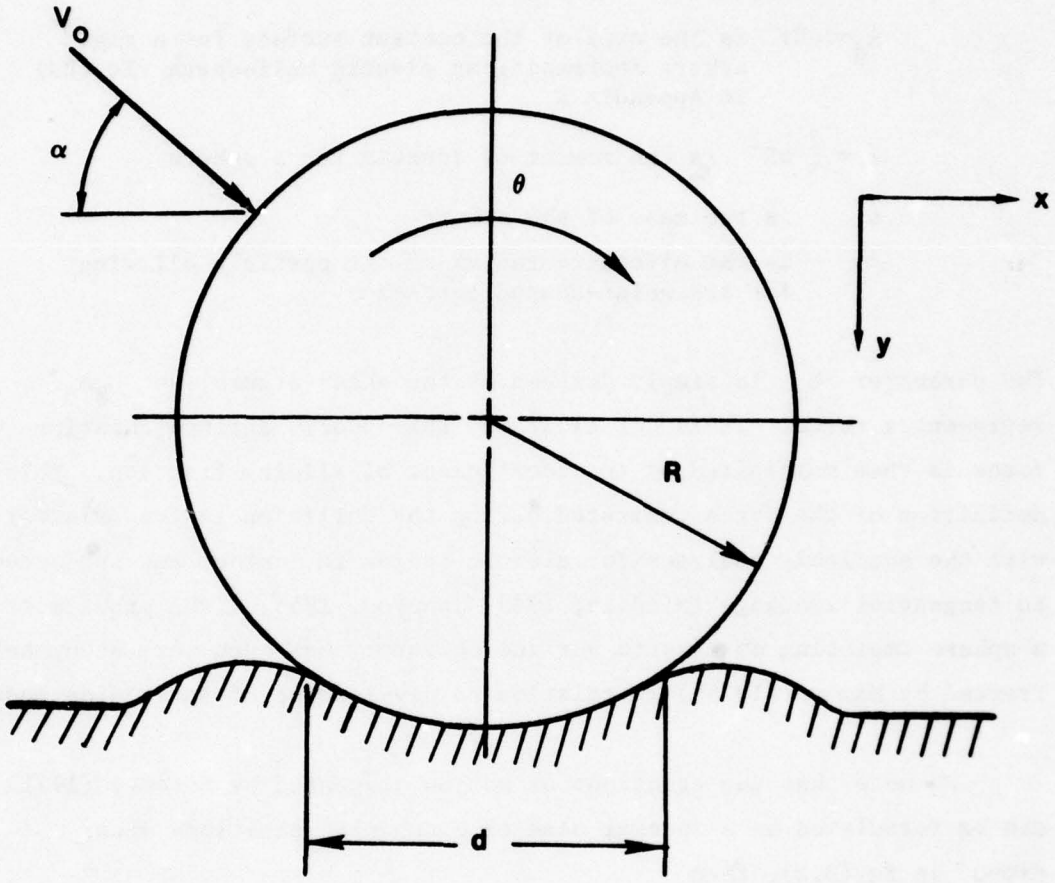

Figure 3.14. Coordinate System Used by Surette (1971) and His Idealization of the Deformation Process.

where N is the normal force developed at the interface and is stated explicitly in terms of the Hertzian relation for static indentations in elastic materials

f_s is the coefficient of sliding friction

$A_d = 2\pi Ry$ is the area of the contact surface for a rigid sphere impressing an elastic half-space (Eq.(B3) in Appendix B

$I = \frac{2}{5} mR^2$ is the moment of inertia for a sphere

m is the mass of the sphere

R is the effective radius of the particle allowing for irregular-shaped particles

The parameter σ_s is simply defined as the shear stress, so $\sigma_s A_d$ represent a force. It is not clear why this poorly defined shearing force is then multiplied by the coefficient of sliding friction. This definition of the force generated during the collision is inconsistent with the available analyses for elastic bodies in contact and subjected to tangential loadings (Mindlin, 1949; Johnson, 1955). The problem of a sphere impacting an elastic surface obliquely has been more accurately treated by Mamoun (1975b) in relation to development of an erosion model.

We note that the equations of motion suggested by Surette (1971) can be formulated as a special case of Hutchings' equations when $\beta+\phi=0$ in Eq.(3.2), then

$$\begin{aligned} m\ddot{x} &= -\mu N \\ m\ddot{y} &= -N \\ I\ddot{\theta} &= R\mu N \end{aligned} \qquad (3.62)$$

The imposed condition corresponds to the force acting along the y axis which is representative of a normal collision rather than representing the contact area which would result as a rigid bead ploughs through a ductile target during an oblique impact. In Surette's analysis the

equations of motion are very idealized for oblique impacts and do not conform to a realistic physical model of the collision process. However this simplification permits the equations of motion to be solved analytically. The lack of clarity in Surette's work eventually frustrated this author and his work is left to others to decipher.

Comparing Eq.(3.58) and (3.60) it is seen that both Bitter (1963b) and Surette define the normal force in terms of the Hertzian impact pressure but according to Eq.(3.57) and (3.59) define independent forces for the resistance which develops parallel to the surface of the target. This is contrary to Surette's model but is consistent with Bitter's approach where the particle actually penetrates the surface. Bitter assumes that no material is removed if the oblique impact is purely elastic.

Heuristic arguments are used with the general equations for the assumed model to obtain the final expressions for target volume removal

$$v_{C1} = \frac{2MC(V_o\sin\alpha - V_e)^2 V_o\cos\alpha}{\sqrt{V_o\sin\alpha}} - \frac{2MC^2(V_o\sin\alpha - V_e)^4}{V_o\sin\alpha}\,\phi \qquad \alpha \leq \alpha_o \tag{3.63}$$

$$v_{C2} = \frac{M}{2\phi}\left[V_o^2\cos^2\alpha - K_1(V_o\sin\alpha - V_e)^{3/2}\right] \qquad \alpha \geq \alpha_o \tag{3.64}$$

where

$$C = \frac{0.288}{\sigma_{e\ell}}\left(\frac{\rho_1}{\sigma_{e\ell}}\right)^{1/4} \tag{3.65}$$

$$K_1 = 0.82\,\sigma_{e\ell}^2\left(\frac{\sigma_{e\ell}}{\rho_1}\right)^{1/4}\left(\frac{1-\nu_1^2}{E_1} + \frac{1-\nu_2^2}{E_2}\right)^2 \tag{3.66}$$

and V_e is defined in Eq.(3.48). When $V_o >> K_1^2$ and K, the angle α_o can be found from

$$\frac{\cos\alpha_o}{\sin^{3/2}\alpha_o} = \frac{0.576}{\sigma_{e\ell}} \left(\frac{\rho_1}{\sigma_{e\ell}}\right)^{1/4} V_o^{1/2} \phi \qquad (3.67)$$

Determination of the range of application of Eq.(3.63) and (3.64) is not as simple as for Finnie's analysis. Bitter's expression in Eq.(3.63) shows the dependence of the erosion rate on impact velocity to be essentially $V_o^{5/2}$ since the second term on the right-hand side will generally be small compared to the first term. Thus a velocity exponent different than 2 is a result of Bitter's analysis. Removal of this velocity squared restriction was the objective for the models and corresponding analyses undertaken by Sheldon and Kanhere (1972) and Finnie and McFadden (1978). It is also interesting to note that the first and dominant term in Eq.(3.63) can be evaluated explicitly without knowing the empirical factor ϕ .

The experimental erosion rate data obtained as a function of impingement angle is now represented by the sum of the contributions due to deformation wear and cutting wear. Thus, from Eq.(3.53), (3.63) and (3.64),

$$W_T = W_D + W_{C1} \qquad \text{when } \alpha \leq \alpha_o \qquad (3.68)$$

$$= W_D + W_{C2} \qquad \text{when } \alpha \geq \alpha_o \qquad (3.69)$$

In order to fit the erosion data the empirical parameters ξ and ϕ have to be determined. Two experimental data points are required. From Eq.(3.53) it is seen that ξ can be evaluated directly when $\alpha=90°$. The W_D curve can then be constructed. A second data point for $\alpha_o<\alpha<<90°$ provides the equation

$$W_{C2} = W_T - W_D \qquad (3.70)$$

for the evaluation of ϕ . W_{C1} can then be constructed if $\sigma_{e\ell}$ is known for the target material. The value of α_o is found graphically from the intersection W_{C1} and W_{C2} .

Bitter (1963b) shows that Eq.(3.64) is equivalent to Finnie's Eq.(3.30) when $K_1=0$. However he notes that Finnie's Eq.(3.31) for $\alpha<\alpha_o$ includes the implicit assumption that the time required for penetration of the particle is equal to the time required for its egress which can be seen upon differentiating Eq.(3.26). Bitter's observation is that if the normal velocity of the particle becomes zero before the tangential velocity component, the particle is pressed out of the target by the elastic reaction forces while its cutting action continues (due to the non-zero tangential velocity). This is consistent with Finnie's analysis but is not consistent with the assumption that the target material is perfectly plastic. For this case there is no elastic restoring force; it can be presumed the cutting action of the particle would continue tangential to the target's surface until the tangential velocity (and corresponding kinetic energy) was dissipated. Bitter's formulation of the problem, Eq.(3.57) and (3.58) accounts for this condition. Bitter thus comments that Finnie has utilized a relation describing the contact duration for the collision of a spherical body with a plane surface, although his model is based on oblique impacts by angular particles.

3.5 Neilson and Gilchrist

Neilson and Gilchrist (1968) devised a purely empirical scheme for fitting the experimental erosion data (erosion rate as a function of impact angle) based on their own test results and the analyses of Finnie and Bitter. Their correlation procedure will be described.

Neilson and Gilchrist note that the following observations should be included in any correlation of the experimental data.

The kinetic energy of the impacting particles normal to the target is imparted to the specimen and accounts for deformation wear.

There is a threshold velocity component normal to the surface, κ, above which erosion occurs: principally for deformation wear. The kinetic energy of the impacting particles parallel to the target is responsible for cutting wear.

There is a critical impingement angle, α_o, above which the particles come to rest in the target and below which the particles leave the surface with a velocity V_p parallel to the surface.

Neilson and Gilchrist further observe that tests on ductile materials using a constant impact velocity indicate that as the impingement angle, α, increases from zero, the erosion rate increases initially at a rapid rate which decreases as the impingement angle increases. They assume that the cutting action of the particles when $\alpha \leq \alpha_o$ can be represented by a function of the form

$$\left(\frac{V_p}{V\cos\alpha}\right)^2 = 1-\sin n\alpha \qquad (3.71)$$

where n is a constant. Then,

$$V_p = V_o \qquad \text{when } \alpha = 0 \qquad (3.72)$$

$$V_p = 0 \text{ and } \alpha_o = \frac{\pi}{2n} \qquad \text{when } \alpha = \alpha_o \qquad (3.73)$$

The above observations are contained in the following relations,

$$W_T = W_D + W_C$$

$$= \frac{1}{2\Xi}(V_o \sin\alpha - \kappa)^2 + \frac{1}{2\Phi}(V_o^2 \cos^2\alpha - V_p^2) \qquad (3.74)$$

or, introducing Eq.(3.71),

$$W_T = \frac{1}{2\Xi}(V_o \sin\alpha - \kappa)^2 + \frac{1}{2\Phi} V_o^2 \cos^2\alpha \sin n\alpha \quad \text{when } \alpha \leq \alpha_o \qquad (3.75)$$

and

$$W_T = \frac{1}{2\Xi}(V_o \sin\alpha - \kappa)^2 + \frac{1}{2\Phi} V_o^2 \cos^2\alpha \qquad \alpha \geq \alpha_o \qquad (3.76)$$

where Φ denotes the amount of kinetic energy which has to be absorbed to remove one unit mass of material from the target by the cutting wear mechanism and Ξ is the corresponding parameter for deformation wear. Neilson and Gilchrist described the general features of Eq.(3.75) and (3.76) and provided a procedure for evaluating the parameters n, Φ and Ξ when $\kappa=0$. A self-contained approach for carrying out this procedure will be described for use by the interested reader.

First consider erosion rate curves representative of ductile response when the cutting mechanism dominates. In terms of Neilson and Gilchrist's approach, $0 \leq \Phi/\Xi \leq 1$. The maximum erosion rate in the ductile response curve will be determined. Differentiating Eq.(3.75) with respect to α and setting the result equal to zero, yields

$$\sin n\alpha_m - \frac{n \cos n\alpha_m}{2 \tan \alpha_m} = \frac{\Phi}{\Xi} \qquad (3.77)$$

where $\alpha_m \leq \alpha_o$ is the value of α at which the maximum erosion rate occurs. The values of α_m are plotted in Figure 3.15 as a function of n and Φ/Ξ. When

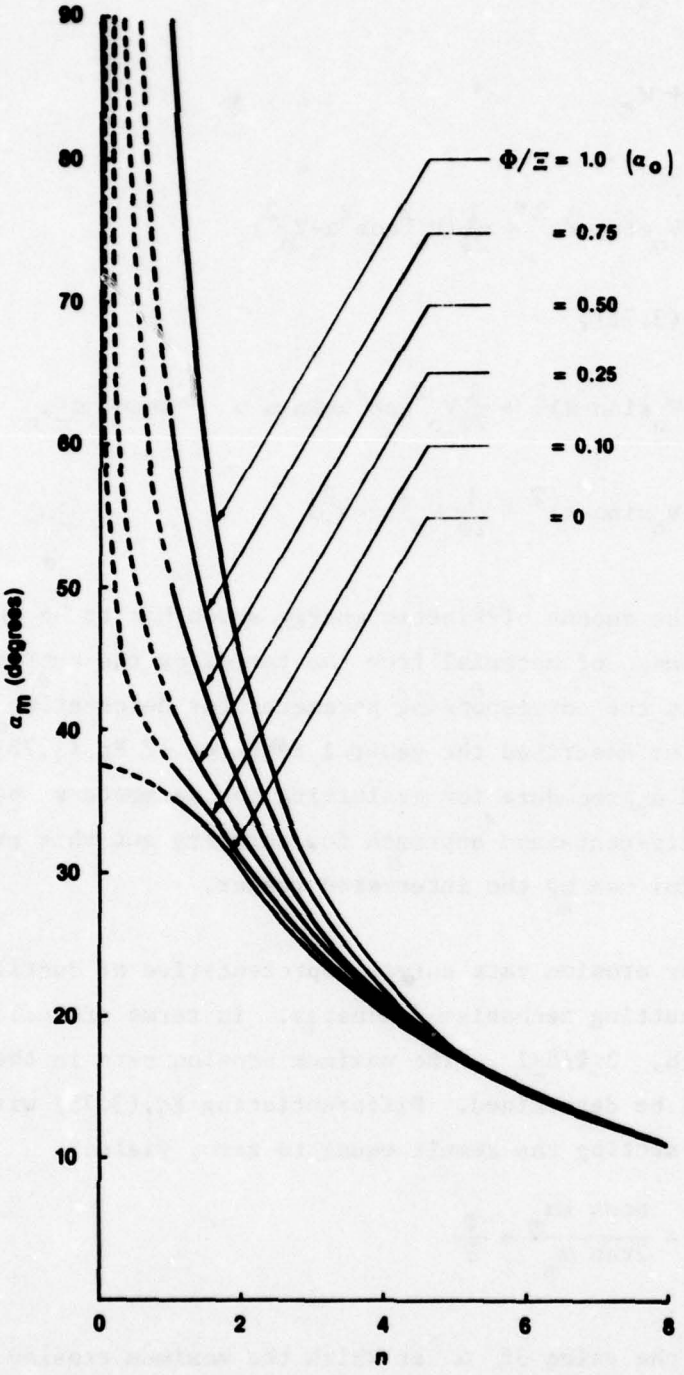

Figure 3.15. The Impingement Angle for Maximum Erosion, α_m, as a Function of the Parameter n (Neilson and Gilchrist, 1968).

$$\Phi/\Xi = 1 ,$$

$$\alpha_m = \alpha_o = \frac{\pi}{2n} \tag{3.78}$$

The procedure for evaluating the parameters n, Φ and Ξ when $\Phi/\Xi \leq 1$ requires experimental data to establish the erosion rate when $\alpha = \pi/2$, the value of α_m, and the maximum in W_c. The steps in constructing the erosion rate curve are illustrated in Figure 3.16.

1. Evaluate Ξ from Eq.(3.76) when $\alpha = \pi/2$,

$$\Xi = \frac{\frac{1}{2} V_o^2}{W_{90°(exp)}}$$

2. Knowing Ξ, draw the curve for the erosion rate associated with the deformation mechanism of removal.

$$W_D = \frac{\frac{1}{2} V_o^2 \sin^2\alpha}{\Xi}$$

3. Subtract W_D from $W_T(exp)$ data points to approximate W_C, the erosion rate due to the cutting mechanism of removal, so

$$W_C = W_T(exp) - W_D$$

4. Determine α_m for W_C.

5. Using the value of $\alpha_m\big|_{W_C}$ determine the value of n from Figure 3.15 when $\Phi/\Xi = 0$ which corresponds to the condition when the erosion is due entirely to the cutting mechanism. The value of $\alpha_o(\Phi/\Xi = 1)$ can now be found from Figure 3.15 for this value of n.

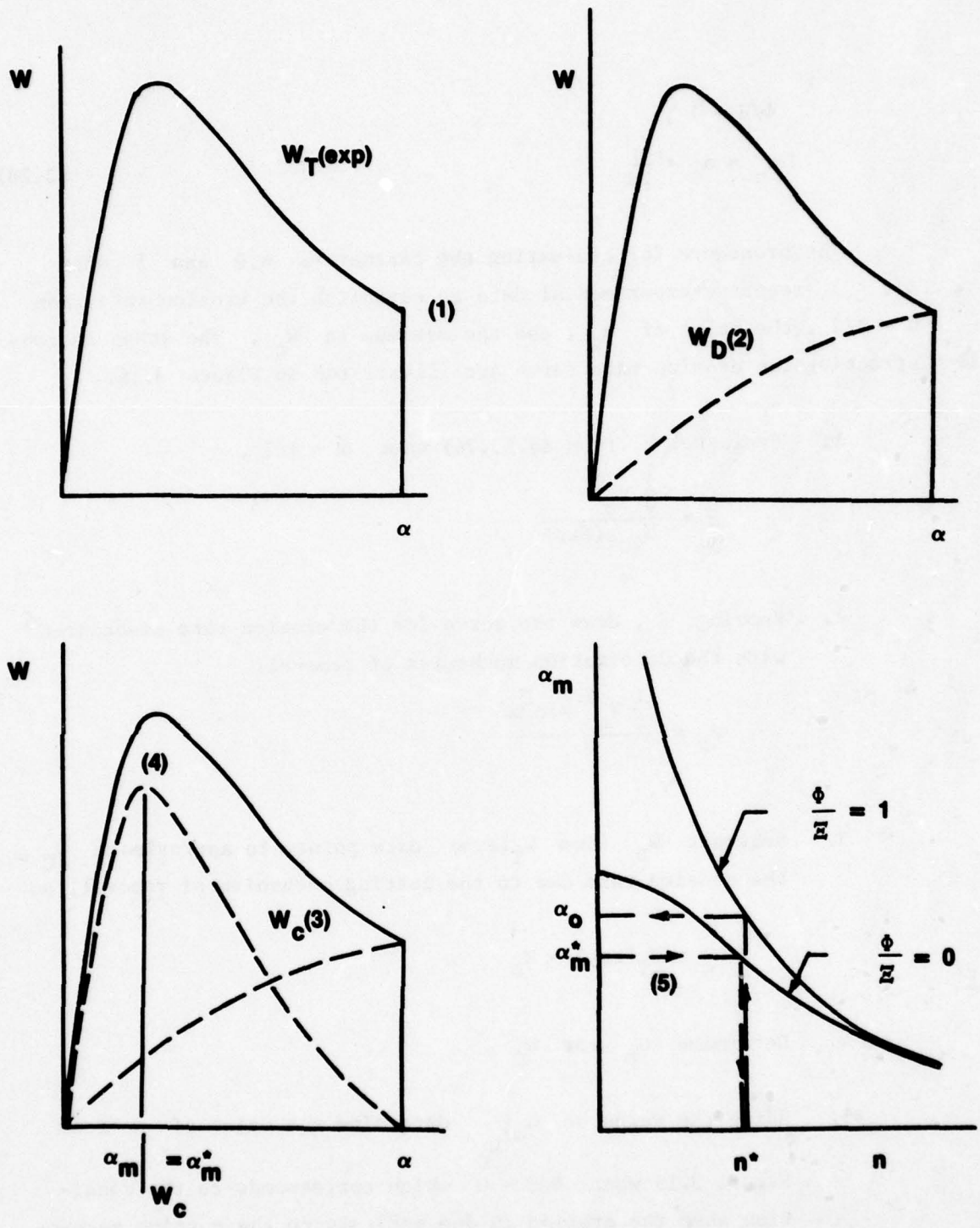

Figure 3.16. Steps in Evaluating the Parameters in Neilson and Gilchrist's Erosion Correlation.

6. Knowing n and having the experimental value of α_m for W_T, the value of Φ/Ξ can be obtained from Figure 3.15. The value of Φ can now be evaluated since Ξ is known.

The curve for W_T based on the parameters n,Φ,Ξ, and α_o can be constructed as an analytical representation for the experimental data.

When $\Phi/\Xi > 1$, $\frac{dW}{d\alpha} > 0$ for all α, the deformation mechanism dominates and the erosion rate curve displays behavior characteristic of brittle materials. For this case Neilson and Gilchrist replace the condition for determining α corresponding to a maximum erosion rate with the arbitrary selection of the value of α (denoted by β) corresponding to the erosion rate which is one-half the erosion rate for $\alpha=\pi/2$. Substituting this condition into Eq.(3.75) and (3.76) yields,

$$\frac{\cos^2\beta \sin n\beta}{1/2 - \sin^2\beta} = \frac{\Phi}{\Xi} \qquad \text{when } \beta \leq \alpha_o \qquad (3.79)$$

and

$$\frac{\cos^2\beta}{1/2 - \sin^2\beta} = \frac{\Phi}{\Xi} \qquad \text{when } \beta \geq \alpha_o \qquad (3.80)$$

The values of β are plotted in Figure 3.17 as a function of n and $\frac{\Phi}{\Xi}$ along with Eq.(3.78). To construct the empirical curve for experimental data displaying brittle response, steps 1 through 5 are used, however the experimental value of W_T corresponding to β is used with the known value of n to determine the value of Φ/Ξ from Figure 3.17.

Neilson and Gilchrist observe that Φ and Ξ are dependent on the particle impact velocity and particle shape but do not appear to depend on the particle size. It is obvious that many additional factors would influence Φ,Ξ, and n.

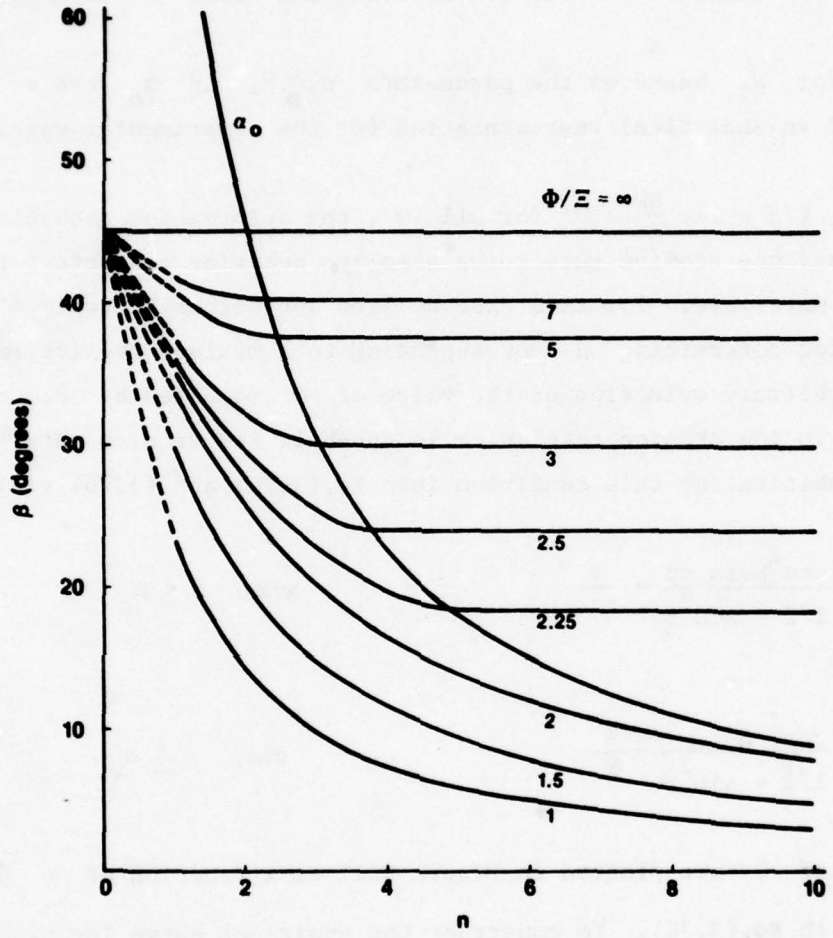

Figure 3.17. The Impingement Angle, β , at which the Erosion is One-half the Erosion at $\alpha=\pi/2$ as a Function of the Parameter n (Neilson and Gilchrist, 1968).

If the parameter κ is equated to Bitter's determination of the maximum velocity, V_e, for which the target material's response in elastic, then an explicit determination of κ can be made using Eq.(3.48). Typically the velocity V_e for ductile materials is quite small, so neglecting this effect is not very significant unless long-term erosion at very low velocities is of interest.

Prior to the publication of Neilson and Gilchrist, Wood (1966) simplified Bitter's Eq.(3.69) to the form

$$W = \frac{1}{2\xi}(V_o \sin\alpha)^2 + \frac{1}{2\phi}(V_o \cos\alpha)^2 \qquad \text{for } \alpha \geq 15° \qquad (3.81)$$

which he used to correlate his erosion data for impacts on metals when $15° \leq \alpha \leq 90°$. Wood evaluated the value of ε and ϕ for all of his test data which included six quartz dusts with different size distributions ranging from an average size of 3 to 50 μm, and nine metals, some with different heat treatments. Both impact velocity (122 to 244 ms^{-1}) and temperature (from ambient to 648°C (1200°F)) were varied. Wood found that the deformation wear factor ϕ and the cutting wear factor ξ do not show any correlation with the Knoop hardness or strain energy. A thirty-fold difference was represented in the hardness values for the target materials selected and a fifty-fold difference in strain energy. The factors ϕ and ξ did however display a dependence on particle size and temperature: the erosion resistance first increased with increasing temperature and then decreased as the temperature increased further.

3.6 Tabakoff and Co-workers

Tabakoff and his associates have studied and modeled solid particle flow trajectories through fairly complex turbomachinery (Clevenger and Tabakoff, 1974; Grant and Tabakoff, 1975; Tabakoff, et al., 1976; Tabakoff and Hamed, 1977; Wakeman and Tabakoff, 1979). Their more recent work examined the effects of solid particle erosion on gas turbine and compressor components. In order to model the multiple interactions a particle may have with the stationary and moving surfaces it encounters as it passes through a gas turbine for example, Tabakoff finds that it is necessary to investigate the rebound characteristics of the particle collisions represented by the coefficient of restitution (Ball and Tabakoff, 1974). The coefficient of restitution is taken to be a measure of the kinetic energy exchanged between the two colliding bodies which characterizes the particle/target interaction. The impact and rebound process is statistical in nature, so statistical distributions were obtained experimentally and empirical equations were fitted to the data. In order to complete the general model of turbomachinery erosion, it is necessary to prescribe the amount of material which will be removed by particle collisions (Grant and Tabakoff, 1973).

Tabakoff and his co-workers found that it was the coefficient of restitution defined in terms of the tangential components of the impact and rebound velocity which was related to the magnitude of the material removed: maximum erosion occurred in ductile metals when the coefficient of restitution for the tangential velocity components was minimum. They conjectured that the coefficient of restitution based on the normal components of the impact and rebound velocities represented the kinetic energy dissipated by plastic flow of the target material without significant material removel.

Let V_o be the magnitude of impact velocity and α the angle of inclination of the velocity vector to the surface as previously defined,

and V_r be the magnitude of the rebound velocity and β its inclination angle with the target's surface, then the tangential restitution ratio, R_T, is

$$R_T = \frac{V_r \cos \beta}{V_o \cos \alpha} \tag{3.82}$$

The experimental data for 410 stainless steel, Ti-6Aℓ-4V, and 2024 aluminum (Ball and Tabakoff, 1973; Grant and Tabakoff, 1973) indicated that

$$R_T \approx 1.0 - 0.0016\, V_o \sin \alpha \tag{3.83}$$

for quartz and alumina particle collisions.

The erosion data for 2024 aluminum (Grant and Tabakoff, 1973) was found to be described by the following equation

$$W = K_1 f(\alpha)\, (V_o \cos \alpha)^2\, (1-R_T^2) + K_3 (V_o \sin \alpha)^4 \tag{3.84}$$

where

$$f(\alpha) = \left[1+\psi\, (K_2 \sin 2\alpha_m) \right]^2 \tag{3.85}$$

$$\psi = 1 \quad \text{for } \alpha \leq 2\alpha_m$$

$$\psi = 0 \quad \text{for } \alpha > 2\alpha_m \tag{3.86}$$

The angle α_m is the impingement angle for maximum erosion, K_1, K_2, and K_3 are empirical constants, and R_T is determined from Eq.(3.83). Eq.(3.84) was formulated on the assumption that the erosion process is characterized by two erosion mechanisms: one dominant for small impingement angles and the other applicable for large impingement angles. It can be seen from Eq.(3.84) that the velocity dependence will be greater than the velocity squared for low angles of attack and that the velocity

exponent will be 4 when $\alpha=90°$. The velocity exponent of 4 was found to correlate the erosion test data for a 2024 aluminum alloy impacted by quartz particles (20 to 200 μm) for particle impacts ranging from 300 to 590 ms^{-1} (Grant and Tabakoff, 1973, 1975). For ductile metals this is a high exponent which illustrates the strong dependence on the test procedure and detailed characterization of the collision process, since Wood (1966) was able to show that his data for several metals including a 2017 aluminum alloy also using quartz particles with a maximum size of 50 μm correlated with a velocity exponent of 2 when $\alpha=90°$ as predicted by Bitter's correlation (Bitter, 1963a). Wood used the same values of the empirical constant ξ in Eq.(3.53) over a velocity range from 122 to 244 ms^{-1}. With this wide variation in the form of the correlation for normal collisions, the magnitude of the discrepancies possible between the test procedure used and the analysis of the erosive environment are evident. The consistency of the data reported by both investigators and that of others essentially rules out the possibility that these differences are the result of the material's actual response to the erosive environment.

The empirical constants were found for a number of cases (Grant and Tabakoff, 1975; Tabakoff, et al., 1979). For example, for quartz particles impacting 2024 aluminum these constants are $K_1=3.67\times10^{-6}$, $K_2=0.585$, and $K_3=6.0\times10^{-12}$ when the measure of erosion is in mg/gm of impacting particles (Grant and Tabakoff, 1973, 1975). A slightly modified form of Eq.(3.85) was used for correlating the experimental data obtained by Tabakoff, et al., 1979. There is no explicit dependence on the particle size in Eq.(3.84), however Grant and Tabakoff (1973) indicate there is a significant dependence on the specimen size used in the Tabakoff's wind tunnel facility. The specimen size influences the aerodynamics of the flow field in the test section. Increasing the specimen width decreased the erosion rate. The specimen size effect appears to be dependent on the impact parameters as reflected in the particle interactions at the surface and the nature of the flow field. Tabakoff has

not defined an absolute erosion rate for his experimental data but reports the specimen size with the erosion data. There does not appear to be a simple correlation between the test results obtained from specimens of different sizes.

Tabakoff's experimental facility, test procedures, data analysis, and general correlation all require further consideration, since they represent a significant departure from the more typical sand blast test procedures and data analysis. As stated in Section 2 a greater awareness is developing in solid particle erosion testing concerning the influence of the test parameters on the measured material removal rates. In this regard Tabakoff's work deserves more attention.

Menguturk and Sverdrup (1979) also were concerned with the effects of solid particle erosion in gas turbines. They introduced a generalization of Bitter's equations (Bitter, 1963a,b), Eq.(3.53) and (3.54), proceeding along the lines of Neilson and Gilchrist (1968), using the final forms given in Eq.(3.75) and (3.76), by raising the cutting wear and deformation wear terms to arbitrary exponents, m_1 and m_2, respectively. Neglecting the maximum normal velocity for elastic response and setting $m_1=m_2=m$, Menguturk and Sverdrup find

$$\begin{aligned} \upsilon &= K_1(V_o\cos\alpha)^m \sin n\alpha + K_2(V_o\sin\alpha)^m \quad \text{for} \quad \alpha \leq \alpha_o \\ \upsilon &= K_1(V_o\cos\alpha)^m + K_2(V_o\sin\alpha)^m \quad \text{for} \quad \alpha \geq \alpha_o \end{aligned} \tag{3.87}$$

where K_1, K_2, and m are empirical constants which have to be determined. As in Eq.(3.73) $n = \frac{\pi}{2\alpha_o}$. The procedure for determining the required constants is analogous to that outlined for evaluating Eq.(3.75) and (3.76).

3.7 Mamoun

Mamoun (1975a,b,c,d; 1976) developed estimates of material removal due to spherical particle impacts for both ductile and brittle materials using the Hertzian theory of impact and semi-empirical relations for the fatigue life as a function of strain amplitude. The ultimate objective of Mamoun's modeling study was to develop analytical predictions for the material removal and mechanical property degradation in components subjected to the erosion/corrosion environment associated with coal gasification. The material response was categorized as follows: ductile materials at load levels below the elastic limit (case 1), fully plastic deformations in nonstrain-hardening materials (case 2) and strain-hardening materials (case 3), elastic-plastic deformations (case 4), brittle materials at load levels below the fracture threshold (case 5), and brittle materials above the fracture threshold (case 6). Only the erosion due to normal impacts by spherical particles is considered in the published reports, however analyses for oblique impacts of angular particles have apparently been formulated but remain unpublished (Mamoun, 1979). Thus only the general relations for normal impacts will be outlined here.

The approach used by Mamoun is based on the general assumptions that the impact event is represented by a quasistatic loading condition and that the deformations during the collision are small. The quasistatic condition is hypothesized to be valid if the impact duration is at least four times longer than the natural period of the impacting sphere. For the case of a char or ash particle impacting a steel plate the impact velocity for which quasistatic conditions pertain is on the order of 600 ms^{-1}. The magnitude of the deformations is estimated from the condition that the distance q the two bodies approach each other be less than one-fourth the radius of the impacting sphere. The range of conditions evaluated for the fully plastic case when a char sphere impacts a steel plate shows this condition pertains for impact velocities ranging from 90 to 245 ms^{-1}. On the basis of this comparison Mamoun

concludes that his approach is valid for typical coal gasification conditions where the flow velocities would not be expected to exceed 90 ms^{-1}.

The limitation on the impact conditions encompassed by the results of the model is arbitrarily based on a factor of four and the bounds are established in terms of the analysis which is being evaluated. The hypothesized response of the particle collision may be somewhat distinct from the purely elastic properties assigned to the particle without fracture or crushing being a possibility. The imposed impact velocity constraint requires more adequate substantiation.

Continuing with Mamoun's straightforward mechanics analysis of the erosion problem, the volume of material removed for the six material response regimes previously enumerated will be described. The multiple particle effects are taken into account in terms of a fatigue process for all of the cases considered except for case 6: single particle fracture of brittle materials. The volume removed is expressed in the general form

$$\text{volume loss/impact} = v/N_f \tag{3.88}$$

where v denotes the elemental volume removed and N_f is the number of impacts required to remove this volume. The volume removed is estimated on the basis of assumptions made with regard to the material's response in a multiple impact environment and the number N_f is taken to be the fatigue life for the material determined for uniaxial stress loadings. N_f is thus prescribed in terms of semi-empirical fatigue relationships. Some examples follow. The details of Mamoun's calculations are quite lengthy and parallel the work of Bitter in many aspects of the Hertzian theory; only the general form of the results will be reported here.

For case 1, when V_o is less than the threshold velocity for yielding to occur, Mamoun suggests that microslip takes place producing fatigue cracks which eventually reach a depth of $0.5\, a_{max}$, where a_{max} is the maximum contact radius for a sphere impacting an elastic half-space (Appendix A). Mamoun assumes the elemental volume removed is then equal to a semiellipsoid, which is equivalent to Eq.(B4) if $a_{max} << 1$,

$$v = \frac{1}{2}\left(\pi a^2_{max}\right)\left(\frac{a_{max}}{2}\right) \tag{3.89}$$

and for purely elastic deformations

$$N_f \approx \left(\frac{1}{2H}\, P_{max}\right)^{1/q} \tag{3.90}$$

where P_{max} is the maximum pressure in the Hertzian pressure profile (obtained from Eq.(A4) and Eq.(A35) for spherical body impacts), and H and q are experimental fatigue constants which depend on the target material. The final expression for the volume removed per impact is completely deterministic when the parameters H and q are prescribed (refer to Table 3.2).

$$\upsilon_e = f(H,\nu_1,\nu_2,E_1,E_2\rho_1)\; R^3\; V_o^{\left(\frac{6q-2}{5q}\right)} \tag{3.91}$$

where ρ_1 is the density of the sphere of radius R impacting at a velocity V_o, and E_1, E_2, ν_1, ν_2 are Young's moduli and Poisson's ratios for the sphere and the half-space, respectively.

The volume removed per particle impact for a fully plastic collision is determined from the total kinetic energy imparted to the target by the impacting sphere. The sphere does not rebound from the surface for this impact condition. The volume removed per impact, υ_p, is estimated to be

TABLE 3.2. Constants Employed in Determining the Critical Number of Impacts.

Type of Material	CONSTANTS			
	q	H	s	I
AISI 4130 (soft)	-0.0577	0.00884	-0.627	1.1397
AISI 304 (hard)	-0.132	0.02715	-0.693	0.9765
AISI 4340 (hard)	-0.0996	0.02041	-0.596	0.7482
AISI 4340 (annealed)	-0.0626	0.00824	-0.538	0.6245
AISI 52100	-0.0692	0.02376	-0.563	0.2373
AISI 4130 (hard)	-0.0529	0.01258	-0.693	1.1155
AISI 310 (annealed)	-0.127	0.01124	-0.567	0.8128
Inconel X	-0.138	0.0239	-0.708	1.1679
Titanium 6Al-4V	-0.130	0.0405	-0.738	1.5453
Beryllium	-0.0655	0.00314	-0.353	0.02541
1100 Aluminum	-0.0506	0.00278	-0.685	2.258
2014-T6 Aluminum	-0.12	0.02794	-0.649	0.5296

$$\upsilon_p = \frac{1}{N_f}\left(\frac{1}{2} m_1 V_o^2\right)\frac{1}{\sigma_f} \tag{3.92}$$

where N_f is the fatigue life of the target material in terms of the plastic strain amplitude and σ_f is the plastic flow stress. Mamoun uses the fatigue relations

$$N_f = \left(\frac{\Delta\xi_p}{I}\right)^{1/s} \qquad \text{for } \Delta\xi_p < I \tag{3.93}$$

$$= 10 \qquad \text{for } \Delta\xi_p > I \tag{3.94}$$

where I,s are constants for a given material. Representative values are listed in Table 3.2.

According to Mamoun's definition of the plastic strain amplitude,

$$\Delta\xi_p \approx 0.2\left(\frac{a_{max}}{R}\right) \tag{3.95}$$

and in view of the magnitude of the values for I listed in Table 3.2, the condition that $\Delta\xi_p > I$ is only possible when $a_{max} > R$ which is physically unrealistic. Thus, in contrast to the expressions derived by Mamoun using Eq.(3.92) to (3.94), it is only necessary to consider Eq.(3.92) and (3.94) which would only exclude the erosion of beryllium except for very small deformations. In order for Eq.(3.95) to be consistent with Mamoun's criterion for small deformations, $\Delta\xi_p \leq 0.14$.

For strain-hardening materials, Mamoun finds

$$\upsilon_{ph} = f(\rho_1, I, n)\left(\frac{1}{\sigma_f}\right)^{\frac{4s-1}{s(4+n)}} R^3 V_o^{\frac{2(4s-1)}{s(4+n)}} \tag{3.96}$$

where n is the strain-hardening exponent. The expression in Eq. (3.96) reduces to the nonstrain-hardening condition (case 2) when $n=0$.

A simple but inadequate modification of Eq. (3.96) is used for treating elastic-plastic deformations (case 4). This is the condition which Bitter investigated. Mamoun also investigated material removal due to normal collisions by spherical bodies on brittle materials (cases 5 and 6) which will be described in Section 4.

The final expressions for the volume removed per impact in Eq. (3.91) and (3.96) show that the volume removed is directly proportional to the mass of the impacting sphere (R^3 dependency) but the velocity exponent is a function of the fatigue characteristics of the target material. The range of velocity exponents for elastic and fully-plastic, non-strain-hardening ($n=0$) materials will be considered using the data provided in Table 3.2.

For the elastic case, $-0.138 \leq q < -0.05$. The velocity exponent in Eq. (3.91) therefore ranges from 4.2 to 9.2: the lower value corresponds to Inconel X and the higher value to 1100 aluminum. These values would appear to be fairly high, although the magnitude of the coefficient obtained by evaluating the function f would have to be determined. In addition, the range of application for these equations for ductile metals is only on the order of 10 ms^{-1} at which point plasticity effects become dominant. For the nonstrain-hardening fully plastic case the fatigue parameter s has a smaller range, $-0.738 \leq s \leq -0.538$, excluding beryllium. The velocity exponent according to Eq. (3.96) when $n=0$ ranges then from 2.68 to 2.93. The introduction of the work-hardening parameter n would bring the computed velocity exponents within the range of values typically quoted for ductile metals. The comparison is interesting but will require more definitive confirmation.

The analytical predictions for spherical particles impacting normal to the target's surface are compared with hard angular particle impacts (silicon carbide and alumina particles) impacting normal but in some cases oblique impacts are included in the limited data base Mamoun claimed was available at the time (Mamoun, 1975d, 1976). A more extensive literature survey would have revealed a somewhat expanded amount of experimental results. The materials for which erosion data was reported are 304 and 310 stainless steel (annealed) and 1100 aluminum. The previously determined volume losses are converted to mass loss per mass of impacting particles. However, Mamoun notes that only a percentage of the stated mass of impacting particles actually impact the specimen: this percentage ranges from 33 to 50%. Mamoun's reasoning is that particle-particle collisions occur as well as a particle shielding effect which takes place at the face of the target as illustrated by Moore (1968). The incoming particles collide with the particles rebounding from the surface for near normal impacts and may therefore impact the surface along a different trajectory and impact velocity than assumed in the experiment or not at all. However the specific determination of the magnitude of these effects would have to be based on the manner in which the experiment was conducted and the particle concentration in the flow field. The comparison between experiment and theory is quite tenuous and certainly requires further support before any conclusions can be drawn regarding the merits of Mamoun's approach.

3.8 Head and Co-workers

After completion of an extensive testing program (Head, et al., 1967), Head and Harr (1970) attempted to develop a model applicable to natural soils which included consideration of the energy transferred from the impinging particles to the target, the nature of the response of the target, and the nature of the erosive agent including pertinent descriptors of composition, angularity, hardness, and size distribution. The result of this effort was the development of a weighted regression

analysis program (WRAP model) in which

$$A = f\left(\frac{V^2}{E}, R, \sin\alpha, \cos\alpha, \frac{H}{E}, \frac{B}{E}\right) \tag{3.97}$$

where A is the erosion rate measured in volume removed per unit mass of dust, V is the effective velocity of the mix, R is the effective roundness of the dust particles, α is the particle impingement angle, B is the hardness of the target, and E is the erosion resistance per unit volume of target. Head and Harr use the effective parameters which they define as the sum of the parameters associated with the individual size components of the dust weighted on the basis of the grain-size distribution of the dust. A number of different materials were eroded with four test dusts with a particle size distribution ranging from 10 to 120 μm to supply the data base for the statistical analysis. A different form of interaction between the dependent variables was found for brittle and ductile materials.

The erosion resistance of the target material was measured by simple expressions of the form

$$E = f(\alpha, B, MT) \tag{3.98}$$

where

$$MT = \varepsilon_u\left(\frac{\sigma_{yp} + \sigma_u}{2}\right) \tag{3.99}$$

is the modulus of toughness determined from a uniaxial tension test. The stress and strain at rupture are denoted by σ_u and ε_u, respectively, and σ_{yp} is the yield point stress determined at 2% offset. The uniaxial data was obtained for the metallic specimens at a strain rate of 0.05 in/min up to the yield point and then the strain rate was increased to 0.1 in/min until rupture occurred. For brittle elastic materials, such as glass, the value of MT is determined by assuming a

value of σ_{yp} and ε_u. For this case, it appears that Head and Harr let

$$MT = \frac{1}{2} \varepsilon_u \sigma_{yp} \tag{3.100}$$

where $\varepsilon_u = 0.001$ in/in and $\sigma_{yp} = 10^3$ psi (69 MPa).

The basic concept behind this approach which was considered in earlier work (Finnie, et al., 1967) is that the resistance of the target material to erosion was proportional to the hardness of the material for small impingement angles and to its ability to absorb energy as represented by the modulus of toughness at normal impingements. This idea is most simply represented by a straight line variation

$$E = B - \frac{2\alpha}{\pi} (B-MT) \tag{3.101}$$

Four versions of the model were formulated based on the parameters appearing in Eq. (3.97): two for brittle materials and two for ductile materials. The model is simply a statistical correlation of the test data generated by Head and his colleagues without any consideration for the mechanism for material removal. The data base for brittle materials was not too extensive; the simpler step-wise regression analysis indicated the particle shape factor, R, was not significant and that the erosion rate increased as the erosion resistance of the target, E, increased. The stepwise regression analysis fitted the available data for ductile materials quite well; however, although the parameters appearing in the final expression followed physically reasonable trends, the erosion rate showed an even stronger correlation for increasing as the target's erosion resistance increased. The resulting expressions are

$$A_{BS} = V^{3.06} \alpha^{2.69} H^{2.08} E^{0.03} B^{-3.64} \tag{3.102}$$

for the stepwise regression analysis for brittle materials, and

$$A_{DS} = V^{4.34}\ \alpha^{0.46}\ H^{0.10}\ E^{0.21}\ B^{-2.48} R^{-2.84} \qquad (3.103)$$

for the stepwise regression analysis of ductile materials. The velocity exponent is 3.06 for brittle materials and 4.34 for ductile materials which is highly inconsistent with the most of the erosion data from other sources where the velocity exponent for brittle materials is higher than that for ductile materials for which the velocity exponent typically falls in the range from 2 to 3.

A weighted regression analysis (WRAP model) was then carried out for both ductile and brittle materials. The WRAP model indicated that the volume removed would decrease as the erosion resistance increased. For brittle materials the volume loss is weakly dependent on the impact velocity with a velocity exponent of two. For ductile materials the volume removal is fairly strongly dependent on the impact velocity to the fourth power.

The erosion rates obtained previously for stainless steel, 17-4PH (AMS5643) heat treated to a hardness of RC38, using three natural dusts and silica flour (Head, et al., 1967) were used as a basis for evaluating the WRAP model predictions. The particle shape factor, R values were not available for the three test soils: only for silica flour. The roundness parameters for the test soils were calculated from Eq.(3.103) for each value of α and the values of R averaged over the number of impact angles. The effective particle velocities and effective particle hardnesses were computed and the erosion rates calculated from the WRAP expression for ductile materials. The predicted and observed erosion rates agreed within a factor of two and showed the same general trend for impingement angles between 15 and 75° for three natural soils, but the values at 90° were significantly in error. The predictions of the WRAP model for silica flour using a properly evaluated shape factor showed the closest agreement with the test data for impingement angles

AD-A073 034 EFFECTS TECHNOLOGY INC SANTA BARBARA CA F/G 11/6
ASSESSMENT OF THE STATE OF KNOWLEDGE PERTAINING TO SOLID PARTIC--ETC(U)
JUN 79 W F ADLER DAAG29-77-C-0039
UNCLASSIFIED ETI-CR79-680 ARO-14980.1-MS NL

2 OF 2
AD
A073034

END
DATE
FILMED
9 79
DDC

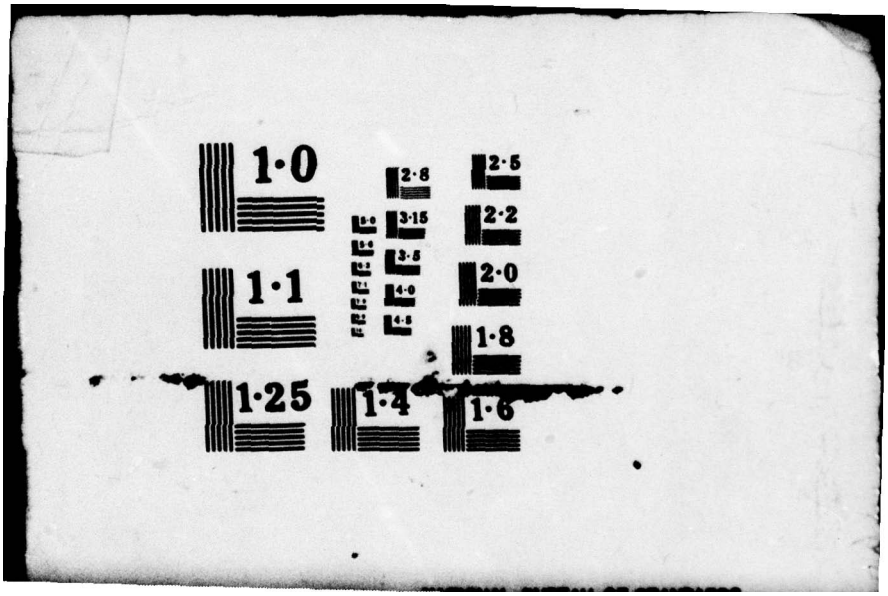
1·0
1·1
1·25
2·8
3·15
3·5
4·0
1·4
2·5
2·2
2·0
1·8
1·6

between 15 and 75°, however the trend in the predicted and observed results is definitely reversed in terms of the curvature of the two curves. Head and Harr consider the agreement to be quite good noting that the predicted curve yields a maximum erosion rate for an impingement angle of 30° while the experimental data, according to them, indicates the maximum erosion rate occurs at 15°. This is a surprising comparison since no maximum erosion rate has been established for the experimental data: the curve is still increasing monotonically at 15°. The data reported by Head and Harr (1970) for the erosion of 17-4PH stainless steel by silica flour displays a similar trend as the predicted curve but the erosion rates are approximately twice as large. The erosion tests carried out by Head and Harr (1970) appear to have been carried out using a different sand blaster than used by Head, et al. (1967), although both erosion apparatus had an 8 mm ID blast tube. This comparison does not evaluate how well the velocity dependence is predicted or if the target material properties selected, hardness and toughness, can adequately differentiate the erosion response of one material from another.

The predictive capability of the WRAP model was subsequently evaluated for two ductile metals (type 302 stainless steel and 6061-T6 aluminum) eroded by 220 mesh (68 μm) alumina particles and 220 mesh fluorite particles (Head, et al., 1973). When the model was adjusted for a higher maximum particle velocity, 300 ms^{-1} as opposed to 185 ms^{-1} in the earlier work imparted by the carrier gas and changes in the dimensions of the blast tube, agreement between the model predictions and the experimental data for alumina particles is claimed for impingement angles between 20° and 60° with good estimates of the maximum erosion rate; however, the general trend of the model predictions and the experimental data as a function of impingement angle show little resemblance to each other. The comparison is less encouraging for fluorite particles where the predicted maximum erosion rates underestimate the actual values by a factor of two for the stainless steel and a factor of four for the aluminum alloy. It is interesting to note that the fluorite particles with a Moh hardness of 4.0 and higher particle roundness

than the alumina were significantly more erosive than the alumina particles with a Moh hardness of 9.0. In the case of 6061-T6 aluminum, there is nearly an order of magnitude difference in the measured erosion rates for these two particles. The WRAP model predicts that the erosion rate increases with particle hardness and roundness. There does not appear to be a sound technical basis for the modified WRAP model; the results are simply adjusted to match the magnitude of the WRAP predictions with the experimental data. Evidently, there are other factors which must be taken into account with regard to particle characterization and testing procedures which have not been identified by Head and his colleagues.

The statistical analyses developed by Head and his co-workers are significant in that this is the only erosion modeling effort which addresses erosion due to a distribution of particle sizes rather than carefully graded particulates generally used in erosion investigations.

3.9 Correlations with the Thermal Properties of the Target Material

Several general correlations relating to the thermal properties of the target material have been proposed. The validity of these correlations has typically been determined by comparison to the erosion resistance for a number of pure metals determined by Finnie, Wolak, and Kabil (1967). The original correlation with Vickers hardness will be described and then the thermally-based correlations will be summarized.

Finnie's theory of ductile erosion indicates that the erosion resistance is inversely proportional to the flow stress, σ_F, of the material [refer to Eq.(3.30) and (3.31)] which is directly related to a measure of hardness. The experimental results of Finnie, Wolak, and Kabil (1967) for various pure metals (and some steels) are reproduced in Figure 3.18. Note that on this log-log plot there are two distinct and parallel "lines," both having a slope which represents a direct proportionality between erosion resistance and Vickers hardness. The one line,

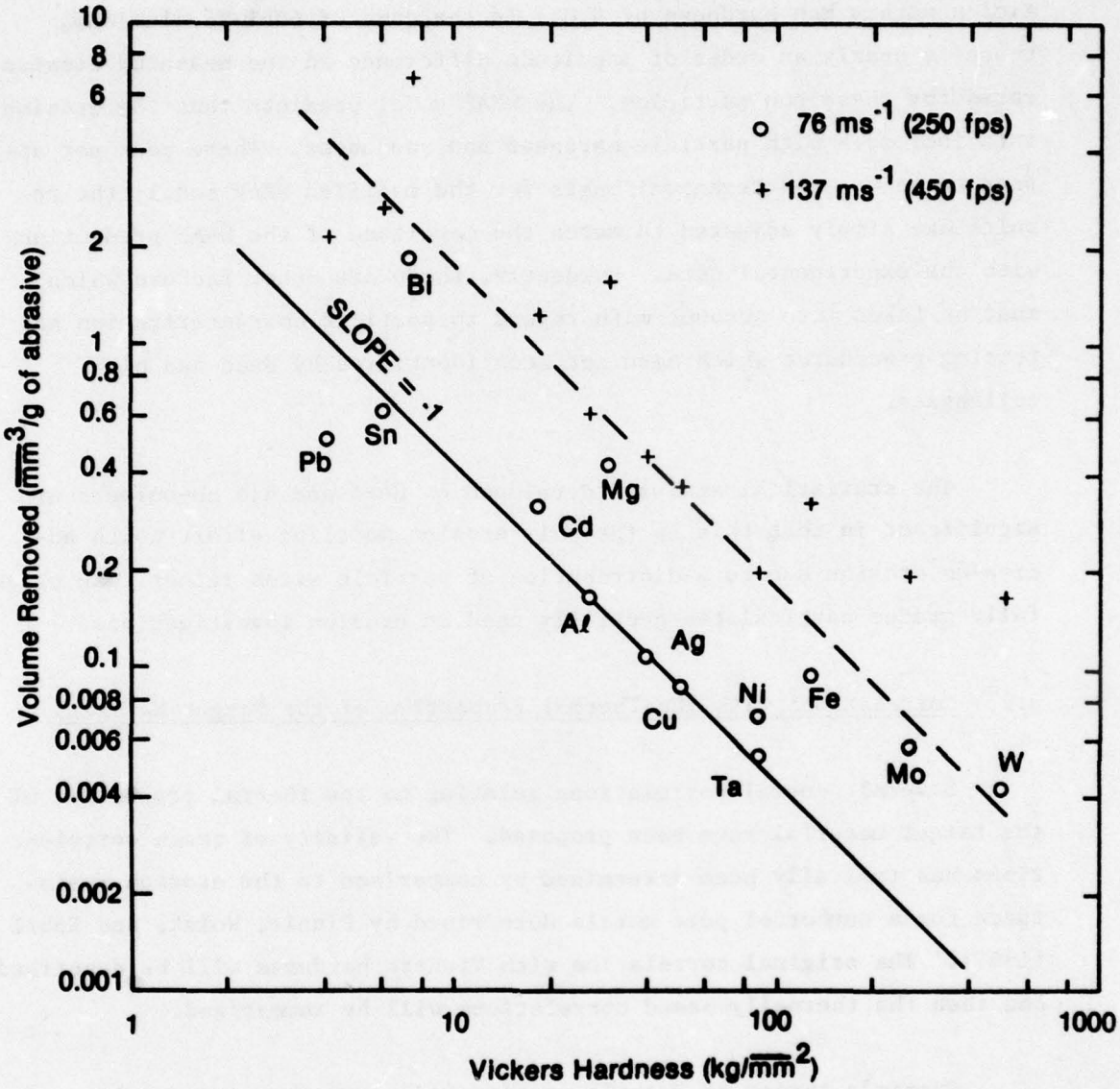

Figure 3.18. Volume Removed as a Function of Vickers Hardness. Metals Eroded by 250 μm (60-mesh) Silicon Carbide Particles at $\alpha=20°$. All Metals except Cadmium were in an Annealed Condition. (Data from Finnie, Wolak, and Kabil, 1967).

which the authors regard as the "main trend," is established by tin, aliminum, silver, copper, tantalum and (with slight deviation) by cadmium and nickel. The other "line" can be imagined to pass through or close to the points for bismuth, magnesium, iron and molybdenum, and represents a resistance about one-third that of the "main trend," for the same hardness. Tungsten exhibits an even worse resistance relative to hardness, although it is the most resistant on an absolute level. Lead, on the other hand, is the most resistant relative to hardness. The authors propose explanations for these results in terms of the microstructure, work-hardening properties and dynamic properties of the various materials, and make comparisons with corresponding results from abrasive wear tests. Goodman, Tilly and Sage (1969) have shown that hardness in combination with other properties may provide some correlation for the erosion resistance of alloys.

Finnie, Wolak, and Kabil (1967) also investigated the effect of prior work-hardening on the erosion resistance of several pure metals and found no effect. Furthermore, the hardening by heat-treatment of several steels not only showed no beneficial effect, but actually reduced the erosion resistance slightly. The lack of improved erosion resistance through coldworking and heat treatment of alloys was also found by Smeltzer, et al. (1970), and to a lesser extent by Sheldon and Kanhere (1972). Eq.(3.30) and (3.31) predicts that the annealed specimens with lower flow stresses should erode three to four times more readily than the heat treated specimens. Instead the difference in erosion rates for the annealed and heat treated specimens was less than five percent in all cases.

Smeltzer, et al. (1970), purportedly observed evidence for target material melting based on microscopic examinations of the eroded surfaces of several alloys [2024 Aluminum (annealed), 410 stainless steel, and Ti-6Aℓ-4V (annealed)]. They provide a simple calculation to demonstrate that the kinetic energy for a representative particle and impact

condition is more than sufficient to melt the volume of material (based on pure iron) they believe is removed by this process. Smeltzer and co-workers define two mechanisms (Smeltzer, et al., 1970, p. 216):

> Mechanism 1 (Melting and splattering) - Corner-oriented particle impacts are sufficient to cause localized target melting in the crater region and subsequent spraying or splattering of micron-size droplets of molten and semimolten target metal into the gas stream under the high pressures generated by impact. Below the threshold energy for erosion, there is insufficient energy available for significant metal melting and/or splattering. Metal splattering would be most feasible (reasonable) for the corner-oriented impact, where the particle is decelerated over the smallest total contact area, promoting most intense heat buildup, maximum pressurization, and maximum opportunity for target liquating and spraying.
>
> Mechanism 2 (Melting, bonding, and dislodgement) - Corner-oriented particle impacts also result in broken particle corners being embedded (mechanically bonded) in the impact craters they formed. This bonding is a transient condition; most particles subsequently are extracted from the craters with whatever residual energy they possess or by subsequent particle impacts. But in the extraction process, some bonded target metal may adhere to the particle surface and be removed.

Smeltzer and co-workers could not establish the relative contributions from each of these mechanisms to the total erosion rate but included both mechanisms in an empirical correlation based on the idea that the material removal rate was proportional to the particle kinetic energy. They assume that a percentage of the impacting particles will terminate their trajectories while in contact with the surface of the target and thereby transfer all of their kinetic energy into localized melting of the target. The amount of material melted, W, expressed in

mg/g of impacting particles, is given by the expression

$$W \equiv \phi(\alpha) \frac{V_o^2}{2Q} \tag{3.104}$$

where V_o is the impact velocity, Q is the energy required to heat and melt one gram of target, and $\phi(\alpha)$ is the probability that a particle impacting the target at an angle α will be snagged by the target. The energy Q required for melting one gram of target material may be calculated from the equation

$$Q = C_p \Delta T + H_F \tag{3.105}$$

where C_p is the specific heat of the target, H_F is the heat of fusion of the target, and ΔT is the difference between the actual target temperature and its melting temperature. Smeltzer, et al., assume

$$\phi(\alpha) = \phi(90°)\sin\alpha \tag{3.106}$$

Since the major portion of the melted material is generated in the vicinity of point P (Figure 3.19) on the crater-particle interface, maximum liquation is assumed to occur in the vicinity of the corner of the particle. A portion of the molten material is squeezed out of the vicinity of point P . The amount of material removed by mechanism 1 is estimated to be

$$W_1 = \eta\psi(\alpha)\, W \tag{3.107}$$

where η is the fraction of splattered material which actually escapes from the crater, and

$$\psi(\alpha) = 1 - \sin\alpha \tag{3.108}$$

is the probability for splattering of the molten material at point P .

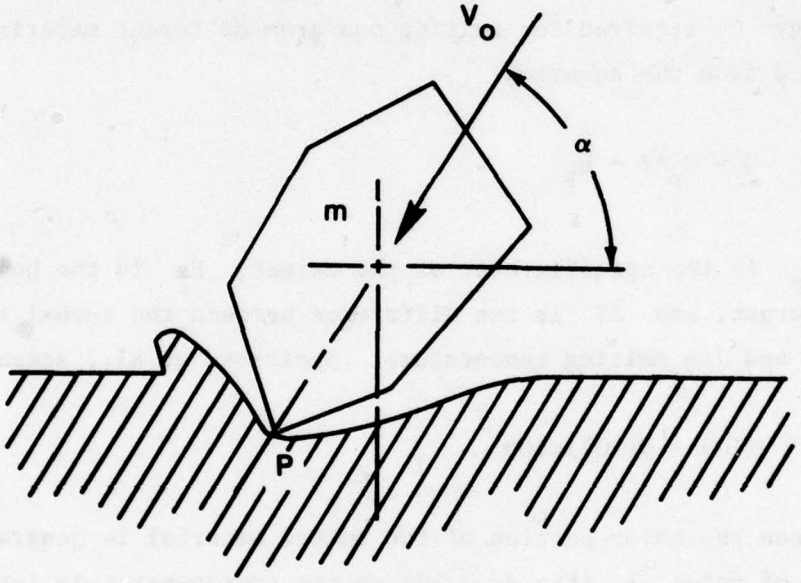

Figure 3.19. Idealized Condition within Impact Craters for Localized Melting due to Corner-Oriented Particle Collisions Suggested by Smeltzer, et al., 1970.

Since $\psi(\alpha)$ is the probability for splattering of the melted material, then $1-\psi$ is the probability that the melted material will remain in the vicinity of point P, and $(1-\psi)W$ represents the amount of target material remaining at the interface. Then

$$W_2 = \zeta[1-\psi(\alpha)]\, W \tag{3.109}$$

where ζ is the fraction of the remaining melted material which is removed in accordance with mechanism 2.

The final form of the correlation is simply the sum

$$\begin{aligned} W_T &= W_1 + W_2 \\ &= \frac{K_1}{2} V_o^2 \left[(1-\sin\alpha)\sin\alpha\right] + \frac{K_2}{2} V_o^2 \sin^2\alpha \end{aligned} \tag{3.110}$$

where

$$K_1 = \frac{\eta\phi(90°)}{Q}, \quad K_2 = \frac{\zeta\phi(90°)}{Q}$$

It is seen from Eq.(3.110) that no material will be removed when $\alpha=90°$ unless mechanism 2 is introduced.

The constants K_1, K_2 are evaluated from the experimental data for W_T as a function of α. When $\alpha=90°$,

$$K_2 = \frac{2W_T(\text{exp})}{V_o^2} \tag{3.111}$$

Knowing K_2, K_1 is determined by fitting the first term on the right-hand side of Eq.(3.110) to the difference

$$W_T(\text{exp}) - \frac{K_2}{2} V_o^2 \sin^2\alpha \qquad (3.112)$$

using K_1 as an adjustable constant. The coefficients K_1 and K_2 are evaluated for the alloys evaluated. It is interesting to note that the maximum erosion rates in the experimental data occur for $30° < \alpha_m < 40°$ in contrast to the predictions of Finnie's model and experimental data of Finnie, Wolak, and Kabil, 1967.

Smeltzer, et al. (1970) provide a brief discussion of the relation of K_1 and K_2 to more fundamental properties of the target material. They indicate that, when the erosion loss for pure metals [the erosion data of Finnie, Wolak, and Kabil (1967)] is plotted against such target material properties as Young's modulus, absolute melting temperature, heat required for melting a unit mass Q in Eq.(3.105), and liquid metal surface tension, they all yield the correct relative ranking of the erosion resistance but without a high degree of absolute predictability. They suggest that erosion might occur simply from decohesion of the target material.

Ascarelli (1971) improved the correlation of erosion resistance and the melting point temperature suggested by Smeltzer, et al. (1970) by defining the thermal pressure for pure metals. Ascarelli notes that according to Finnie's analysis the volume removed per particle impact can be written in the form

$$\upsilon \approx C \frac{1}{2} m V_o^2 f(\alpha) \qquad (3.113)$$

where C is a constant dependent on the material properties of the target material, has the dimensions of the inverse of an energy density or pressure, and is proportional to the volume removed per unit energy of the impinging particles. In order to determine the explicit material

dependence of C , Ascarelli introduced the concept of target melting suggested by Smeltzer and co-workers but did not prescribe a specific mechanism by which material is removed except that the melted material will be carried off by the stream of impinging particles. He observes that while large plastic deformations do occur as part of the erosion process, they may contribute little to the actual volume removal mechanism. This is the motivation for attempting to correlate erosion resistance with the physical properties of the target material which, even without a detailed analysis of the mode of material removed, may be simply related to such properties as crystal structure, compressibility, melting point, thermal expansion, and elastic constants.

These observations led Ascarelli to define the thermal pressure as being representative of the pressure corresponding to the localized region within the crater being produced by large plastic deformations which reaches the melting point of the target material. Then

$$C \propto p_T \equiv \frac{\alpha_t (T_m - T_o)}{\chi} \tag{3.114}$$

where

α_t is the linear coefficient of expansion

T_m is the melting temperature

T_o is the temperature of the test

χ is the isothermal compressibility

By introducing the concept of thermal pressure, Ascarelli states that isothermal compressibility is the primary parameter characterizing the erosion resistance of both brittle and ductile metals.

A comparison is made of the volume removed determined by combining Eq.(3.113) and (3.114) with the experimental data of Finnie, Wolak, and Kabil (1967) where $\alpha = \alpha_m$. The experimental data falls within $\pm$ 25% of

the predicted values for volume removal.

Ascarelli also considered the form of the function $f(\alpha)$ in Eq.(3.113) which he relates to the surface roughness which evolves as part of the erosion process. The derivation of Eq.(3.107) is generalized accounting for surface roughness. The final form of Ascarelli's expression for volume removal is

$$\upsilon \propto \frac{0.5m\, V_o^2}{\alpha_t (T_m - T_o)/\chi}\, f(\theta) \tag{3.115}$$

where

$$f(\theta) = \frac{\sin(2k\sin^2\theta)\ (2\cos^2\theta - 1)}{4k\sin^2\theta} + \frac{\sin(k\sin^2\theta)}{k\sin\theta} - \frac{1}{2} \tag{3.116}$$

The angle θ replaces α as the impingement angle and is defined as the actual angle of impingement between the particle and the eroded surface where $\theta-\theta^* \leq \theta \leq \theta+\theta^*$ is taken to be spread in the values of the actual impingement angle. k is an empirical roughness parameter which has to be determined from the experimental data when $\alpha=90°$ which Ascarelli indicates is inversely proportional to the ductility of the material. It is seen that using Eq.(3.115) eliminates the need for introducing Smeltzer's mechanism 2, Eq.(3.109), which yields a non-zero value of the material removed for normal collisions, since this condition is accommodated in Eq.(3.116) when $k \neq 0$. When $k=0$, Eq.(3.109) results.

Ascarelli (1971) suggests that the temperature dependence of erosion results from the competition of two contrasting effects. The first is that the ductility of metals increases with increasing temperature which leads to larger deformations (for constant impinging particle velocity) and reduces the probability of energy localization. However, this is contrasted by the reduced energy necessary to get a region of the metal to the melting point. He indicates that due to the difficulty

in predicting or describing the ductility of metals, it is indeed a difficult problem to make predictions for the temperature dependence of erosion for temperature larger than say $0.5\,T_m$. According to Ascarelli temperature dependent erosion behavior should be similar to the temperature dependent behavior of the shear modulus or of Young's modulus. Brauer and Kriegel (1965) and Truitt (1974) found some correspondence between erosion resistance and Young's modulus for certain metals and alloys.

The experimental work of Jennings, et al. (1976), supported the possibility for target melting previously reported by Smeltzer, et al. (1970). Following a procedure similar to that used by Head and Harr (1970), they obtained the following correlation between the target volume loss per unit mass of impacting particles, A, and the properties of the target material.

$$A = \left[\frac{K_T^{5/2}}{R} \cdot \left(\frac{G^{1/3}}{\rho^{1/3}\, k T_m\, \Delta H_m} \right) \right] S \qquad (3.117)$$

where

K_T is the kinetic energy transferred from the impacting particles to the target per unit mass of particles

R is the particle roundness parameter

G is the gram molecular weight of the target

ρ is the density of the target

k is the thermal conductivity of the target

T_m is the melting temperature of the target

ΔH_m is the enthalpy of melting for the target

S is a dimensionless scaling factor coupling the calculated values with the erosion facility.

Comparisons with the experimental data are provided but will not be considered here.

The kinetic energy transferred expressed as

$$K_T = \frac{V_o^2}{2}(1-e^2) \quad , \tag{3.118}$$

where e is the coefficient of restitution, was evaluated by examining photographic records of the incoming and rebounding particles. The average conditions were estimated, however the detailed statistical analyses undertaken by Tabakoff and his co-workers (Grant and Tabakoff, 1973; Ball and Tabakoff, 1974) were not pursued. A constant velocity exponent of five results when Eq.(3.118) is substituted into Eq.(3.117) which is considerably in excess of any of the experimental values reported for ductile metals. This observation should be kept in mind in relation to the sensitivity of the model verification provided by Jennings, et al. (1976).

In contrast to Smeltzer, et al. (1970), Jennings et al. (1976) acknowledge that material removal is occurring by both mechanically and thermally activated processes, although they cannot determine the portion of the volume removed which should be contributed to each of these processes. In addition to the evidence they claim is observed in support of material melting based on microscopic examination of eroded surfaces, they note that the erosion rates for ductile materials do not change appreciably beyond a material-dependent level of the kinetic energy. After this condition is reached the impact velocity as well as the particle shape are ineffectual in modifying the volume loss.

Hutchings (1975) finds that the data of both Finnie, Wolak, and Kabil (1967) and that of Tadolder (1966) for pure metals can be correlated with the product

$$C\rho(T_m - T_o) \tag{3.119}$$

where C is the specific heat of the material at room temperature

ρ is the density of the target material.

Hutchings states that the one set of data (Finnie, Wolak, and Kabil, 1967) can be fitted within the limits indicated by Ascarelli in terms of the thermal pressure, Eq.(3.114), but that comparable agreement is not found for Tadolder's (1966) results. The relation in Eq.(3.119) compares more favorably with the expanded data base. For pure metals Vijh (1976) demonstrated that the same erosion data correlated with the inverse of the atomic bonding energies representative of the cohesion of the metals tested. These correlations are for pure metals; modified relations would be required for metal alloys.

Jennings, et al. (1976), among others, point out the general observation in solid particle erosion that the macro-mechanical properties of the target do not significantly affect the erosion behavior of ductile materials. However, in view of the above, there does not seem to be a shortage of thermal and physical material properties which show a correspondence with the erosion data.

4.0 EROSION CORRELATIONS AND ANALYSES: BRITTLE MATERIALS

In recent years the fracture morphologies in ceramics associated with indentation and impact by both spherical and angular particles have been investigated in some depth. The current view of particle impingement on brittle ceramics divides the fractures produced into two distinct categories: the elastic response regime and the elastic-plastic response regime.

The elastic response regime is characterized by segmented circumferential cracks surrounding the impact site analogous to the Hertzian cone cracks in glass when impacted or indented with a spherical body. Investigations of these characteristic cone-shaped cracks in glass are fairly extensive (for example, Tillett, 1956; Benbow, 1960; Tsai and Kolsky, 1967; Oh and Finnie, 1967; Fisher, 1967; Frank and Lawn, 1967; Hamilton and Rawson, 1970; Evans, 1973; Knight, Swain, and Chandhri, 1977; Chaudhri and Walley, 1978; Kirchner and Gruver, 1978).

The fractures characteristic of the elastic-plastic response regime are typically produced by pointed indenters or angular particle impacts. Evans and Wilshaw (1976) indicate that for spherical indenters of small radii the elastic-plastic regime applies and the hardness of the target is the controlling material parameter. For radii above a critical value the Hertzian fracture analysis is appropriate and the controlling material properties are the fracture toughness and the surface flaw size distribution. The fracture sequences are material dependent and have been described in a number of papers (Tsai and Kolsky, 1967; Lawn and Swain, 1975; Lawn, Swain, and Phillips, 1975; Lawn and Fuller, 1975; Swain and Hagan, 1976; Evans and Wilshaw, 1976, 1977; Knight, Swain and Chaudhri, 1977; Perrott, 1977). Fracture development due to a small spherical indenter on a semi-brittle ceramic is shown schematically in Figure 4.1. Lawn and co-workers (1975) do not observe the radial cracks as the initial fractures in the brittle materials they investigated when

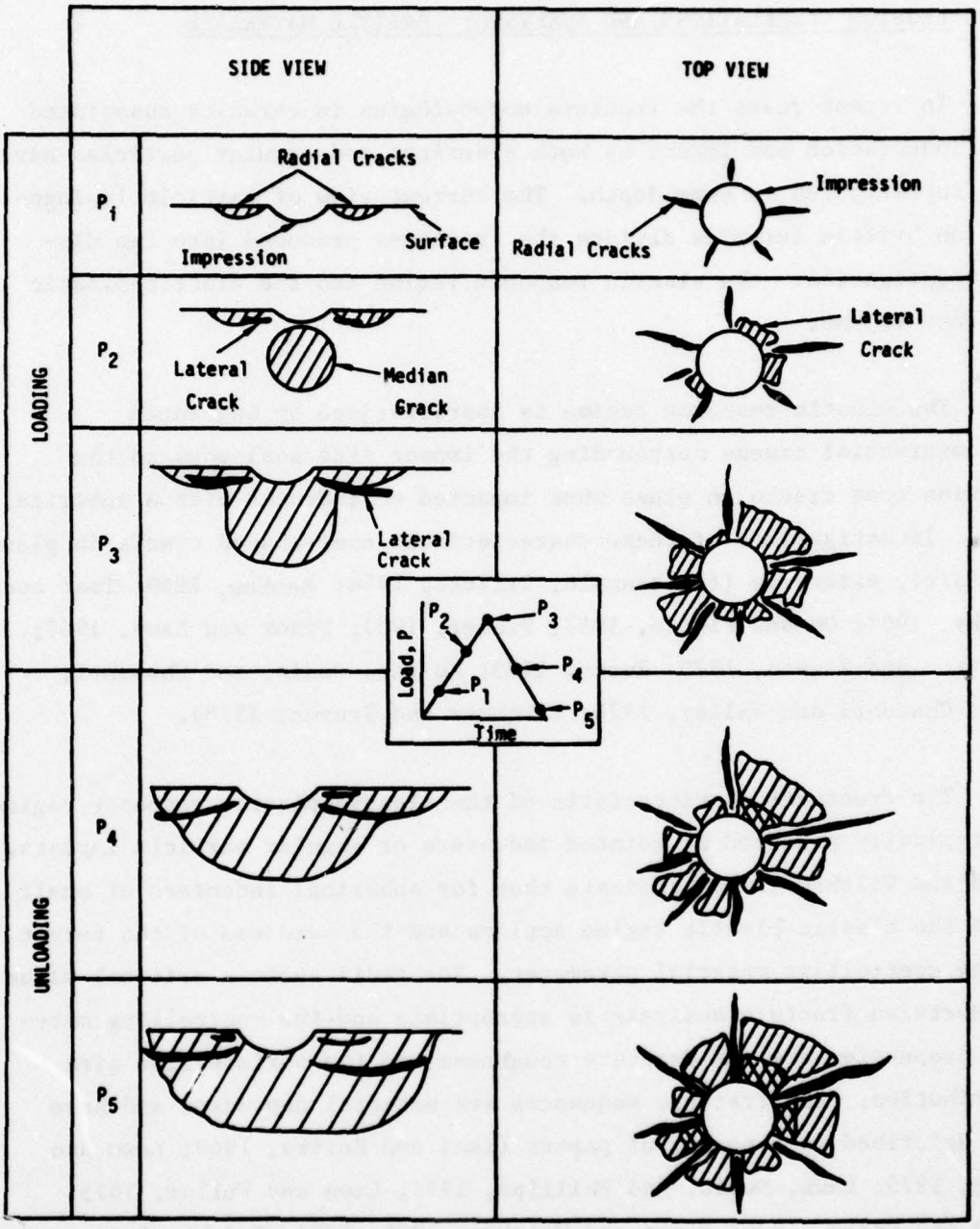

Figure 4.1. Schematic of the Crack Formation and Growth Sequence during Loading and Unloading by a Small Spherical Indenter (Evans and Wilshaw, 1976).

loaded with a pointed indenter; their observations were made on silicon, quartz, fused silica, and soda lime glass. As the sharp indenter penetrates the target it is thought to produce a localized elastic-plastic zone surrounding the indentation site. It is the modern view of indentations in ceramics that localized plastic deformations, even in essentially brittle materials, play a critical role in the crack formation process. During loading a penny-shaped crack forms below the pointed indenter, assuming a normal, axisymmetric loading condition. During the unloading phase the penny-shaped crack, referred to as a median vent fracture will reseal, and lateral cracks will propagate outward from the impact site due to residual stress effects. These cracks initiate in the vicinity of the base of the penetration zone, extend outward nearly parallel to the face of the specimen, and then tend toward the surface. These are referred to as lateral vent fractures.

The fracture sequence shown in Figure 4.1 is characteristic of indentations with a small spherical indenter in chemically vapor deposited (CVD) zinc sulfide, hot-pressed (HP) silicon nitride, single crystal spinel, and single crystal sapphire (Evans and Wilshaw, 1976). The observations by Evans and Wilshaw (1976) for glass were consistent with those of Lawn and Swain (1975) in that radial and lateral vent cracks did not form on loading and on unloading the median vent cracks propagated to the surface and at near zero load lateral cracks developed. Kirchner and Gruver (1978) demonstrated the transitions in fracture modes for glass plates impacted by 3 mm diameter glass beads by heating the specimens to 770°C. Hertzian cone cracks were observed at temperatures up to about 700°C. Radial cracks were also found: the number of radial cracks increased with increases in temperature and particle impact velocity. Returning to the experiments of Evans and Wilshaw (1976), it is noted that radial and median vent cracks in CVD zinc selenide occurred in accordance with the sequence shown in Figure 4.1, but lateral vent fractures would only result through spatial interaction of serveral adjacent indents.

Analyses of the fractures described here have been formulated by a number of authors as previously cited. For the elastic response regime the Hertzian cone cracks have been considered as the basis for erosion theories of brittle materials by Sheldon and Finnie (1966b), Mamoun (1975a), and Adler (1976a,b). In view of the current understanding of the elastic-plastic response regime for ceramics, the median vent fractures and radial cracks are considered to contribute to general strength degradation of the ceramic component when subjected to quasistatic loadings, while the lateral vent fractures contribute to the erosion of the exposed surface.

4.1 Elastic Response Regime

Bitter (1963a) indicated his deformation wear analysis (Section 3.4) developed for ductile materials was also applicable to brittle materials, such as, cement and glass. According to Bitter these materials have no capacity to absorb plastic energy, so presumably the ultimate embrittlement of work hardening ductile materials is present at the initial impact. At "not too high velocities" the crack pattern in glass is taken to be the same as in embrittled ductile materials. Bitter concludes that the amount of material removed from a glass surface is proportional to the diameter of the impacting spherical body and inversely proportional to the one-dimensional strain energy of the target (as obtained from a uniaxial tension test). The maximum principal stress difference employed by Bitter as a fracture criterion is a compressional stress state which is a secondary failure mode in glass which is more susceptible to tensile failures. The maximum tensile stresses for an elastic sphere indenting an elastic half-space occurs at the periphery of the contact radius [Eq.(A33)]. On the basis of the Hertzian stress distribution summarized in Appendix A, it is seen that the critical stress difference defined by Bitter is not proportional to the radius of the impacting sphere but is a more complex function of the sphere radius. Even along the axis of symmetry the dependence on the critical stress difference would not be proportional to the radius of the sphere.

A theoretical analysis for the erosion of brittle materials was presented by Sheldon and Finnie (1966b). Whereas Bitter's deformation wear analysis is based on an elastic-plastic model, Sheldon and Finnie's analysis is based on an elastic-brittle model. The penetration of the particle into the material specimen is calculated from the Hertzian theory of impact and a region of cone cracks is assumed to spread around the impact point.

Sheldon and Finnie apply the Hertzian theory for the normal collision of a rigid sphere on an elastic half-space to irregularly-shaped particles by introducing an idealized sphere of radius R' as shown in Figure 4.2. The radius R is that of a sphere of equal mass to that of the particle, while R' is the radius which is involved in causing fracture. As the indentation process continues material which is already cracked will transmit load to as yet uncracked material causing further fracture. When the particle finally comes to rest, the condition depicted in Figure 4.2 is the basis for the model. The new effective radius of the particle, R^*, for determining the volume removal is then estimated to be the radius of a sphere which just produces cracking when indenting to a depth q_m. The volume removed per particle, υ, is taken proportional to the volume of the spherical cap defined by R^*, a^*, and q_m

$$\upsilon = C_1 \frac{\pi}{2} a^{*2} q_m \tag{4.1}$$

According to Sheldon and Finnie (1966b) the value of the coefficient C_1 should be on the order of unity and can be estimated from measurements of volume removal per particle in erosion tests and calculations of a^* and q_m.

Finnie and co-workers (Oh, et al., 1972) subsequently defined the volume removed per particle as

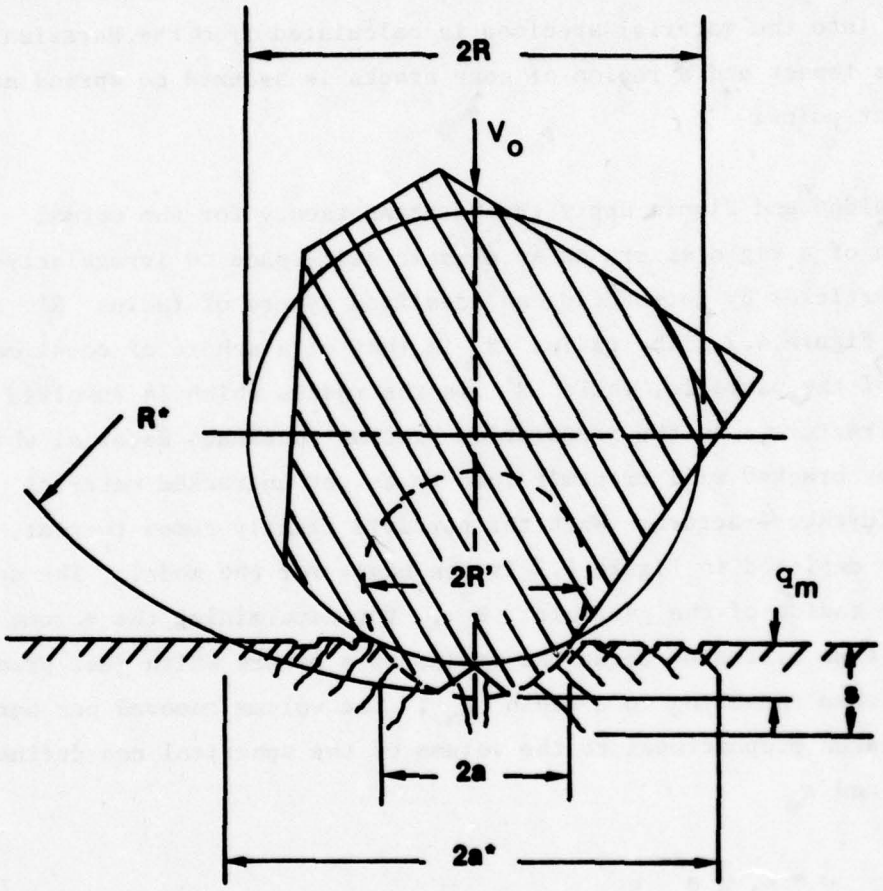

Figure 4.2. Schematic View of Cracking Due to Particle Impact as Idealized by Sheldon and Finnie (1966b).

$$\upsilon = C_2 \pi R^* S^2 = C_2 \frac{\pi}{2} a^{*2} S \tag{4.2}$$

using Eq.(B5) which includes the complete cracked zone, however they then let S be proportional to q_m, so Eq.(4.1) once again represented the volume.

The erosion of brittle materials is based on the idea that the volume removed per spherical bead impact, υ, is proportional to the product of the statistical average of the square of the radius of the outermost ring crack (a^{*2}) and the depth of the inner ring fracture. Using the statistical flaw theory of Oh and Finnie (1967) and the usual Hertzian relations, the primary result of the analysis is that

$$\upsilon = C R^a V_o^b \tag{4.3}$$

where for spherical particles

$$a = (3m-2)/(m-2),\ b \approx 0.8(3m-2)/(m-2) \tag{4.4}$$

and for angular particles

$$a = 1.2(3m-2)/(m-2),\ b = 0.8(3m-2)/(m-2) \tag{4.5}$$

The parameter m is the exponent for a Weibull distribution which is assumed to be constant for a given material. It is seen that the velocity exponent is the same for both spherical and angular particles. The experimental data for hardened steel, graphite, alumina, and magnesia shows the velocity exponent to range from 2.53 to 2.74 for SiC grit in agreement with the theory and identical values for graphite and magnesia impacted by steel shot. The experimental value of the velocity exponent for steel shot impacting plate glass deviates significantly from the calculated value.

Ruff and Wiederhorn (1979) note that

> "although the theory by Sheldon and Finnie provides a reasonable description in brittle materials, its physical basis must be questioned because it assumes Hertzian crack formation, whereas lateral crack formation is the main cause of material removal during erosion."

This is a fairly subjective view. The Hertzian crack formations are responsible for material removal from brittle material surfaces for spherical particles for particular ranges of bead diameters, materials, and impact velocities. Finnie (1970) noted that

> "in our treatment of erosion due to perpendicular impingement by solid particles, we took the volume removed by a single particle as proportional to the cracked volume produced by a single particle striking a smooth surface. Thus, at least one erosion test must be made on the chosen material before quantitative predictions can be made. We took this approach because the intersection of the fracture patterns from many particles will be a complex process, and more work needs to be done on this topic before a complete quantitative treatment of erosion is possible."

Such a program was pursued by Adler (1974a,b; 1976b).

Adler (1976b) investigated the progression of material removal from the initial single particle impacts, to a few interacting impacts, and then to significant levels of mass removal. In the usual solid particle erosion tests the incubation period for mass loss (described in Section 2) occurs so rapidly that the interaction of the impacts on the starting surface go unnoticed. It is only when the particle concentrations are low and short incremental exposures are used that the manner in which the initial surface is obscured can be observed. The progression of erosion mechanisms operative on flat surfaces of borosilicate glass specimens (Corning Glass Works designation Pyrex 7740) and fused silica specimens (Corning 7940) impacted by 70, 135, and 290 micron glass beads were established through detailed microscopic investigation of a number of progressively eroded surfaces.

The objective for this research was the development of an analytical model for the overall particle erosion process. The model was based on a concept of preferential erosion pit nucleation and growth (Adler, 1976a) which is more characteristic of liquid drop impingement, however, the initial effort simplified the erosive medium by employing glass beads and reduced the complexity of the response of the target material by considering elastic-brittle materials. The functional requirements in the general theory were explicitly evaluated for this special case. The complexity of pursuing a detailed, mechanism-oriented model became apparent (Adler, 1976b). This effort represents the only known attempt in the solid particle literature to mechanistically relate the initial single particle impact event with the mode of removal during the steady-state period for material removal.

Mamoun's formulation for material removal due to normal collisions of spherical bodies on brittle materials will now be considered (Mamoun, 1975a). As noted in Section 3.7 impacts above and below the fracture threshold are treated separately (cases 5 and 6). For case 5, Mamoun views crack nucleation and propagation as the result of a microslip process and therefore uses the same formulation for the material removed as for case 1 (Section 3.7). No information is provided on how the elastic fatigue constants are to be obtained for brittle materials, such as, inorganic glasses or alumina.

A different point of view is adopted when the impact velocity is sufficient to produce brittle fractures which are taken to be in the form of Hertzian cone cracks. Mamoun comments that the crack depth can be determined for statically applied loads using fracture criteria from fracture mechanics however acceptable fracture criteria are not available for predicting the extent of the fracture due to an impacting sphere. Mamoun therefore resorted to an energy relation by assuming that the energy difference between the initial kinetic energy with which the sphere impacts the target and that which it has when it leaves the target

surface is equal to the energy expended in creating the Hertzian fracture surface. The Hertzian fracture is in the form of a truncated cone which increases in radius with depth. These fracture surfaces have been studied extensively in glass (as already indicated in the references provided). The depth of penetration, q, of the cone crack is determined from the ratio of the energy supplied to that required to form a cylindrical fracture surface with a radius equal to the Hertzian contact radius,

$$q = \frac{1}{2\pi \gamma a_{max}} (1-e^2) \left(\frac{1}{2} m_1 V_o^2\right) \tag{4.6}$$

where e is the coefficient of restitution and γ is the surface energy per unit surface area. The volume removed is assumed to equal to the cylindrical volume described above, so the volume loss per impact is

$$\upsilon = \frac{1}{N_f} (\pi a_{max}^2 q) \tag{4.7}$$

Using Eq.(4.6) and the expression for a_{max} based on the Hertzian theory of impact

$$\upsilon = \frac{(1-e^2)}{4\gamma N_f} \left[\frac{1280\pi^6 \rho_1^6}{243} \left(\left(\frac{1-\nu_1^2}{E_1}\right) + \left(\frac{1-\nu_2^2}{E_2}\right)\right)\right]^{1/5} R_t^4 V^{2.4} \tag{4.8}$$

For this case N_f is not prescribed, so the above result is incomplete. The form of the mass removal expression subsequently presented by Mamoun (1975d) differs from the form in Eq.(4.8), however only a brief description is provided concerning the derivation of the revised form.

Mamoun (1975d) compared his analysis with what he claimed was the existing experimental data which consists of a single data point: 127 μm silica carbide particles impacting high-purity alumina at 152 ms^{-1} (Sheldon and Finnie, 1966a). Although Sheldon and Finnie (1966a) provide erosion data for glass, graphite, and magnesia, Mamoun ignores its existence.

4.2 Elastic-Plastic Response Regime

After fairly extensive investigations of quasistatic spherical bead indentations and particle impacts by single spherical beads at normal incidence on ceramics, Evans and co-workers (Evans and Wilshaw, 1976, 1977; Evans, et al., 1978) formulated two semi-empirical erosion models based on semi-empirical relations between the magnitude of the lateral fractures produced and the relevant target and projectile parameters. The semi-empirical relations are obtained from an approximate stress analysis of the indentation process and fracture mechanics (quasistatic erosion analysis) or from an approximate analysis of the impact dynamics and fracture mechanics (dynamic erosion analysis).

The upper bound for material removal per particle impact is determined from the cylindrical volume encompassed by the radial extent of the lateral cracks, C_ℓ , and their maximum depth, q . Thus,

$$\upsilon = \pi C_\ell^2 q \tag{4.9}$$

For the quasistatic impact condition, Evans and Wilshaw (1976) find that

$$\upsilon \propto N G_t^{4/5} \rho_p^{6/5} R^4 V_o^{12/5} / K_D^{3/2} H_D^{1/2} \tag{4.10}$$

Evans observes that little interaction occurs between lateral fractures from adjacent impacts, so a first order approximation to the material removal process would be a simple summation of the volume removed per particle. The total number of impacting particles is N, G_t is the shear modulus for the target material, and ρ_p is the density of the impacting particle. The dynamic fracture toughness and dynamic hardness, K_D and H_D , are introduced without comment.

Evans and Wilshaw apparently felt that the values for dynamic loadings should replace the static values in their analysis but do not indicate how they might be evaluated or provide justification for this modification. (Compare Evans and Wilshaw, 1977.)

The derivation of Eq.(4.10) is obtained from an experimental data base for spherical indenters with a liberal interchange of the loads and indent dimensions for a Vickers indenter with the loads and contact zone radii for a spherical bead indentation. The crack dimensions are related to the fracture toughness, however the depth of the lateral fractures is conjectured to be proportional to the radius of the contact zone which is the then equated to the length of the hardness impression: all without experimental verification. The load on the spherical indenter and the Vickers indenter are also considered equivalent and for the low-velocity impact condition the load is expressed in terms of the impact velocity according to the Hertzian theory of impact [Eq.(A35) in Appendix A] as is evident in the form of the parameters other than K_D and H_D appearing in Eq.(4.10). The derivation, although lacking in rigor, introduces an explicit dependence on the fracture toughness and hardness into the expression for material removal which is intuitively appealing.

The basis for the dynamic analysis is somewhat more refined: the relation between q and the contact zone is experimentally defined and the characterization procedures, experimental damage measurements, and analytical procedures have expanded (Evans, et al., 1978). Based on the implicit assumption that the lateral crack dimensions are proportional to the radial crack sizes for which an expression was derived, the input to Eq.(4.9) is now

$$C_\ell \propto C_r \propto \frac{\left(\rho_p \rho_t G_p G_t\right)^{1/3}}{\left(\sqrt{\rho_p G_p} + \sqrt{\rho_t G_t}\right)^{4/3}} \quad \rho_p^{2/3} \left(\frac{(RV_o)^2}{K_c}\right)^{2/3} \tag{4.11}$$

and

$$q \propto \left(\sqrt{\frac{\rho_p}{H}}\, R^2 V_o\right)^{1/2} \tag{4.12}$$

Eq.(4.9) becomes

$$U \propto \frac{\left(\rho_p \rho_t G_p G_t\right)^{2/3}}{\left(\sqrt{\rho_p G_p} + \sqrt{\rho_t G_t}\right)^{8/3}} \rho_p^{19/12} R^{11/3} V_o^{19/6} K_c^{-4/3} H^{-1/4} \tag{4.13}$$

as given by Evans (1979).*

The quasistatic elastic-plastic indentation experiments indicate that the lateral cracks propagate outward from the region of the plastic zone (Lawn and Swain, 1975). This observation prompted specification of an alternative form of the material removal volume in Eq.(4.9), as reported by Ruff and Wiederhorn (1979). Eq.(4.11) is used, however the depth of the lateral cracks is taken to be proportional to the depth of the maximum particle penetration. Eq.(4.12) is replaced by

$$q \propto \left(\rho_p R^3 V_o^2 H^{-1}\right)^{1/3} \tag{4.14}$$

Then

$$U \propto \frac{\left(\rho_p \rho_t G_p G_t\right)^{2/3}}{\left(\sqrt{\rho_p G_p} + \sqrt{\rho_t G_t}\right)^{8/3}} \rho_p^{11/9} R^{11/3} V_o^{22/9} K_c^{-4/3} H^{1/9} \tag{4.15}$$

The significance for this modified form is not clear.

---

*Note that Ruff and Wiederhorn (1979) comment that Evans, et al., (1978) found a weak experimental dependence of C_r on ρ_p and eliminated ρ_p from Eq.(4.11). However since ρ_p enters the theory again in establishing the erosion rate, the dependence on ρ_p is included. This is the reason for the difference in the form of Eq.(4.13) as found in Evans, et al. (1978), compared with Ruff and Wiederhorn (1979) and Evans (1979).

The relation between the volume removed per particle and the parameters $(K_c^{4/3} H^{1/4})$ was compared with Gulden's data (Gulden, 1979a) for four ceramics impacted by 115 μm quartz particles at from 98 to 180 ms^{-1} to show that the correlation was nonlinear (Evans, et al., 1978). The inclusion of hot-pressed silicon nitride may not be a valid comparison, since the impact conditions were below the lateral fracture threshold. Thus, while material was being removed, it was not being removed in accordance with the mechanism upon which Eq.(4.13) is based. The correlation with the remaining data points appears reasonable. On the other hand, the relation $v \propto (H^{1/3}/K_c^{4})^{1/3}$ in Eq.(4.15) shows a much stronger nonlinear correlation of the experimental values. Thus, Eq.(4.13) appears to be a better form for representing the material properties.

The particle velocity and size dependence indicated in Eq.(4.13) are in excellent agreement for magnesium fluoride impacted by quartz particles ranging in the size from 10 to 385 μm over a velocity range from 50 to 285 ms^{-1} (Gulden, 1979b). Reaction-bonded silicon nitride also showed good correlation with $R^4V_o^4$ for quartz particles when the impact condition was above the threshold for lateral crack formation, however the volume removed per particle impact for glass bonded alumina and hot-pressed silicon nitride impacted by quartz particles showed very good agreement with a R^3V_o (the particle momentum) correlating factor (Gulden, 1979a). When hot-pressed silicon nitride was impacted by 10 to 940 μm silicon carbide particles, the data was consistent with an $R^4V_o^4$ correlating parameter which indicates the significance of the particle target interaction. The determination of the range of application of the correlation in Eq.(4.13) certainly requires further consideration.

Due to the similarities in the nature of the fractures formed for quasistatic and dynamic loadings in the elastic-plastic response regime, there is some motivation to use the quasistatic fracture measurements. Evans has maintained an awareness of the transient nature of the particle impact event. This approach appears to be warranted in that the experimental data shows that the radial and lateral cracks lengths for zinc sulfide and magnesium fluoride normalized with respect to the impression radius for spherical beads are significantly larger for the dynamic loading conditions compared with the quasistatic loadings. The difference ranges from a factor of two to four for the larger plastic indentation radii. Knight, Swain, and Chaudhri's (1977) work on glass also indicates that a quasistatic analysis of impact damage significantly underestimates the extent of the damage.

5.0 DISCUSSION

Both the experimental and analytical approaches to solid particle erosion phenomena as found in the publications dating from the early 1930's to the present time were reviewed. Some of the deficiencies in solid particle erosion testing will be indicated, although this subject has not been adequately treated in this report. Then some of the observations regarding solid particle erosion modeling will be summarized.

5.1 Solid Particle Erosion Testing

The experimental work has revealed general trends in the erosive response of materials exposed to multiple solid particle impacts, but an accurate and reproducible quantitative evaluation of the erosion of materials still has not been achieved. The lack of a reliable data base is due to the need for a test facility which will provide impact conditions corresponding to the impact parameters which have been used in the past (impingement angle, impact velocity, particle mass and shape, and so on) to correlate the experimental determination of mass removal. Concern over the nature of the particulate flow and the actual impact conditions at the surface of the target has been expressed by several investigations in relation to the results they obtained in their erosion facilities. Since this problem is beginning to receive attention, due to the need for more refined and reliable erosion measurements, the available experimental results and procedures were examined but no coherent treatment of this work evolved which would be of value to current and future investigations.

The survey of the solid particle erosion testing facilities and procedures indicates that there is a definite need for devising a facility to provide an accurate measure of the erosive response of materials and/or to provide detailed charaterization of the actual impact parameters for existing facilities. This is not a simple under-

taking due to the number of parameters which are associated with multiple collisions of irregular-shaped particles on a material surface whose general topography and properties are changing with the length of the exposure. The characterization process for a single particle type and material is in itself quite extensive. Many factors have to be evaluated to develop accurate measures of the mass of particles actually contacting the surface, their impact velocity and impingement angle, and the nature of the particles delivered to the surface compared with the initial properties and sizes of the particles (especially for soft particulates). Concentration effects are obviously important. Particle concentration can influence the extent of particle shielding at the surface (the accumulation of particles on the surface which prevents the incoming particles from making direct contact with the target's surface), particle rebound characteristics which change as a function of exposure time also affect the trajectories of the incoming particles, and the occurence of particle embedding in the target's surface modifies the measured erosive response of the base material. Current interests are directed toward evaluating the response of materials at elevated temperatures and in corrosive environments which introduces additional complications into an already complicated evaluation procedure.

In the past the above considerations would generally have been dismissed as being overstated, but the experimental work underway in several laboratories is demonstrating that these issues have to be resolved. The statistical nature of the multiple particle erosion process has to be recognized, so it may not be possible to provide a definitive result: the erosive response for restricted impact conditions may have to be expressed in terms of bounds on the measure of erosion. However even defining reliable bounds on the magnitude of the erosive response which are independent of the test procedure used would be an accomplishment in view of the present state of affairs. Therefore careful examination of what is really required from a pragmatic viewpoint should be undertaken and then a general methodology for achieving

a realistic testing objective established. It is therefore suggested that a significant contribution to the solid particle erosion field would be to fully characterize existing test facilities and test procedures in order to establish: (1) a set of design requirements for minimizing the influence of the test apparatus on erosion evaluations, (2) operating procedures to further assure that the test parameters are within specified limits, and (3) reporting procedures which will supply adequate information for reproducing the test conditions in other laboratories in order to confirm or extend the experimental data.* It is almost imperative that such as investigation be a necessary prerequisite to any large-scale test and evaluation program.

5.2 Solid Particle Erosion Modeling

The various solid particle erosion analyses which have been developed have been reviewed and compiled for future reference. This report does not replace reference to the original work, which is strongly advised, but attempts to highlight the basis for the approach adopted, provides some perspective on the general interrelationships among the various analyses, and re-examines the validity of the analytical procedures employed. During the course of presenting the analytical work, the solid particle experiments sometimes used as the basis for the modeling effort have also been examined.

Hutchings' work has made a significant contribution to providing a more realistic view of the material removal process due to oblique impacts of both rounded and angular rigid particles on ductile materials. Reasonable correlation with the mass loss for spherical body impacts is achieved if numerical integration of the equations of motion for the progression of the particle through the material replaces the re-

*Round-robin tests are being conducted by members of the ASTM Subcommittee G2.20 on Erosion by Solid Particle Impingement to begin to assess what can be done to address these problems. If these criteria are to be established within a reasonable time frame, the magnitude of this effort will have to be considerably expanded.

strictive assumptions which have to be imposed to analytically integrate the equations of motion (Finnie, 1958; Surette, 1971). The model used by Hutchings is still highly idealized and requires further modifications before it may adequately reproduce the volume removal rates. However Hutchings' work demonstrates the benefits of a well-characterized experimental arrangement for gaining insights into the mechanics of the material removal process and in clarifying by direct observation the effectiveness of the modes of material removal possible. This latter consideration is usually a matter of conjecture in the modeling approaches (Finnie, 1958; Bitter, 1963a,b).

Both Sheldon and Kanhere (1972) and Finnie and McFadden (1978) attempted to develop analyses which would provide a velocity exponent greater than two. It is this investigator's finding that if Sheldon and Kanhere's analysis is correctly carried out, a velocity exponent of two results instead of three as they conclude. Furthermore, it is this investigator's observation that Finnie and McFadden artifically introduce the desired velocity dependence into the analysis, so the model they propose is not really representative of the outcome of their derivation. Bitter's analysis (1963b) is somewhat overshadowed by the oft-quoted simplification of the correlation presented by Neilson and Gilchrist (1968), however Bitter's result, although based on heuristic arguments yields a velocity exponent of 5/2 or less when $\alpha \leq \alpha_o$ [refer to Eq. (3.63)].

Velocity exponents not equal to two were the result of Mamoun's analysis (which is an elaboration of Bitter's mechanics analysis which views the erosion of ductile metals as a fatigue process), Head's statistical analysis, and Tabakoff's modifications of Neilson and Gilchrist's purely empirical correlations. Mamoun's published work is only applicable to normal collisons of spherical particles, however, the introduction of empirical fatigue correlations results in material dependent velocity exponents. Several assumptions are made with regard

to the volume of material removed and in correlating the experimental data which weakens Mamoun's contention that he developed a definitive predictive theory. Head's statistical approach suffered in part from an inadequately characterized erosion apparatus: significant differences were found in the erosion data when a slightly modified test arrangement was used (cp. Head and Harr, 1970, and Head, et al., 1973). Although velocity exponents different than two were obtained, the inconsistency in the results essentially invalidates their usefulness. A much better correlation with their experimental data is claimed than can be supported by the comparisons provided. Head's work does not rule out the use of statistical correlative procedures, as is sometimes suggested in the solid particle erosion literature since it has been attempted, but simply illustrates that meaningful results cannot be obtained from a testing program which does not adequately address the prerequisites listed at the end of Section 5.1. Subsequent analysis along the same lines (Jennings, et al., 1976) indicated the velocity exponent had a constant value of five which does not correspond to the available test results for which the velocity exponent rarely exceeds three for ductile metals. Tabakoff investigated the statistics of the particle rebound characteristics in his erosion facility which he described empirically. Introduction of these empirical correlations inherent in his erosion facility into a modified form of Neilson and Gilchrist's volume removal relations also yields a velocity exponent greater than two for ductile metals which reaches a constant value of four for normal impacts which appears to describe Tabakoff's experimental data. The strong dependence of the erosion data on the size of the specimen in Tabakoff's wind tunnel facility has to be resolved in order to differentiate the material's response from the aerodynamics of particulate-laden gases.

It is seen that the physical basis for the correlations (analyses) of solid particle erosion of ductile materials is almost negligible. It may be that the process is too complex to be described by other than semi-empirical correlations of the test data, however there are still

considerable advances which can be made in this regard. The best potential for progress is a closer association with the microscopic details of the particle/target interactions responsible for material removal as observed for idealized, but well characterized, experimental conditions. The review of past work indicates that this approach has not yet been extensively pursued for solid particle erosion of ductile metals. Target surface melting was suggested by Smeltzer, et al. (1970) and Jennings, et al. (1976) based on their microscopic observations of eroded metallic surfaces. The significance of localized melting during solid particle impingements is still a controversial matter. As the number of investigators examining the microscopic details of eroded surfaces increases, the role of localized melting should be clarified.

The approach suggested above has been pursued by Evans for normal collisions of primarily spherical particles on polycrystalline ceramics. A number of useful observations have been made including an estimate of volume removal per particle impact. This semi-empirical correlation indicates an explicit velocity exponent of 3.17 for all ceramics such that the impact conditions are within the elastic-plastic response regime: allowance is made for additional velocity dependence in the proportionality coefficient, Eq. (4.13). However Evans was more concerned with material properties which affect the extent of the damage due to single particle impacts. Fracture toughness and hardness are identified as the most significant material properties. The dependence of the volume removed per particle on $K_c^{-4/3}H^{-1/4}$, where K_c is the fracture toughness and H is the Vickers hardness of the target material, shows moderate correlation with the experimental data (Evans, et al., 1978) but the correspondence leaves room for improvement. The dependence of $K_c^{-4/3}H^{1/9}$ reported by Ruff and Wiederhorn (1979) shows little correlation with the experimental data.

Although the general character of the fractures produced in ceramics by quasistatic loading conditions appear similar to those observed for particle collisions, Evans' quantitative measurements of the extent of the fracture surfaces show the dynamic loading conditions produce significantly larger cracks than quasistatic loadings for comparable contact zone radii. A transient stress analysis is therefore required to adequately estimate the extent of the crack growth during the loading/unloading cycle.

The anlaytical representations for volume removal from brittle materials are quite crude in relation to the physical process of removal [Eq.(4.1), (4.7), and (4.9)], and as defined, would overestimate the volume of material removed. As long as the primary contributors to the removal process are identified and are assigned the proper functional dependence, this volume discrepancy should appear in the proportionality coefficient. All of the brittle erosion analyses assume that the conditions for the initial particle impact prevail during the erosion process. That this was not the case was shown by Adler (1974b, 1976b) for a very idealized experimental condition, and a counter example is provided by Gulden (1979b). The particular application would determine if conditions during the incubation period would be most significant or if the steady state removal rates are the desired erosion measure. In most applications the incubation period is quite short and not generally an important factor.

There is an obvious need to obtain better material property relations in order to improve the predictive capability of the existing brittle erosion models and to generalize the results to oblique impacts (a simple generalization was proposed by Hockey, et al. (1977)). In contrast to the erosion models developed for ductile materials, the recent semi-empirical correlations for brittle materials include definable material properties for the target materials. These correlations are based on direct observations of single particle impact damage and incorporate concepts from fracture mechanics and stress wave propagation in deformable media.

APPENDICES

APPENDIX A

Hertzian Theory of Impact

A number of solid particle erosion theories employ the Hertzian theory of impact, although the limits of application for the results from this theory are often greatly exceeded. The advantage of using the Hertzian theory is that explicit expressions for the stresses in an elastic half-space can be evaluated with very simple expressions for the surface of the half-space which includes the location of the critical stress condition for fractures in brittle materials. The stresses in an elastic half-space impacted by a spherical body with different elastic properties than the half-space will be considered in some detail, since there does not appear to be a readily available source for obtaining explicit expressions for both the stress and displacement components.

The problem originally solved by Hertz (1896) was the evaluation of the stress distribution associated with two isotropic elastic bodies which touch each other over a very small part of their surface and exert upon each other a finite pressure over the common area of contact. Hertz determined the form of the common surface, the distribution of pressure over it, and the relation between the distance the bodies approach each other. The results given here will be restricted to the case of a spherical elastic body indenting an elastic half-space which is adequate for the analyses in the erosion literature. A detailed account of the stress distribution for this case was given by Huber (1904) and the principal stress trajectories were computed by Fuchs (1913) from Huber's formulas for the stress components.

The radius a of the circle of contact and the distance of approach q for an elastic sphere indenting a thick elastic plate are given by

$$a = (KPR)^{1/3} \tag{A1}$$

$$q = \frac{a^2}{R} \tag{A2}$$

where P is the normal load on the indenter, R is the indenter radius, and

$$K = \frac{3}{4}\left[\left(\frac{1-\nu_1^2}{E_1}\right) + \left(\frac{1-\nu_2^2}{E_2}\right)\right] \tag{A3}$$

where ν_1, E_1 are Poisson's ratio and Young's modulus for the sphere and ν_2, E_2 are the elastic constants for the half-space. The interfacial contact pressure between the sphere and the half-space is found to have the general form

$$p(\rho) = \frac{3P}{2\pi a^2}\left(1-\rho^2/a^2\right)^{1/2} \tag{A4}$$

for $0 \leq \rho \leq a$.

The non-vanishing stress and displacement components in the half-space for the Hertz-Huber theory can be evaluated from the analysis found in a paper by Love (1929). The notation used is defined in Figure A1.

$$\sigma_{\rho\rho} = \frac{3P}{2\pi a^2}\left[\frac{(1-2\nu)}{3\xi^2}(1-\eta^3) + \frac{\eta^5}{\eta^4+\zeta^2} + \frac{(1-\nu)\eta\zeta^2}{\eta^2+\zeta^2} + (1+\nu)\zeta\tan^{-1}(\eta/\zeta) - 2\eta\right] \tag{A5}$$

$$\sigma_{\theta\theta} = \frac{-3P}{2\pi a^2}\left[\frac{(1-2\nu)}{3\xi^2}(1-\eta^3) + \frac{(1-\nu)\eta\zeta^2}{\eta^2+\zeta^2} - (1+\nu)\zeta\tan^{-1}(\eta/\zeta) + 2\nu\eta\right] \tag{A6}$$

$$\sigma_{\rho z} = \frac{3P}{2\pi a^2}\,\xi\,\frac{\zeta\eta^5}{(\eta^2+\zeta^2)(\eta^4+\zeta^2)} \tag{A7}$$

$$\sigma_{zz} = \frac{-3P}{2\pi a^2}\,\frac{\eta^5}{(\eta^4+\zeta^2)} \tag{A8}$$

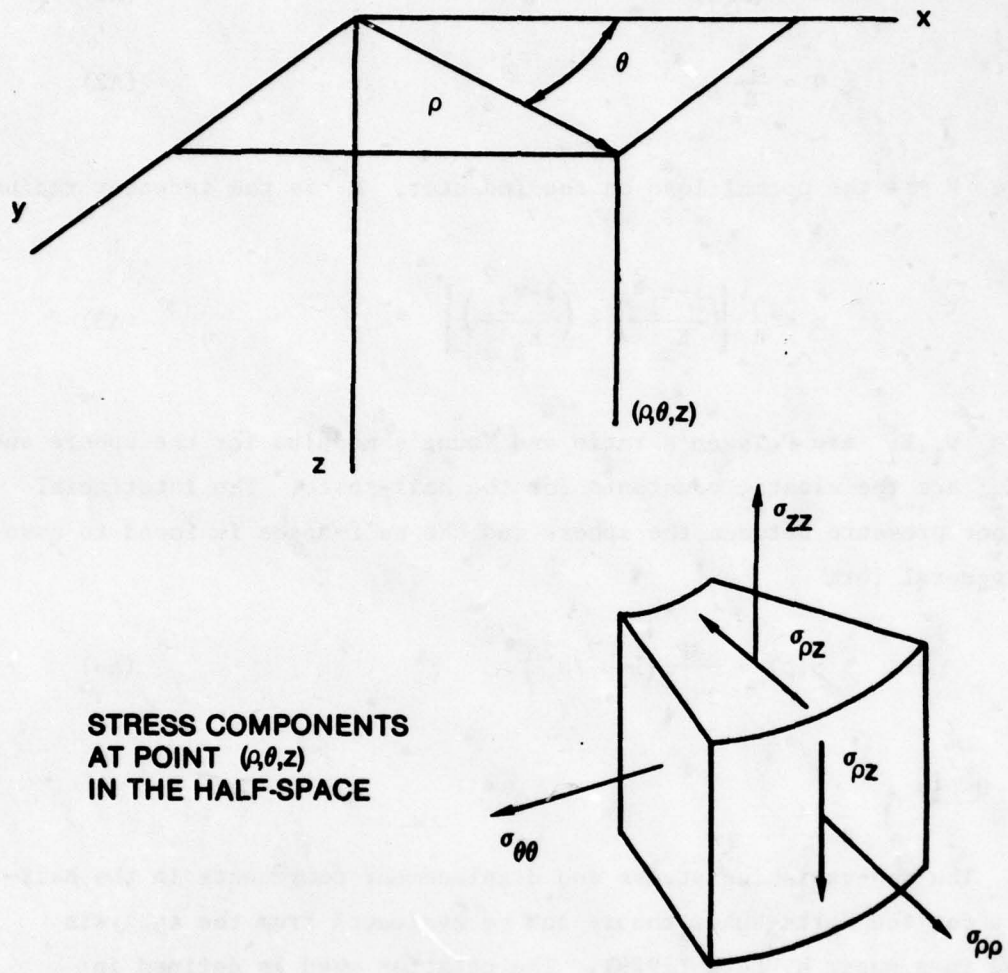

Figure A1. Notation Used in Hertzian Stress Analysis.

The displacement components are

$$u_\rho = \frac{-P}{2\pi aE}(1+\nu)\frac{1}{\xi}\left\{(1-2\nu)\left[1+\frac{3}{2}\zeta\xi^2\left(\eta/\zeta-\tan^{-1}(\eta/\zeta)\right)-\frac{1}{2}\eta(3-\eta^2)\right]\right.$$
$$\left.+\frac{3}{2}\zeta\xi^2\left(\frac{\eta\zeta}{\eta^2+\zeta^2}-\tan^{-1}(\eta/\zeta)\right)\right\} \qquad \text{(A9)}$$

$$u_z = \frac{3P}{2\pi aE}(1+\nu)\left\{(1-\nu)\left[\left(1-\frac{1}{2}\xi^2+\zeta^2\right)\tan^{-1}(\eta/\zeta)+\frac{1}{2}\xi^2\frac{\eta\zeta}{\eta^2+\zeta^2}-\eta\zeta\right]\right.$$
$$\left.+\zeta^2\left(\eta/\zeta-\tan^{-1}(\eta/\zeta)\right)\right\} \qquad \text{(A10)}$$

where

$\xi = \rho/a$, $\zeta=z/a$, $\eta=z/\lambda$, E,ν are Young's modulus and Poisson's ratio, and $\lambda^2=(\Lambda a)^2$ is the positive root from

$$\Lambda^2 = \frac{1}{2}(\xi^2+\zeta^2-1) \pm \frac{1}{2}\left[(\xi^2+\zeta^2-1)^2+4\zeta^2\right]^{1/2} \qquad \text{(A11)}$$

Numerical evaluations of Eq.(A5) to (A10) can be carried out, but the explicit representations for the limiting forms of these equations at the surface of the half-space (z=0) and along the axis of symmetry (ρ=0) will be displayed.

When $\zeta=0$, Eq.(A11) yields

$$\Lambda^2 = (\xi^2-1)\ ,\ 0 \qquad \text{(A12)}$$

With the restriction that Λ is the positive root of Eq.(A11), two cases must be considered

$$\Lambda^2 = \xi^2-1 \qquad \text{when } \xi \geq 1$$
$$\Lambda^2 = 0 \qquad \text{when } \xi < 1 \qquad \text{(A13)}$$

Then from the definitions of the dimensionless parameters

$$\eta^2 = \frac{\zeta^2}{\Lambda^2} = 1 - \frac{\xi^2}{1+\Lambda^2} \tag{A14}$$

whereby

$$\begin{aligned} \lim_{\zeta \to 0} \eta^2 &= 0 \qquad \text{when } \xi \geq 1 \\ &= 1 - \xi^2 \quad \text{when } \xi < 1 \end{aligned} \tag{A15}$$

Introducing these limiting forms into EQ.(A5) to (A10), we find for $\zeta = 0$

$$\sigma_{\rho\rho} = \frac{3P}{2\pi a^2}\left[\frac{(1-2\nu)}{3\xi^2}\left(1-(1-\xi^2)^{3/2}\right) - (1-\xi^2)^{1/2}\right] \quad \text{when } \xi<1 \tag{A16}$$

$$= \frac{3P}{2\pi a^2}\ \frac{(1-2\nu)}{3\xi^2} \qquad \text{when } \xi\geq 1$$

$$\sigma_{\theta\theta} = \frac{-\ 3P}{2\pi a^2}\left[\frac{(1-2\nu)}{3\xi^2}\left(1-(1-\xi^2)^{3/2}\right) + 2\nu(1-\xi^2)^{1/2}\right] \quad \text{when } \xi<1 \tag{A17}$$

$$= \frac{-\ 3P}{2\pi a^2}\ \frac{(1-2\nu)}{3\xi^2} \qquad \text{when } \xi\geq 1$$

$$\sigma_{zz} = \frac{-\ 3P}{2\pi a^2}\ (1-\xi^2)^{1/2} \qquad \text{when } \xi<1 \tag{A18}$$

$$= 0 \qquad \text{when } \xi\geq 1$$

$$\sigma_{\rho z} = 0 \tag{A19}$$

$$u_\rho = \frac{-P(1+\nu)(1-2\nu)}{2\pi a E\xi}\left[1-(1-\xi^2)^{3/2}\right] \qquad \text{when } \xi<1 \tag{A20}$$

$$= \frac{-P(1+\nu)(1-2\nu)}{2\pi a E\xi} \qquad \text{when } \xi\geq 1$$

$$u_z = \frac{3P(1-\nu^2)}{2\pi aE}\,\frac{\pi}{4}\,(2-\xi^2) \qquad \text{when } \xi<1$$

$$= \frac{3P(1-\nu^2)}{4\pi aE}\left[(\xi^2-1)^{1/2} - (\xi^2-2)\tan^{-1}(\xi^2-1)^{-1/2}\right] \text{when } \xi\geq 1 \qquad \text{(A21)}$$

The limiting forms when $\xi=0$ follow. Now Eq.(A11) yields

$$\Lambda^2 = \zeta^2,\ 0 \qquad \text{(A22)}$$

which is equivalent to

$$\eta = 1\ . \qquad \text{(A23)}$$

Using this condition in conjunction with the limit as $\xi\to 0$ in Eq.(A5) to (A8),

$$\sigma_{\rho\rho} = \frac{3P}{2\pi a^2}\left[\frac{1-2\nu}{2}\left(\frac{1}{1+\zeta^2}\right)+\left(\frac{1}{1+\zeta^2}\right)+\frac{(1-\nu)\zeta^2}{1+\zeta^2} + (1+\nu)\zeta\tan^{-1}(1/\zeta)-2\right] \qquad \text{(A24)}$$

$$\sigma_{\theta\theta} = \frac{-3P}{2\pi a^2}\left[\frac{1-2\nu}{2}\left(\frac{1}{1+\zeta^2}\right)+\frac{(1-\nu)^2}{1+\zeta^2} -(1+\nu)\zeta\tan^{-1}(1/\zeta)+2\nu\right] \qquad \text{(A25)}$$

$$\sigma_{zz} = \frac{-3P}{2\pi a^2}\left(\frac{1}{1+\zeta^2}\right) \qquad \text{(A26)}$$

$$\sigma_{\rho z} = 0 \qquad \text{(A27)}$$

Using either Eq.(A16) to (A18) and letting $\xi\to 0$, or using Eq.(A24) to (A26) and letting $\zeta\to 0$, we have the following limiting cases at the initial point of contact $\xi=0,\zeta=0$,

$$\sigma_{\rho\rho} = \frac{-3P}{4\pi a^2}\,(1+2\nu) \qquad \text{(A28)}$$

$$\sigma_{\theta\theta} = \frac{-3P}{4\pi a^2}\,(1+2\nu) \qquad \text{(A29)}$$

$$\sigma_{zz} = \frac{-3}{2}\frac{P}{\pi a^2} \tag{A30}$$

The corresponding displacements are,

$$u_\rho = 0 \tag{A31}$$

$$u_z = \frac{3P(1+\nu)}{2\pi aE}\left\{(1-\nu)\left[(1+\zeta^2)\tan^{-1}(1/\zeta)-\zeta\right]+\zeta^2\left[1/\zeta-\tan^{-1}(1/\zeta)\right]\right\} \tag{A32}$$

The generally quoted results follow from the limiting cases for stress components. From Eq.(A16) and (A17) it is seen that the circumferential stress component, $\sigma_{\theta\theta}$, is compressive over the entire surface and of the same magnitude as $\sigma_{\rho\rho}$ for $\rho \geq a$. The σ_{zz} stress component is compressive and corresponds to the loading condition specified in Eq.(A4). According to Eq.(A24) to (A26), $\sigma_{\rho\rho}$, $\sigma_{\theta\theta}$, and σ_{zz} are all compressive along the z-axis (axis of symmetry) between the surface and a critical depth which depends on ν. At this depth both $\sigma_{\rho\rho}$ and $\sigma_{\theta\theta}$ vanish and are tensile for all greater depths. The σ_{zz} stress component is always compressive along the axis of symmetry. The maximum radial tensile stress is located at the circular boundary of the contact surface which according to Eq.(A16) has the magnitude

$$\sigma_{\rho\rho} = \frac{(1-2\nu)P}{2\pi a^2} \tag{A33}$$

The general stress and displacement components in Eq.(A16) to (A21) can be readily programed for digital computer evaluation at any point in the half-space.

Hertz assumed that the collision of two bodies could be regarded as a statical problem; the compression at the place of contact is regarded as gradually applied and as subsiding completely by reversal of the process by which it was produced. To study the impact of a spherical body on an elastic surface, the previous relations from the Hertzian

theory are restated in terms of the impact velocity V_o instead of the load P which is now an unknown. In order to establish a relation between P and V_o, the kinetic energy of the impacting sphere is equated to the strain energy at the time of maximum impression.

$$\frac{1}{2}\left(\frac{4}{3}\rho_1\pi R^3\right) V_o^2 = \int_o^{qmax} P(\alpha)d\alpha \qquad \text{(A34)}$$

where ρ_1 is the density of the impacting sphere. Using Eq.(A2)

$$P_{max} = \left(\frac{5}{3}\pi\rho_1\right)^{3/5} K^{-2/5} V_o^{6/5} R^2 \qquad \text{(A35)}$$

The duration of contact T between the two impacting bodies is given by

$$T = 2.943\left(\frac{5}{3}\pi\rho_1 K\right)^{2/5} \frac{R}{V_o^{1/5}} \qquad \text{(A36)}$$

Thus knowing the elastic properties of the colliding bodies, the load P in Eq.(A16) to (A21) can be replaced by Eq.(A35) in terms of the impact velocity V_o so the stress and displacement components can be evaluated for the Hertzian impact conditions.

APPENDIX B

Geometrical Relations for a Rigid Sphere Indenting a Compressible Half-Space

The volume of material removed from a material surface due to particle impingement is often related to the volume included within a spherical segment. The geometrical relations for a spherical segment are summarized for general reference. The geometry of the indent is shown in Figure B1.

$$R^2 = (R-y)^2 + (d/2)^2 \tag{B1}$$

$$d^2 = 4(2Ry-y^2)$$

and

$$d = 2\sqrt{2Ry-y^2} \approx 2\sqrt{2Ry} \tag{B2}$$

The approximation to d can be used when the depth of the indent is small.

The surface area of the indent is

$$S = \int_{-R}^{-(R-y)} 2\pi x \sqrt{1+\left(\frac{dx}{dy^*}\right)^2}\, dy^*$$

$$- 2\pi \int_{-R}^{-(R-y)} R\, dy^* = 2\pi Ry \tag{B3}$$

where the geometric relation in Eq.(B1) was used.

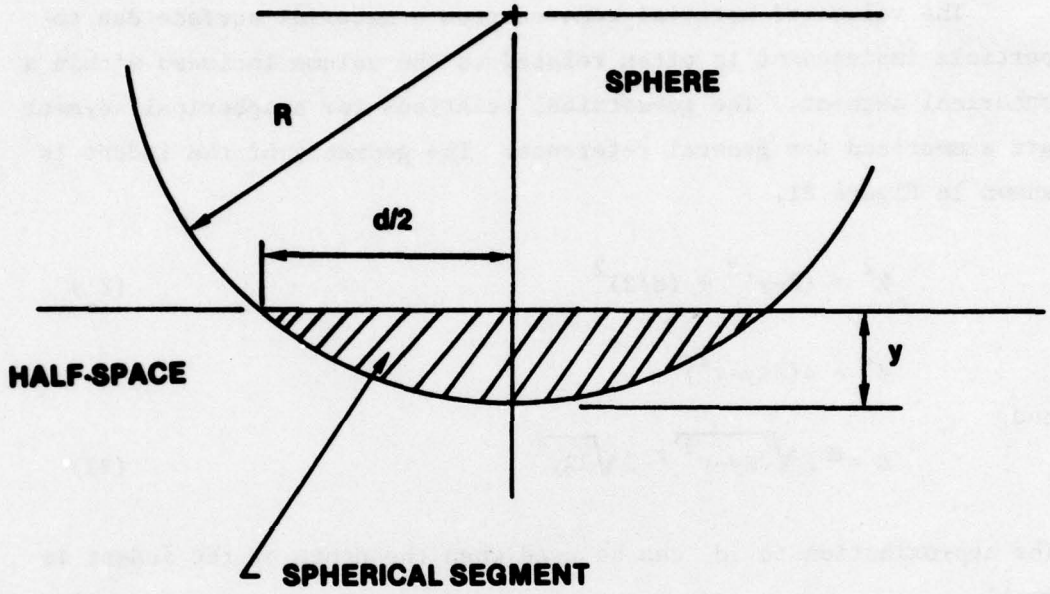

Figure B1. Geometry of Sphere Indenting a Half-Space.

The volume of the spherical indent is determined from

$$\upsilon = \pi \int_{-R}^{-(R-y)} x^2 dy^* = \pi \int_{-R}^{-(R-y)} (R^2 - y^{*2}) dy^*$$

$$= \pi \left[R^2 y^* - \frac{1}{3} y^{*3} \right]_{-R}^{-(R-y)}$$

$$= \pi \left(R y^2 - \frac{1}{3} y^3 \right) \qquad \text{(B4)}$$

For $y \ll 1$,

$$\upsilon \approx \pi R y^2 = \frac{\pi}{2} \left(\frac{d}{2}\right)^2 y \qquad \text{(B5)}$$

using Eq.(B2).

REFERENCES

Adler, W.F. (1961). Factors Influencing the Coefficient of Restitution, M.S. Thesis, Mechanics Department, Illinois Institute of Technology.

Adler, W.F. (1974a). "Erosion of Fused Silica by Glass Beads," Erosion, Wear, and Interfaces with Corrosion, ASTM STP 567. American Soceity for Testing and Materials, 294-315.

Adler, W.F. (1974b). Analysis of Multiple Particle Impacts on Brittle Materials, AFML-TR-74-210 (September, 1974).

Adler, W.F. (1976a). "Analysis of Particulate Erosion," Wear, 37, 345-352.

Adler, W.F. (1976b). "Analytical Modeling of Multiple Particle Impacts on Brittle Materials," Wear, 37, 353-364.

Adler, W.F., Morris, W., Jr., and Wahl, N.E. (1972). Supersonic Rain and Sand Erosion Research: Characterization and Development of Erosion Resistant Materials . Air Force Materials Laboratory Report AFML-TR-72-85 (May, 1972).

Ascarelli, P. (1971). Relation Between the Erosion by Solid Particles and the Physical Properties of Metals. U.S. Army Materials and Mechanics Reserach Center Technical Report 71-47, (November, 1971).

Ball, R., and Tabakoff, W. (1974). An Experimental Investigation of the Particle Dynamics of Quartz Sand Impacting 6Al-4V Titanium and 410 Stainless Steel in an Erosive Environment, University of Cincinnati, Technical Report No. 74-43 (October, 1974).

Benbow, J.J. (1960). "Cone Cracks in Fused Silica," Proc. Phys. Soc. (London), 75, 697-699.

Bitter, J.G.A. (1963a). "A Study of Erosion Phenomena, Part I," Wear, 6, 5-21.

Bitter, J.G.A. (1963b). "A Study of Erosion Phenomena, Part II," Wear, 6, 169-185.

Brauer, H. and Kriegel, E. (1965). "Verschleiss von Rohrkrümmern beim pneumatischen und hydraulischen Feststofftransport," Chem. Ing. Tech., 37, 265-276.

Chaudhri, M.M., and Walley, S.M. (1978). "A High-Speed Photographic Investigation of the Impact Damage in Soda-Lime and Borosilicate Glasses by Small Glass and Steel Spheres," Fracture Mechanics of Ceramics 3 (R.C. Bradt, D.P.H. Hasselemann, and F.F. Lange, ed.). New York: Plenum Press, 349-364.

Clevenger, W.B. and Tabakoff, W. (1974). "Similarity Parameters for Comparing Erosive Particle Trajectories in Hot Air and Cold Air Radial Inflow Turbines," J. Eng. Power, Trans. ASME, 96, Series A, 358-364.

Davies, R.M. (1949). "The Determination of Static and Dynamic Yield Stresses Using a Steel Ball," Proc. R. Soc. Lond, A197, 416-432.

de Haller, P. (1939). "Erosion and Kavitations - Erosion," Handbuch der Werkstoffprüfung, Zweiter Band, (E.Siebel, ed.) 471-488. Berlin: Julius Springer.

Engel, P.A. (1976). Impact Wear of Materials, New York: Elsevier Scientific Publishing Company.

Evans, A.G. (1973). "Strength Degradation by Projectile Impacts," J. Am. Ceram. Soc., 56, 405-409.

Evans, A.G. (1979). "Impact Damage Mechanics: Solid Projectiles," Treatise on Materials Science and Technology, 16, Materials Erosion (C.M. Preece, ed.). New York: Academic Press.

Evans, A.G., Gulden, M.E., and Rosenblatt, M. (1978). "Impact Damage in Brittle Materials in the Elastic-Plastic Response Regime," Proc. R. Soc. Lond., A361, 343-356.

Evans, A.G., and Wilshaw, T.R. (1976). "Quasi-Static Solid Particle Damage in Brittle Solids - 1. Observations, Analysis and Implications," Acta Met., 24, 939-956.

Evans, A.G., and Wilshaw, T.R. (1977). "Dynamic Solid Particle Damage in Brittle Materials: An Appraisal," J. Mater. Sci., 12, 97-116.

Finnie, I. (1958). "The Mechanism of Erosion of Ductile Metals," Proceedings Third National Congress on Applied Mechanics, 527-532.

Finnie, I. (1960). "Erosion of Surfaces by Solid Particles," Wear, 3, 87-103.

Finnie, I. (1970). Study of the Mechanisms of Sand and Dust Erosion, U.S. Army Aviation Material Laboratories Technical Report 70-70 (December, 1970).

Finnie, I. (1972). "Some Observations on the Erosion of Ductile Metals," Wear, 19, 81-90.

Finnie, I., and Kabil, Y.H. (1965). "On the Formation of Surface Ripples during Erosion," Wear, 8, 60-69.

Finnie, I., Levy, A., and McFadden, D.H. (1979). "Fundamental Mechanisms of the Erosive Wear of Ductile Metals by Solid Particles," Erosion: Prevention and Useful Applications, ASTM STP 664 (W.F. Adler, ed.) American Society for Testing and Materials, 36-58.

Finnie, I. and McFadden, D.H. (1978). "On the Velocity Dependence of the Erosion of Ductile Metals by Solid Particles at Low Angles of Incidence," Wear, 48, 181-190.

Finnie, I., Wolak, J. and Kabil, Y. (1967). "Erosion of Metals by Solid Particles," J. Mat. 2, 682-700.

Fisher, G.M.C. (1967). "The Auerbach Range in the Hertzian Fracture of Glass," J. Appl. Phys., 38, 1781-1786.

Frank, F.C. and Lawn, B.R. (1967). "On the Theory of Hertzian Fracture," Proc. R. Soc. Lond., A299, 291-306.

Fuchs, S. (1913). "Hauptspannungstrajektorien bei du Berührung einer Kugel mit einer Platt," Physik. Zeitschr., 14, 1282-1285.

Gary, M. (1904). "Versuche mit dem Sandstrahlgebläse," Mitt. dtsch. Mat.-Prüf.-Anst., 22 (3), 103-123.

Goldsmith, W. Impact, London: Edward Arnold Ltd., 1960.

Goodwin, J.E., Sage, W., and Tilly, G.P. (1969). "Study of Erosion by Solid Particles," Proc. Inst. Mech. Engrs., 184, 279-292.

Grant, G., and Tabakoff, W. (1973). An Experimental Investigation of the Erosive Characteristics of 2024 Aluminum Alloy, University of Cincinnati, Technical Report No. 73-37 (June, 1973).

Grant, G. and Tabakoff, W. (1975). "Erosion Prediction in Turbomachinery Resulting from Environmental Solid Particles," J. Aircr., 12, 471-478.

Gulden, M.E. (1979a). "Solid Particle Erosion of High-Technology Ceramics (Si_3N_4, Glass-Bonded Al_2O_3, and MgF_2)," Erosion: Prevention and Useful Applications, ASTM STP 664 (W.F. Adler, ed.). American Society for Testing and Materials, 101-122.

Gulden, M. (1979b). Study of Erosion Mechanisms of Engineering Ceramics, Seventh Interim Technical Report, Effect of Number of Impacts on Erosion in the Elastic-Plastic Response Regime, Office of Naval Research Contract N00014-73-C-0401 (March, 1979).

Hamilton, G. and Rawson, H. (1970). "The Determination of the Flaw Distributions on Various Glass Surfaces from Hertz Fracture Experiments," J. Mech. Phys. Solids, 18, 127-147.

Head, W.J. and Harr, M.E. (1970). "The Development of a Model to Predict the Erosion of Materials by Natural Contaminants," Wear, 15, 1-46.

Head, W.J., Lineback, L.D. and Manning, C.R. (1973). "Modification and Extension of a Model for Predicting the Erosion of Ductile Materials," Wear, 23, 291-298.

Head, W.J., Pacala, T. and Poole, J. (1967). Final Report on Phase I of the Allison-Purdue Dust Technology Program. Paper presented at the Man-Mobility-Serviceability Forum, General Motors, 11-12 April 1967.

Hertz, H. (1896). "On the Contact of Elastic Solids" and "On the Contact of Rigid Elastic Solids and on Hardness," Miscellaneous Papers, London: MacMillan and Company, 146-183.

Heyman, F.J. (1968). Erosion by Cavitation, Liquid Impingement and Solid Impingement--A Reivew, Westinghouse Electric Corp. Eng. Report E-1460.

Hockey, B.J., Wiederhorn, S.M., and Johnson, H. (1978). "Erosion of Brittle Materials by Solid Particle Impact," Fracture Mechanics of Ceramics 3 (R.C. Bradt, D.P.H. Hasselman, and F.F. Lange, ed.). New York: Plenum Press, 379-402.

Huber, M.T. (1904). "Zur Theorie der Berührung fester elastischer Körper," Annalen der Physik, 14(4), 153-163.

Hutchings, I.M. (1975). "Predictions of the Resistance of Metals to Erosion by Solid Particles," Wear, 35, 371-374.

Hutchings, I.M. (1977). "Deformation of Metal Surfaces by the Oblique Impact of Square Plates," Int. J. Mech. Sci., 19, 45-52.

Hutchings, I.M. (1978). Personal communication, February 21, 1978.

Hutchings, I.M. (1979). "Mechanisms of the Erosion of Metals by Solid Particles," Erosion: Prevention and Useful Applications, ASTM STP 664 (W.F. Adler, ed.). American Society for Testing and Materials, 59-76.

Hutchings, I.M., and Winter, R.E. (1974). "Particle Erosion of Ductile Metals: A Mechanism of Material Removal," Wear, 27, 121-128.

Hutchings, I.M. and Winter, R.E. (1975). "The Erosion of Ductile Metals by Spherical Particles." J. Appl. Phys., 8, 8-14.

Hutchings, I.M., Winter, R.E., and Field, J.E. (1976). "Solid Particle Erosion of Metals: the Removal of Surface Material by Spherical Projectiles," Proc. R. Soc. Lond., A348, 379-392.

Jennings, W.H., Head, W.J., and Manning, Jr., C.R. (1976). "A Mechanistic Model for the Prediction of Ductile Erosion," Wear, 40, 93-112.

Johnson, K.L. (1955). "Surface Interaction Between Elastically Loaded Bodies Under Tangential Forces," Proc. R. Soc. Lond., A230, 531-549.

Kirchner, H.P., and Gruver, R.M. (1978). "Localized Impact Damage in a Viscous Medium (Glass)," Fracture Mechanics of Ceramics 3 (R.C. Bradt, D.P.H. Hasselman, and F.F. Lange, ed.). New York: Plenum Press, 365-377.

Kleis, I. (1969). "Probleme der Bestimmung des Strahlverschleisses bei Metallen," Wear, 13, 199-215.

Knight, C.G., Swain, M.V., and Chaudhri, M.M. (1977). "Impact of Small Steel Spheres on Glass Surfaces," J. Mater. Sci., 12, 1573-1586.

Lapides, L., and Levy, A. (1979). "The Halo Effect in Jet Impingement Solid Particle Erosion Testing of Ductile Metals," in Erosion/Corrosion Newsletter (A. Levy) Pub-304, Lawrence Berkeley Laboratory, University of California (May 1979).

Lawn, B.R. and Fuller, E.R. (1975). "Equilibrium Penny-Like Cracks in Indentation Fracture," J. Mater. Sci., 10, 2016-2024.

Lawn, B.R. and Swain, M.V. (1975). "Microfracture Beneath Point Indentations in Brittle Solids," J. Mater. Sci., 10, 113-122.

Lawn, B.R., Swain, M.V., and Phillips, K. (1975). "On the Mode of Chipping Fracture in Brittle Solids," J. Mater. Sci., 10, 1236-1239.

Love, A.E.H. (1929). "The Stresses Produced in a Semi-infinite Solid by Pressures on Part of the Boundary," Proc. R. Soc. Lond., A228, 377-420.

Maji, J. and Sheldon, G.L., (1979). "Mechanisms of Erosion of a Ductile Material by Solid Particles," Erosion: Prevention and Useful Applications, ASTM STP 664, (W.F. Adler, ed.). American Society for Testing and Materials, 136-147.

Mamoun, M. (1975a). Argonne National Laboratory, Materials Science Division Second Quarterly Report to the Office of Coal Research (Contract W-31-109-Eng 38) for period ending March 15, 1975. ANL-75-XX-2.

Mamoun, M. (1975b). Argonne National Laboratory, Materials Science Division Third Quarterly Report to Division of Fossil Energy, ERDA, for period ending June 15, 1975.

Mamoun, M. (1975c). Argonne National Laboratory, Materials Science Division Coal Technology Fourth Quarterly Report, July - September 1975. ANL-76-7.

Mamoun, M. (1975d). Argonne National Laboratory, Materials Science Division Coal Technology Sixth Quarterly Report, January - March 1976. ANL-76-60.

Mamoun, M. (1976). Argonne National Laboratory, Materials Science Division Coal Technology Fifth Quarterly Report, October - December 1975. ANL-76-22.

Mamoun, M. (1979). Personal communication, June 1979.

Menguturk, M. and Sverdrup, E.F. (1979). "Calculated Tolerance of a Large Electric Utility Gas Turbine to Erosion Damage by Coal Gas Ash Particles, " Erosion: Prevention and Useful Applications, ASTM STP 664 (W.F. Adler, ed.). American Society for Testing and Materials, 193-224.

Mindlin, R.D. (1949). "Compliance of Elastic Bodies in Contact," J. Appl. Mech. 16, 259-268.

Moore, M.B. (1968). Mechanisms of Erosion of Ductile Metals by Solid Impingement. U.S. Atomic Energy Commission Report NYO-3477-12.

Neilson, J.H. and Gilchrist, A. (1960). "Erosion by a Stream of Solid Particles," Wear, 11, 111-122.

Oh, H.L. and Finnie, I. (1967). "The Ring Cracking of Glass by Spherical Indenters," J. Mech. Phys. Solids, 15, 401-411.

Oh, H.L., Oh, K.P.L., Vaidyanathan, S. and Finnie, I. (1972). "On the Shaping of Brittle Solids by Erosion and Ultrasonic Cutting." The Science of Ceramic Machining and Surface Finishing (S.J. Schneider, Jr. and R.W. Rice, ed.). National Bureau of Standards Special Publication 348, 119-132.

Perrott, C.M. (1977). "Elastic-Plastic Indentation; Hardness and Fracture," Wear, 45, 293-309.

Preece, C.M. and Macmillan, N.H. (1977). "Erosion," Annual Review of Materials Science (R.A. Huggins, R.H. Bube, and R.W. Roberts, ed.). Palo Alto, CA: Annual Reviews, Inc., 95-121.

Ruff, A.W. and Wiederhorn, S.M. (1979). "Erosion by Solid Particle Impact," Treatise on Materials Science and Technology, 16, Materials Erosion (C.M. Preece, ed.). New York: Academic Press.

Sargent, G.A., Mehrotra, P.K., and Conrad, H. (1979). "Multi-particle Erosion of Pyrex Glass," Erosion: Prevention and Useful Applications, ASTM STP 664 (W.F. Adler, ed.). American Society for Testing and Materials, 77-100.

Sheldon, G.L. and Finnie, I. (1966a). "On the Ductile Behavior of Nominally Brittle Materials during Erosive Cutting," J. Eng. Ind. Nov. 1966, 387-392.

Sheldon, G.L. and Finnie, I. (1966b). "The Mechanism of Material Removal in the Erosive Cutting of Brittle Materials," J. Eng. Ind. Nov. 1966, 393-400.

Sheldon, G.L. and Kanhere, A. (1972). "An Investigation of Impingement Erosion Using Single Particles," Wear, 21, 195-209.

Smeltzer, C.E., Gulden, M.E., McElmury, S.S., and Compton, W.A. Mechanisms of Sand and Dust Erosion in Gas Turbine Engines, U.S. Army Aviation Material Laboratories, Technical Report 70-36, (August, 1970).

Surette, R.G. (1971). Erosion of Ductile Materials by Impaction of Solid Particles. Aerospace Research Laboratory Report ARL-71-0019.

Swain, M.V. and Hagan, J.T. (1976). "Indentation Plasticity and the Ensuing Fracture of Glass," J. Phys. D: Appl. Phys., 9, 2201-2214.

Tabakoff, W. and Hamed, A. (1977). "Aerodynamic Effects on Erosion in Turbomachinery," Presented at the 1977 Tokyo-Joint Gas Turbine Conference, 22-27 May, 1977.

Tabakoff, W., Hosny, W., and Hamed, A. (1976). "Effect of Solid Particles on Turbine Performance," J. Eng. Power, Trans. ASME, 98 (series A) 47-52.

Tabakoff, W., Kotwal, R., and Hamed, A. (1979). "Erosion Study of Different Materials Affected by Coal Ash Particles," Wear, 52, 161-173.

Tabakoff, W. and Wakeman, T. (1979). "Test Facility for Material Erosion at High Temperature," Erosion: Prevention and Useful Applications, ASTM STP 664 (W.F. Adler, ed.). American Society for Testing and Materials, 123-135.

Tabor, D. (1951). The Hardness of Metals, Oxford: Clarendon Press.

Tadolder, Y.A. (1966). "Influence of Abrasive Grain Geometry on the Solid Particle Erosion of Metals," Tr. Tallin. Politekh. Inst., Ser. A, 237, 15-22.

Tillett, J.P.A. (1956). "Fracture of Glass by Spherical Indenters," Proc. Phys. Soc. (London) B69 (1956) 47-54.

Tilly, G.P. (1969a). "Erosion Caused by Airborne Particles," Wear, 14, 63-79.

Tilly, G.P. (1969b). "Sand Erosion of Metals and Plastics: a Brief Review," Wear, 14, 241-248.

Tilly, G.P. and Sage, W. (1970). "The Interaction of Particle and Material Behaviour in Erosion Processes," Wear, 16, 447-465.

Truitt, D.A. (1974). "Erosion Tests of Metallic Coatings," Proceedings of the Fourth International Conference on Rain Erosion and Associated Phenomena, (A.A. Fyall and R.B. King, ed). Royal Aircraft Establishment, Farnborough, England, 677-699.

Tsai, Y.M. and Kolsky, H. (1967). "A study of the Fracture Produced in Glass Blocks by Impact," J. Mech. Phys. Solids, 15, 263-278.

Umois, H. and Kleis, I. (1975). "A Critical Analysis of Erosion Problems which have been Little Studied," Wear, 31, 359-371.

Vijh, A.K. (1976). "Resistance of Metals to Erosion by Solid Particles in Relation to the Solid State Cohesion of Metals," Wear, 39, 173-175.

Wahl, H. and Hartstein, F. (1946). "Strahlverschleiss." Stuttgart: Franckh'sche Verlangshandlung.

Wakeman, T. and Tabakoff, W. (1979). "Turbomachinery Affected by Environmental Solid Particles," Presented at the 17th Aerospace Meeting of the AIAA, 15-17 January, 1979, in New Orleans.

Wellinger, K. (1949). "Sandstrahlverschleiss an Metallen," Z. Metallkunde. 40, 361-364.

Wellinger, K. and Uetz, H. (1955). "Gleitverschleiss, Spülverschleiss, Strahlverschleiss unter der Wirkung von körnigen Stoffen." VDI-Forschungsheft 449, Ansgabe B. Band 21, Düsseldorf: Verlag der Vereins deutscher Ingenieure.

Winter, R.E. and Hutchings, I.M. (1974). "Solid Particle Erosion Studies Using Single Angular Particles," Wear, 29, 181-194.

Wolak, J., Worm, P., Patterson, I., and Bodoin, J. (1977). "Parameters Affecting the Velocity of Particles in an Abrasive Jet," J. Eng. Mat. Tech., 99, 147-152.

Wood, C.D. (1966). Dust Research Studies, Southwest Res. Inst. Report No. AR-572.

Young, J.P. and Ruff, A.W. (1977). "Particle Erosion Measurements on Metals," J. Eng. Mat. Tech., 99, 121-125.